

12-2012

Synthesis and Characterization of Complexes of $[\text{Rh}_2(\text{NPhCOCH}_3)_4]$ and Nitriles.

Jennie Tan

East Tennessee State University

Follow this and additional works at: <https://dc.etsu.edu/honors>

 Part of the [Chemistry Commons](#)

Recommended Citation

Tan, Jennie, "Synthesis and Characterization of Complexes of $[\text{Rh}_2(\text{NPhCOCH}_3)_4]$ and Nitriles." (2012). *Undergraduate Honors Theses*. Paper 49. <https://dc.etsu.edu/honors/49>

This Honors Thesis - Open Access is brought to you for free and open access by the Student Works at Digital Commons @ East Tennessee State University. It has been accepted for inclusion in Undergraduate Honors Theses by an authorized administrator of Digital Commons @ East Tennessee State University. For more information, please contact digilib@etsu.edu.

Synthesis and Characterization of Complexes of $[\text{Rh}_2(\text{NPhCOCH}_3)_4]$ and Nitriles

Thesis submitted in partial fulfillment of Honors

By

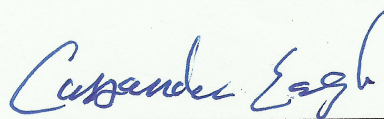
Jennie Tan

The Honors College

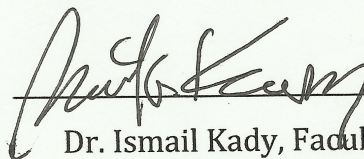
University Honors Program

East Tennessee State University

September 5, 2012



Dr. Cassandra Eagle, Faculty Mentor



Dr. Ismail Kady, Faculty Reader



Dr. Thomas Jones, Faculty Reader

Abstract

The rhodium carboxamide $[\text{Rh}_2(\text{NPhCOCH}_3)_4]\text{L}$ (L=axial ligand), has applications as a catalyst for carbenoid transformations. To explore the nature of the rhodium-carbene bond, studies between $\text{Rh}_2(\text{NPhCOCH}_3)_4$ and nitriles were proposed. Trials of the benzonitrile, o-tolunitrile, and m-tolunitrile have been performed and characterized on the 2,2-*trans* $[\text{Rh}_2(\text{NPhCOCH}_3)_4]$ complex via NMR spectroscopy, IR spectroscopy, and X-ray crystallography.

Table of Contents

1. Introduction	7
1.1 Dirhodium catalysts.....	7
1.2 Cyclopropanes.....	10
1.3 X-ray Crystallography Introduction.....	21
1.4 X-ray Characteristics.....	22
2. Methods	26
2.1 Synthesis of $[\text{Rh}_2(\text{NPhCOCH}_3)_4]$	26
2.2 Synthesis of 2,2-trans $[\text{Rh}_2(\text{NPhCOCH}_3)_4] \cdot \text{nitriles}$	38
2.3 Crystallization process of 2,2-trans $[\text{Rh}_2(\text{NPhCOCH}_3)_4] \cdot \text{nitriles}$	39
2.4 X-ray Crystallography.....	40
3. Results and Discussion	41
3.1 ^1H NMR.....	41
3.11 Benzonitrile.....	42
3.12 2,2-trans $[\text{Rh}_2(\text{NPhCOCH}_3)_4] \cdot 2\text{NC}(\text{C}_6\text{H}_4)$	45
3.13 o-tolunitrile.....	51
3.14 2,2-trans $[\text{Rh}_2(\text{NPhCOCH}_3)_4] \cdot 2 \text{ o-NC}(\{2\text{-CH}_3\}\text{C}_6\text{H}_4)$	57
3.15 m-tolunitrile.....	63
3.16 2,2-trans $[\text{Rh}_2(\text{NPhCOCH}_3)_4] \cdot 2 \text{ m-NC}(\{3\text{-CH}_3\}\text{C}_6\text{H}_4)$	68
3.2 FTIR data.....	74
3.3 X-ray Diffraction data.....	77
3.31 Bond lengths.....	87
3.32 Bond angles.....	88
3.33 Torsion angles.....	89
3.34 Packing diagrams.....	90
4. Conclusion	92
References	94

List of Figures

1. Tetrakis(carboxylate) dirhodium(II), tetrakis(acetate) dirhodium(II).....	7
2. Molecular structure of $\text{Rh}_2(\text{O}_2\text{CCH}_3)_2(\text{O}_2\text{CPh}_3)_2 \cdot (\text{CH}_3\text{CN})_2$	8
3. Tetrakis(carboxylamidate) dirhodium(II) fractions, Isomers I-IV.....	9
4. Sigma (σ) bonding and pi (π)-backbonding.....	10
5. <i>N</i> -phenylacetamide.....	11
6. Formation of <i>cis</i> and <i>trans</i> cyclopropanes with 2,2- <i>cis</i> [$\text{Rh}_2(\text{NPhCOCH}_3)_4$], formation of <i>cis</i> and <i>trans</i> cyclopropanes with 2,2- <i>trans</i> [$\text{Rh}_2(\text{NPhCOCH}_3)_4$] (middle), dotted lines were used to show bonds of the cyclopropane (bottom).....	12
7. Formation of <i>cis</i> and <i>trans</i> cyclopropane isomers.....	14
8. The cycle of the generation of cyclopropanes (<i>cis</i> and <i>trans</i>) and the regeneration of L_nM	15
9. 2,2- <i>cis</i> tetrakis (<i>N</i> -phenylacetamide) dirhodium(II), 2,2- <i>trans</i> tetrakis (<i>N</i> - phenylacetamide) dirhodium(II), 3,1 tetrakis (<i>N</i> -phenylacetamide) dirhodium(II).....	18
10. Tentative binding modes at bridging nitrile molecule.....	20
11. Adduct formation between ligand molecules (L) and dirhodium complex $\text{Rh}_2[(\text{R})\text{-MTPA}_4]$ (Rh-Rh; MTPA-H \equiv methoxytrifluoromethylphenylacetic acid = Mosher acid).....	21
12. Bravais lattices of triclinic and monoclinic structures (above); C-centered monoclinic unit cell (below).....	25
13. ^1H NMR of Fraction I.....	30
14. Resonance of benzene ring attached <i>N</i> -phenylacetamide, proton locations on benzene ring attached <i>N</i> -phenylacetamide.....	31
15. ^1H NMR of Fraction II.....	33
16. ^1H NMR of Fraction II from 6.7 to 7.6 ppm.....	34
17. ^1H NMR of Fraction III.....	36
18. ^1H NMR of Fraction IV.....	37
19. ^1H NMR of benzonitrile from 0-8 ppm.	42

20. ^1H NMR of benzonitrile from 7.2-7.7 ppm.....	43
21. ^1H NMR of 2,2- <i>trans</i> $[\text{Rh}_2(\text{NPhCOCH}_3)_4] \bullet 2\text{NC}(\text{C}_6\text{H}_4)$ from 0.0-8.0 ppm.....	45
22. Proton labels for 2,2- <i>trans</i> $[\text{Rh}_2(\text{NPhCOCH}_3)_4] \bullet 2\text{NC}(\text{C}_6\text{H}_4)$	46
23. ^1H NMR of 2,2- <i>trans</i> $[\text{Rh}_2(\text{NPhCOCH}_3)_4] \bullet 2\text{NC}(\text{C}_6\text{H}_4)$ from 6.0-7.6 ppm.....	47
24. ^1H NMR of 2,2- <i>trans</i> $[\text{Rh}_2(\text{NPhCOCH}_3)_4] \bullet 2\text{NC}(\text{C}_6\text{H}_4)$ from 0.7-2.3 ppm.....	50
25. ^1H NMR of o-tolunitrile.	51
26. ^1H labels for o-tolunitrile.	52
27. ^1H NMR of o-tolunitrile from 7.2 ppm to 7.7 ppm.....	53
28. ^1H NMR of o-tolunitrile from 1.6 ppm to 2.7 ppm.....	55
29. ^1H NMR of 2,2- <i>trans</i> $[\text{Rh}_2(\text{NPhCOCH}_3)_4] \bullet 2$ o-NC($\{2\text{-CH}_3\}\text{C}_6\text{H}_4$).....	57
30. Proton labels for 2,2- <i>trans</i> $[\text{Rh}_2(\text{NPhCOCH}_3)_4] \bullet 2$ o-NC($\{2\text{-CH}_3\}\text{C}_6\text{H}_4$).....	58
31. ^1H NMR of 2,2- <i>trans</i> $[\text{Rh}_2(\text{NPhCOCH}_3)_4] \bullet 2$ o-NC($\{2\text{-CH}_3\}\text{C}_6\text{H}_4$) from 6.0-7.8 ppm.....	59
32. ^1H NMR of 2,2- <i>trans</i> $[\text{Rh}_2(\text{NPhCOCH}_3)_4] \bullet 2$ o-NC($\{2\text{-CH}_3\}\text{C}_6\text{H}_4$) from 2.5-1 ppm.....	62
33. ^1H NMR of m-tolunitrile.....	63
34. ^1H NMR of m-tolunitrile from 6.0 ppm to 8.0 ppm.....	64
35. ^1H NMR of m-tolunitrile from 7.3-8.0 ppm.....	65
36. ^1H NMR of m-tolunitrile from 2.6 ppm to 1.7 ppm.....	67
37. Proton labels for 2,2- <i>trans</i> $[\text{Rh}_2(\text{NPhCOCH}_3)_4] \bullet$ m-NC($\{3\text{-CH}_3\}\text{C}_6\text{H}_4$).....	68
38. ^1H NMR of 2,2- <i>trans</i> $[\text{Rh}_2(\text{NPhCOCH}_3)_4] \bullet$ m-NC($\{3\text{-CH}_3\}\text{C}_6\text{H}_4$).....	69
39. ^1H NMR of 2,2- <i>trans</i> $[\text{Rh}_2(\text{NPhCOCH}_3)_4] \bullet$ m-NC($\{3\text{-CH}_3\}\text{C}_6\text{H}_4$) from 6.0 to 7.4 ppm.....	70
40. ^1H NMR of 2,2- <i>trans</i> $[\text{Rh}_2(\text{NPhCOCH}_3)_4] \bullet$ m-NC($\{3\text{-CH}_3\}\text{C}_6\text{H}_4$) from 1.1 to 2.4 ppm.....	73
41. IR spectrum of o-tolunitrile. $\text{C}\equiv\text{N}$ functional group's stretching frequency at 2223.92 cm^{-1}	75
42. IR spectrum of 2,2- <i>trans</i> $[\text{Rh}_2(\text{NPhCOCH}_3)_4] \bullet 2$ o-NC($\{2\text{-CH}_3\}\text{C}_6\text{H}_4$). $\text{C}\equiv\text{N}$ functional group's stretching frequency at 2320.37 cm^{-1}	76
43. IR spectrum of m-tolunitrile. $\text{C}\equiv\text{N}$ functional group's stretching frequency at 2227.78 cm^{-1}	76

44. IR spectrum of 2,2- <i>trans</i> [Rh ₂ (NPhCOCH ₃) ₄]•m-NC({3-CH ₃)C ₆ H ₄).....	77
45. ORTEP of 2,2- <i>trans</i> -[Rh ₂ (NPhCOCH ₃) ₄]• 2NC({2-CH ₃)C ₆ H ₄).....	83
46. ORTEP of 2,2- <i>trans</i> -[Rh ₂ (NPhCOCH ₃) ₄]• 2 o-NC({2-CH ₃)C ₆ H ₄).....	83
47. ORTEP of 2,2- <i>trans</i> [Rh ₂ (NPhCOCH ₃) ₄]• m-NC({3-CH ₃)C ₆ H ₄).....	84
48. Packing diagram of 2,2- <i>trans</i> [Rh ₂ (NPhCOCH ₃) ₄]• 2 o -NC({2-CH ₃)C ₆ H ₄).....	86
49. X-ray crystallography packing diagram of 2,2- <i>trans</i> [Rh ₂ (NPhCOCH ₃) ₄]• m-NC({3-CH ₃)C ₆ H ₄).....	87

List of Tables

1. Comparison of tetrakis(<i>N</i> -phenylacetamide) dirhodium(II) isomers using different alkenes.....	17
2. ¹ H NMR of Fraction I.	31
3. ¹ H NMR of Fraction II.	35
4. Benzonitrile phenyl protons.....	44
5. 2,2- <i>trans</i> [Rh ₂ (NPhCOCH ₃) ₄]• 2NC(C ₆ H ₄) phenyl protons.	49
6. o-tolunitrile phenyl protons.....	54
7. 2,2- <i>trans</i> [Rh ₂ (NPhCOCH ₃) ₄]• 2 o-NC({2-CH ₃ }C ₆ H ₄) phenyl protons.....	61
8. m-tolunitrile phenyl protons.....	66
9. 2,2- <i>trans</i> [Rh ₂ (NPhCOCH ₃) ₄]• m-NC({3-CH ₃ }C ₆ H ₄) phenyl peaks.....	72
10. X-ray quality crystals and solvent in the formation of: 2,2- <i>trans</i> [Rh ₂ (NPhCOCH ₃) ₄]• 2NC(C ₆ H ₄); 2,2- <i>trans</i> [Rh ₂ (NPhCOCH ₃) ₄]• 2 o-NC({2-CH ₃ }C ₆ H ₄); and 2,2- <i>trans</i> [Rh ₂ (NPhCOCH ₃) ₄]• m-NC({3-CH ₃ }C ₆ H ₄).....	77
11. 2,2- <i>trans</i> [Rh ₂ (NPhCOCH ₃) ₄]• 2NC(C ₆ H ₄) X-ray crystallography data.....	79
12. 2,2- <i>trans</i> [Rh ₂ (NPhCOCH ₃) ₄]• 2 o-NC({2-CH ₃ }C ₆ H ₄) X-ray crystallography data.....	80
13. 2,2- <i>trans</i> [Rh ₂ (NPhCOCH ₃) ₄]• m-NC({3-CH ₃ }C ₆ H ₄) X-ray crystallography data.....	82
14. X-ray Crystallography bond lengths, bond angles, and torsion angles (x=1 or x=2).....	85

1. Introduction

1.1 Dirhodium catalysts

Dirhodium carboxylates and carboxylamidates are effective metal catalysts, which affect the successful synthesis of pyrethroid insecticides, as well as other pharmaceutical and agrochemical products.¹ Pyrethroid insecticides have high toxicity to insects, low toxicity to mammals, and pose a low risk to the environment, and thus have been used commercially in bug repellants, aerosols, pet shampoos, lice treatments, and other products.

There are three traditional categories of rhodium catalysts: carboxylamidates, perfluorinated carboxylates, and carboxylates.² Tetrakis(carboxylate) dirhodium(II) molecules are homogeneous, soluble metal catalysts capable of stereoselectivity in cyclopropanation reactions. The most commonly used tetrakis(carboxylate) dirhodium(II) is tetrakis(acetate) dirhodium(II), $[\text{Rh}_2(\text{OOCCH}_3)_4]$.³ $[\text{Rh}_2(\text{OOCCH}_3)_4]$ has two Rh atoms bound together in a +2 oxidation state, surrounded by four acetate groups that each carry a -1 charge. (See Figure 1.)

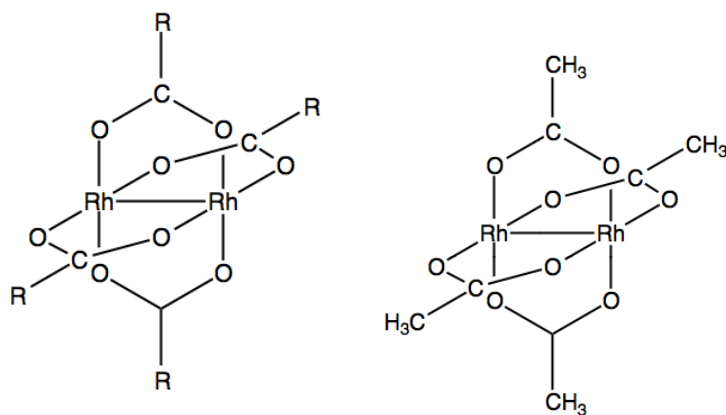


Figure 1. Tetrakis(carboxylate) dirhodium(II) (left), tetrakis(acetate) dirhodium(II) (right).

Tetrakis(carboxylamidate) dirhodium(II) compounds are easier to manipulate than tetrakis(carboxylate) dirhodium(II) to produce higher

stereoselectivity.⁴ Stereoisomers are isomers that have their atoms connected in the same order but have different three-dimensional arrangements. Stereoselectivity indicates the preference of the formation of a certain stereoisomer when a reaction produces an unequal mixture of stereoisomers due to, for example, steric or electronic effects.⁵

The R group (see Figure 1) of the tetrakis(carboxylate) compound can be manipulated to produce steric bulk and increase stereoselectivity; however, this is difficult and cannot be used commercially. Cotton and Thompson synthesized dirhodium(II) carboxylates with bulky R groups: adamantanecarboxylate, biphenylcarboxylate and triphenylacetate.⁶ The third compound in their research contains two acetate ligands and two triphenylacetate ligands, shown in Figure 2.

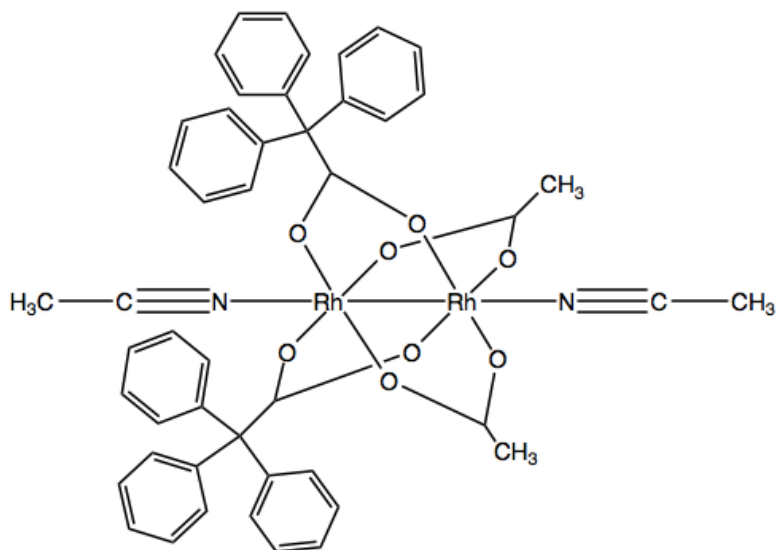


Figure 2. Molecular structure of $\text{Rh}_2(\text{O}_2\text{CCH}_3)_2(\text{O}_2\text{CPh}_3)_2 \cdot (\text{CH}_3\text{CN})_2$.

To synthesize $\text{Rh}_2(\text{O}_2\text{CCH}_3)_2(\text{O}_2\text{CPh}_3)_2 \cdot (\text{CH}_3\text{CN})_2$, anhydrous rhodium acetate (0.20 mmol) and triphenylacetic acid (1.2 mmol) were reacted together in an atmosphere of nitrogen gas. The bulky ligands (Ph_3CCO_2) were desired to provide the compound with steric bulk. However, only two triphenylacetate groups replaced two (out of the four) acetate groups. It was speculated that four triphenylacetate groups did not fit around Rh-Rh because of the steric hinderance of each triphenylacetate group. Additional Ph_3CCO_2 ligands may be forced to add to the

molecule later, but this process would involve extra steps to perform the synthesis, which may not be an efficient process for commercial applications.⁶ Therefore, tetrakis(carboxylamidate) dirhodium(II) compounds can be used to produce sterically bulky dirhodium(II) compounds instead.

The Rh atoms in tetrakis(carboxylate) dirhodium(II) are bound to oxygen atoms and not nitrogen atoms, whereas the Rh atoms in the tetrakis(carboxylamidate) dirhodium(II) are bound to both nitrogen and oxygen atoms. Because tetrakis(carboxylamidate) dirhodium(II) has nitrogen atoms, an additional substituent or molecular group can be bound to the nitrogen. This property allows tetrakis(carboxylamidate) dirhodium(II) to be manipulated to produce higher stereoselectivity than tetrakis(carboxylate) dirhodium(II).

During synthesis of the tetrakis(carboxylamidate) dirhodium(II) molecules, multiple isomers form. (See Figure 3.)

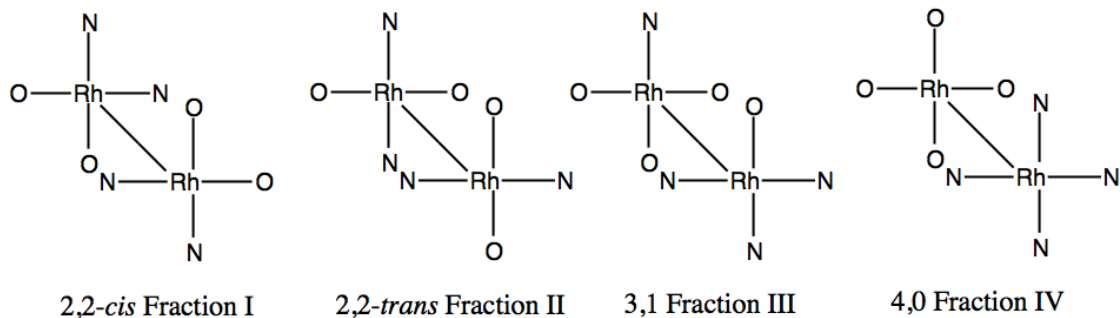


Figure 3. Tetrakis(carboxylamidate) dirhodium(II) fractions (also referred to as isomers), Isomers I-IV.

The 2,2-*cis* and 2,2-*trans* tetrakis(carboxylamidate) dirhodium(II) isomers are very effective for catalytic applications.⁴ These tetrakis(carboxylamidate) dirhodium(II) complexes can facilitate the synthesis of insecticides, which are pesticides designed to kill or deter insects. The type of insecticides in this research refers to pyrethroid insecticides, which are synthetic versions of pyrethrum. (Pyrethrum is a natural compound extracted from an East African plant.) Pyrethroid insecticides, commonly called pyrethroids, have rapid toxicity to insects and low toxicity to mammals and can be made reliably to meet market demands and possess stability towards light and air.⁷ The cyclopropane ring is the active part of the

pyrethroid insecticides. However, the most challenging part of the synthesis of pyrethroid insecticides is the formation of the cyclopropane functional group in this complex.⁸ Through studying the formation of cyclopropanes, more efficient catalysts for the synthesis of pyrethroid insecticides can be proposed.

1.2 Cyclopropanes

A cyclopropane is the product of the reaction between a carbene and an alkene. A carbene is a neutral, yet reactive and unstable molecule because of the two unshared valence electrons on the carbon. When the carbene forms a bond with the rhodium atom, it becomes stabilized. The metal-stabilized carbene is formed by both sigma (σ) bonding and pi (π) backbonding. The carbene donates electron density to the metal (rhodium) through σ bonding. Through "backbonding," the electrons (e^-) move back from the atomic orbital of the metal to the π^* anti-bonding orbital of the carbene. When the electrons of the d orbital of the metal (rhodium) move to the empty p orbital of the carbene, π -backbonding occurs.⁹ See Figure 4.

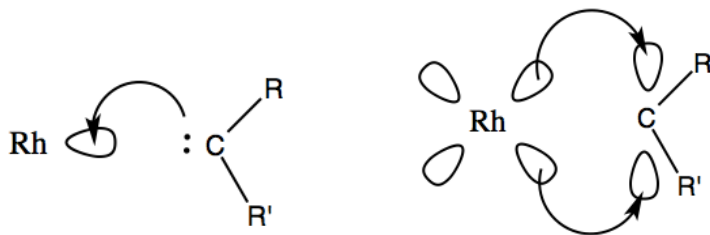


Figure 4. Sigma (σ) bonding and pi (π)-backbonding.

During the cyclopropane reaction, the dirhodium(II)-carbene bond is often difficult to isolate and study because of its transient nature. The rhodium-carbene bond occurs at the beginning of the carbenoid transformation. A carbenoid is a reactive intermediate with similar reaction characteristics to a carbene. A carbenoid can react with an alkene to form a cyclopropane with similar reaction characteristics to a carbene (further explained on page 7), with the increased potential for stereoselectivity based on the catalyst used.

As a catalyst, tetrakis(carboxylamidate) dirhodium(II) offers the advantageous feature of providing a group near the catalytic site, which can affect product formation via steric bulk and electronic influences. To manipulate the type of group attached to the tetrakis(carboxylamidate) dirhodium(II), certain bulky amides can be chosen.

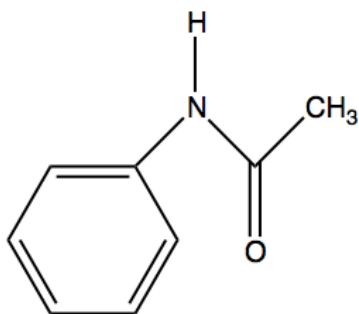


Figure 5. *N*-phenylacetamide.

One amide compound used to produce steric bulk is *N*-phenylacetamide. *N*-phenylacetamide has a phenyl group with the potential for producing steric bulk at the catalytic site. By selecting acetamide ligands with phenyl groups, the bulky phenyl groups can potentially sterically hinder the typically more stereoselectively favorable conformation (*trans* cyclopropanes) to produce the more desired isomer of cyclopropanes (*cis* cyclopropanes) to be used for pyrethroid insecticide applications.

Equatorial ligands bound to the tetrakis(carboxylamidate) dirhodium(II) have electronic control over the reactivity of the intermediate carbenoid; an electron-withdrawing ligand produces a more reactive and less selective carbenoid. Since steric bulk on the rhodium, near the catalytic site, influences the position of the approaching alkene by decreasing the stability and increasing the reactivity of the metal-stabilized carbene, the alkene is more likely to approach the carbene from the least sterically hindered position. The bulky group, *N*-phenylacetamide, bound to a tetrakis(carboxylamidate) dirhodium(II) can increase the steric bulk close to the site of the carbene formation, without blocking the site.

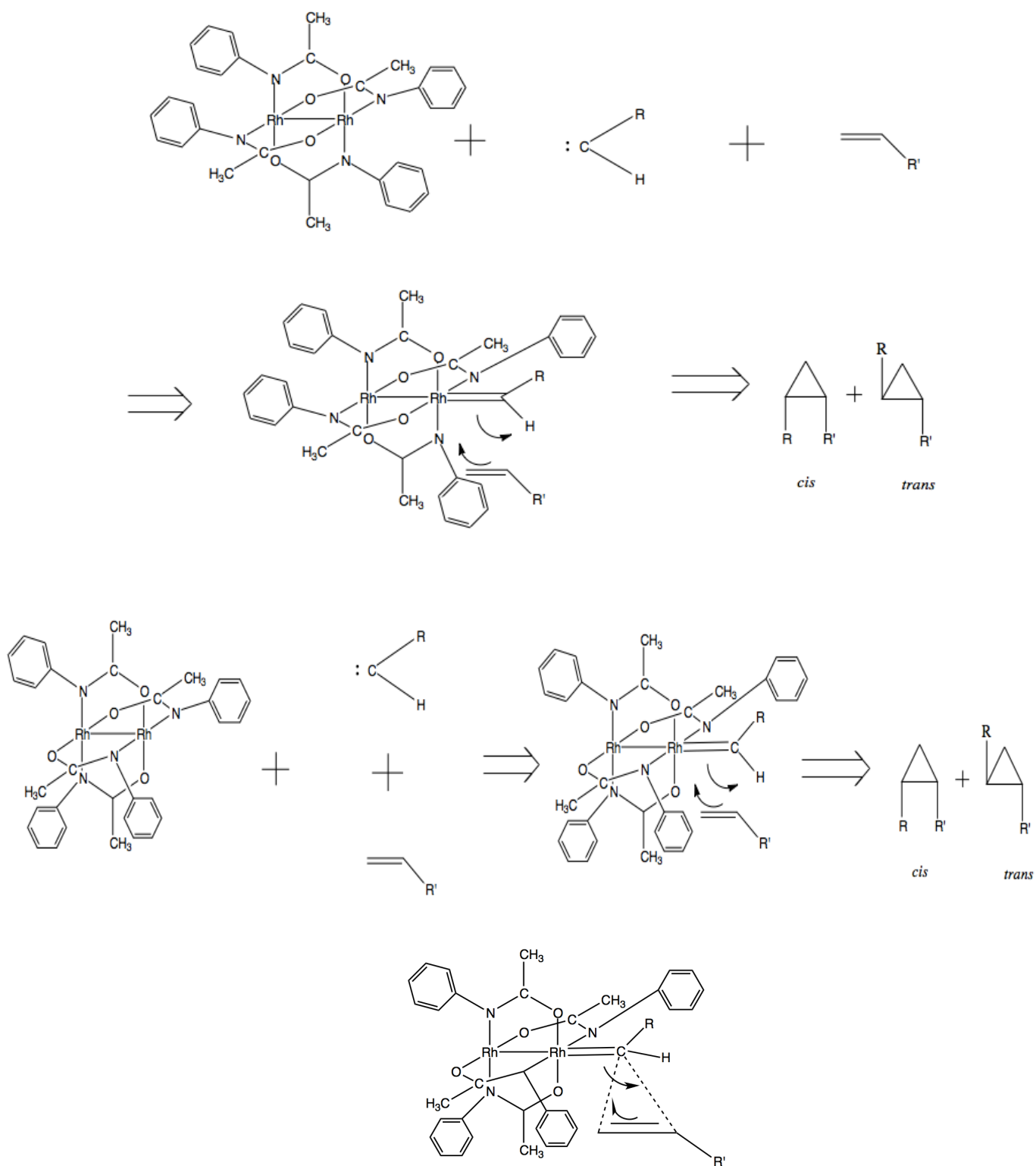


Figure 6. Formation of *cis* and *trans* cyclopropanes with 2,2-*cis* [Rh₂(NPhCOCH₃)₄] (top). Formation of *cis* and *trans* cyclopropanes with 2,2-*trans* [Rh₂(NPhCOCH₃)₄] (middle). Dotted lines were used to show bonds of the cyclopropane (bottom).

The position in which the alkene approaches the metal-stabilized complex determines the ratio of *cis* to *trans* cyclopropanes. The alkene approaches the catalytic site in a position that is both parallel to the carbene and not sterically hindered by phenyl groups (which is the least sterically hindered orientation.) The *trans* cyclopropane is the more favored conformation of the cyclopropane reaction. The electrons of the carbene close the cyclopropane ring.¹⁰ After the formation of the cyclopropane (both *cis* and *trans* cyclopropanes; discussed below), the tetrakis(carboxylamidate) dirhodium(II) compound is released to catalyze another cyclopropane reaction.¹¹ The *cis* cyclopropane is the active conformation for the pyrethroid insecticides. Unfortunately, there have been less successful syntheses of *cis* cyclopropanes than *trans* cyclopropanes.

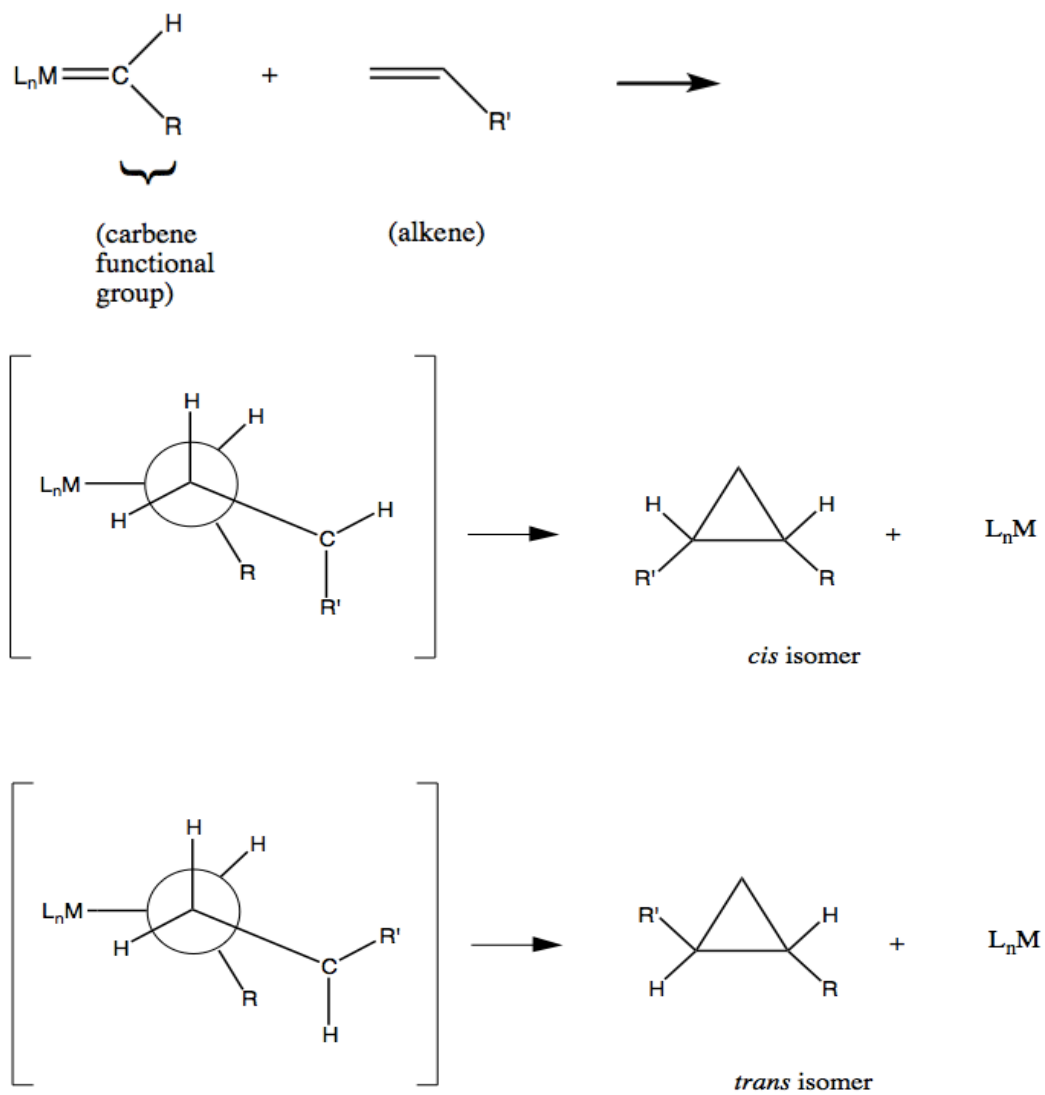


Figure 7. Formation of *cis* and *trans* cyclopropane isomers. (L_nM represents the tetrakis(carboxylamidate) dirhodium(II) compound.)

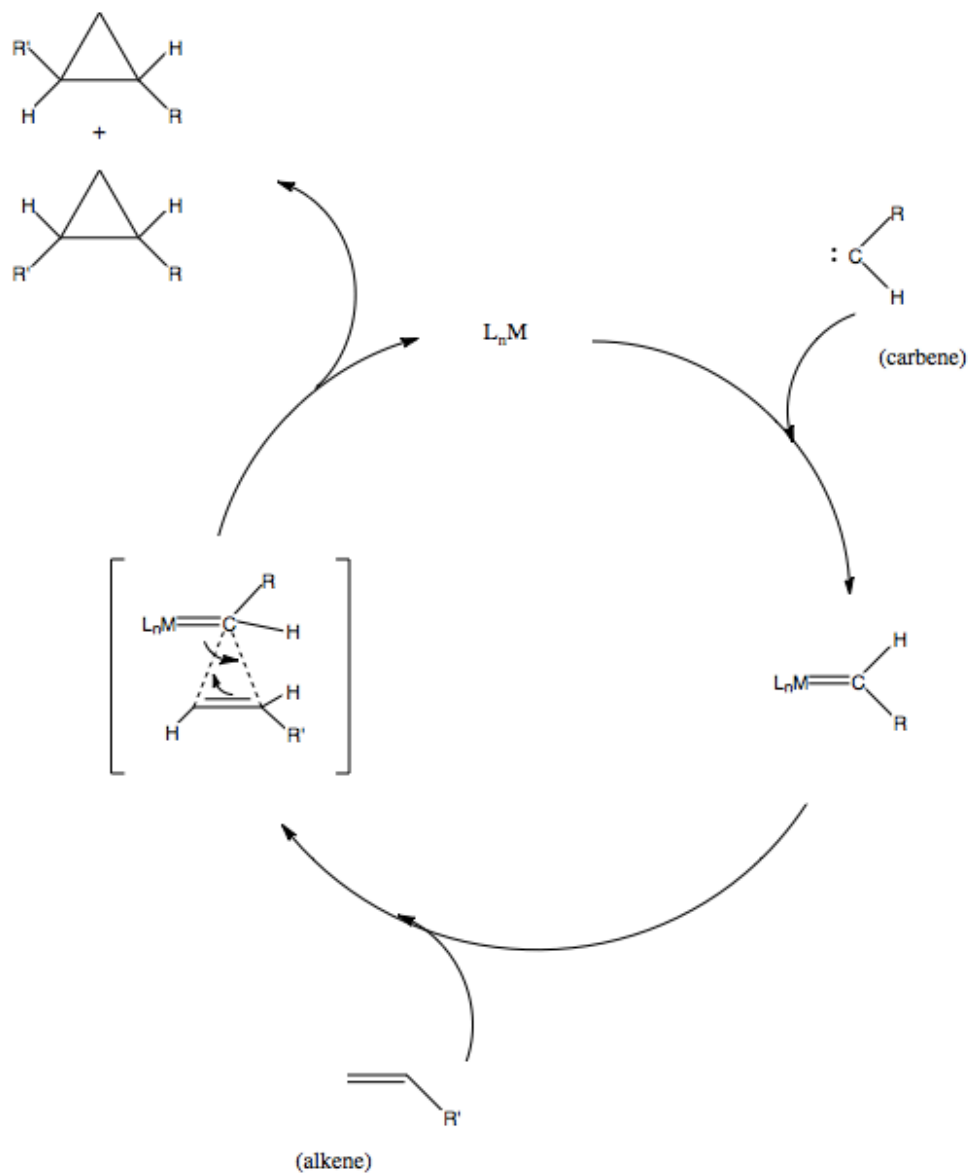


Figure 8. The cycle of the generation of cyclopropanes (*cis* and *trans*) and the regeneration of L_nM .

The nitrogen of an amide in tetrakis(carboxylamidate) dirhodium(II) donates electron density to the rhodium center and increases the production of the *trans* isomer. As the stability of the rhodium-carbene bond increases, the selectivity of the alkene orientation also increases. Over the course of the reaction, the least sterically hindered orientation becomes favored, which produces the *trans* cyclopropane. The steric hindrance of the phenyl group on the *N*-phenylacetamide can increase the

probability of *cis* cyclopropane formation via steric bulk, but the phenyl group alone is not adequate enough to favor the *cis* isomer. Eagle and co-workers discovered that the tetrakis(acetate) dirhodium(II), $[\text{Rh}_2(\text{OOCCH}_3)_4]$, produced 10% more *cis* cyclopropanes than the tetrakis(acetamide) dirhodium(II), $[\text{Rh}_2(\text{NHCOCH}_3)_4]$, due to the electron donating property of nitrogen; however, the tetrakis(*N*-phenylacetamide) dirhodium(II) produced more *cis* cyclopropanes than the tetrakis(acetate) dirhodium(II) because of the steric bulk created by the phenyl groups.⁴ Using *N*-phenylacetamide groups as equatorial ligands produces the unique combination of the electron-donating N and steric bulk of the phenyl groups. As a result, tetrakis(*N*-phenylacetamide) dirhodium(II) possesses two properties to assist in increasing the ratio of *cis* cyclopropanes to *trans* cyclopropanes: 1) *cis* cyclopropane-directing abilities through steric bulk (because of the ability to vary the substituents on the amide nitrogen), 2) σ -bonding and π -backbonding capabilities.

As the bulk of the alkene R' group ($\text{CH}_2=\text{CHR}'$) increases by selecting an alkene with a bulkier R' group, the *cis-trans* ratio of cyclopropanes using the tetrakis(*N*-phenylacetamide) dirhodium(II) isomers increases as well. Eagle and co-workers discovered that for the three tetrakis(*N*-phenylacetamide) dirhodium(II), $[\text{Rh}_2(\text{NPhCOCH}_3)_4]$, isomers (2,2-*cis*, 2,2-*trans*, and 3,1 isomers), the *cis* to *trans* ratios of the cyclopropanes formed in a ratio of 1.78 to the bulkiest alkene, trimethyl styrene (see Table 1). After the formation of the metal-carbene, the steric bulk of the phenyl group forces the approaching alkene to react away from the steric bulk of the ligand. To undergo a *cis* cyclopropane reaction, bulky equatorial ligands on the catalyst will push the substituents R and R' (see Figure 8) into a *cis* conformation instead of a *trans* conformation. It has been previously observed that increasing the bulk of the alkene R' increases the ratio of *cis* to *trans* cyclopropanes when the catalyst is 2,2-*cis* tetrakis(*N*-phenylacetamide) dirhodium(II), 2,2-*cis* $[\text{Rh}_2(\text{NPhCOCH}_3)_4]$. For 2,2-*cis* $[\text{Rh}_2(\text{NPhCOCH}_3)_4]$, as the size of the R' group on the alkene increases from ethoxy to trimethylphenyl, the *cis-trans* ratio increases from 1.0 to 1.8. The 2,2-*trans* (*N*-phenylacetamide) dirhodium(II) isomer shows an increase in the *cis-trans* ratio with increasing size of R', from 0.6 for ethoxy, to 1.2

for trimethylphenyl. For the 3,1 [Rh₂(NPhCOCH₃)₄] isomer, the *cis-trans* increases from 0.7 to 1.0. It was expected that the axial catalytic side with the three *N*-phenylacetamide would cause steric repulsion (“3” side), forcing the cyclopropane reaction to occur on the least sterically hindered catalytic side. The approaching alkene would orient the R’ group toward the carbene’s R group, forming *cis* cyclopropanes. However, the single *N*-phenylacetamidate ligand on the less sterically hindered catalytic side (“1” side) was not enough to cause selectivity for the 3,1 tetrakis (*N*-phenylacetamide) dirhodium(II) isomer. ⁴

	R'	<i>cis-trans</i> ratio
2,2- <i>cis</i> tetrakis (<i>N</i> -phenylacetamide) dirhodium(II)	ethoxy	1.0
	trimethylphenyl	1.8
2,2- <i>trans</i> tetrakis (<i>N</i> -phenylacetamide) dirhodium(II)	ethoxy	0.6
	trimethylphenyl	1.2
3,1 tetrakis (<i>N</i> -phenylacetamide) dirhodium(II)	ethoxy	0.7
	trimethylphenyl	1.0

Table 1. Comparison of tetrakis(*N*-phenylacetamide) dirhodium(II) isomers using different alkenes.

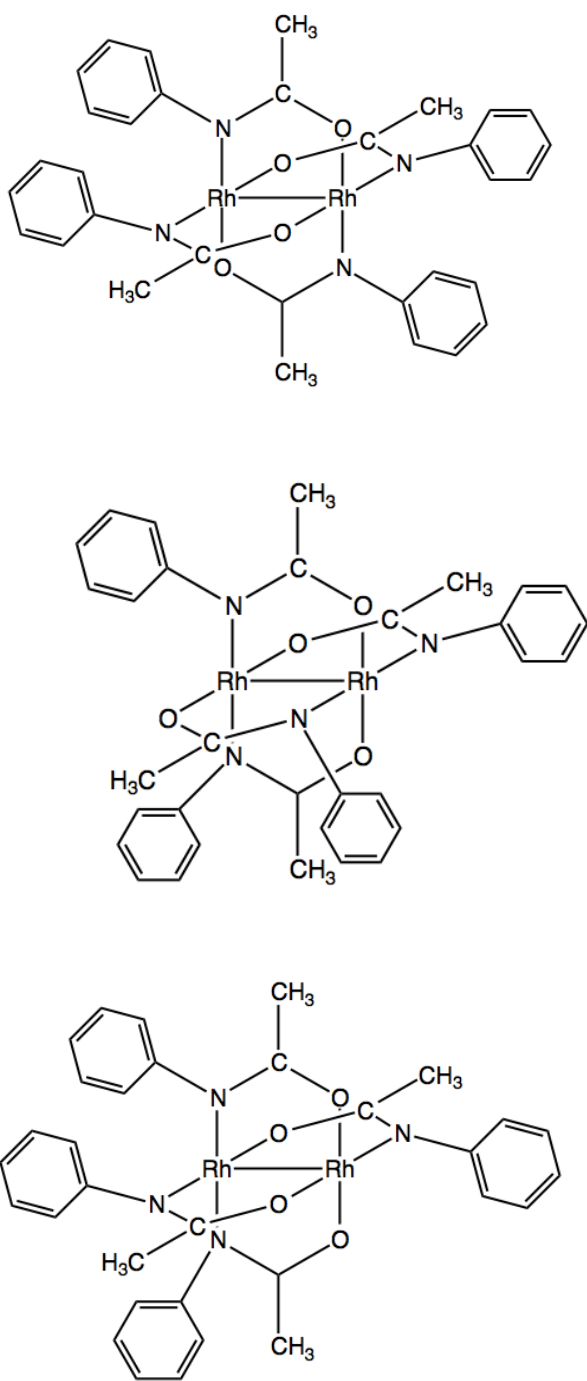


Figure 9. 2,2-*cis* tetrakis (*N*-phenylacetamide) dirhodium(II), (top),
 2,2-*trans* tetrakis (*N*-phenylacetamide) dirhodium(II), (middle),
 3,1-tetrakis (*N*-phenylacetamide) dirhodium(II), (bottom)

In order to continue to learn how to obtain a higher percentage of *cis* cyclopropanes, parameters relevant to the catalytic process can be manipulated, or the catalytic sites can be probed through using a stable analog. The purpose of this research is the latter: to use nitriles as axial ligands (because of their similar bonding properties to carbenes) complexed to tetrakis(*N*-phenylacetamide) dirhodium(II) to study their characteristics. Since the rhodium-carbene bond is highly transient, using a stable analog, such as a dirhodium nitrile compound, creates the opportunity to probe the catalytic site of the dirhodium complex. Since a nitrile can also provide σ -bonding and π -backbonding similar to the carbene, we have chosen it as the axial ligand. Also, benzonitriles with methyl groups are electron-withdrawing, and electron-withdrawing ligands produce more reactive carbenes. Depending on the type of axial ligand used, the ligand may bond on one axial site or on both axial sites of the tetrakis (*N*-phenylacetamide) dirhodium(II). If the axial ligand only bonds at one axial site, the other site may be probed as a catalytic site. A nitrile would be used to block one axial site. Nitriles used in this research will be benzonitrile and benzonitriles with methyl substituents: benzonitrile, *o*-tolunitrile, and *m*-tolunitrile.

The 2,2-*trans* tetrakis(*N*-phenylacetamide) dirhodium(II), also referred to as 2,2-*trans* $[\text{Rh}_2(\text{NPhCOCH}_3)_4]$, was selected for this Honors Research project. By manipulating the electron density of 2,2-*trans* $[\text{Rh}_2(\text{NPhCOCH}_3)_4]$ complexes through axial ligands (L), they can become electron-deficient and used as models for catalysis for chemical reactions, such as cyclopropanation.

An adduct forms when two or more volatile molecules are added to a compound. This results in a molecular complex of the “adduct” existing in between or bound to two or more other structures. Rozwadowski and co-workers have researched the adduct formations of tetrakis(carboxylate) dirhodium(II) ($\text{Rh}_2[(\text{R})\text{-MTPA}_4]$; MTPA-H=methoxytrifluoromethyl-phenylacetic acid), and ligands L (L=nitriles, alkenes, selenides, iodides, epoxides, sulfoxides, and phosphorus chalcogenides). Although there are some differences, Rozwadowski’s research can be used to better understand dirhodium(II) complexes with axial nitrile ligands.¹² Rozwadowski’s research will later be used to understand the adduct shifts

concerning dirhodium(II) complexes with axial nitrile ligands and for comparison of this project's results (see page 79).

Rozwadowski and co-workers determined that axial nitrile ligands form kinetically unstable adducts with tetrakis(carboxylate) dirhodium(II) (instead of tetrakis(carboxylamidate) dirhodium(II)).¹² The nitrile Rozwadowski studied was 2-phenylpropionitrile for its diatomic functional group and π -bond attributes. The product was a dimer of 2 tetrakis(carboxylate) dirhodium(II) molecules bridged by a side on nitrile. On the terminus of each rhodium was a linear, N bound, nitrile. Strongly binding ligands, such as nitriles, prefer $L \rightarrow Rh-Rh \leftarrow L$, whereas weaker ligands, such as alkenes with low steric hindrance, tend to form a dimer of dimers, using ligands as bridging molecules (Figure 10): $***Rh-Rh***L***Rh-Rh***$. (The symbol "*" is used to denote a weak bonds of the bridging ligands to the Rh.) The Rh-Rh adducts are interconnected by bridging 2-phenylpropionitrile at the terminal rhodium atoms, which can be considered as an intermediate during ligand exchange if the molar ratios of the axial nitrile ligand (in this case, 2-phenylpropionitrile), and tetrakis(carboxylate) dirhodium(II) are between 1:1 and 2:1 (Figure 11).¹²

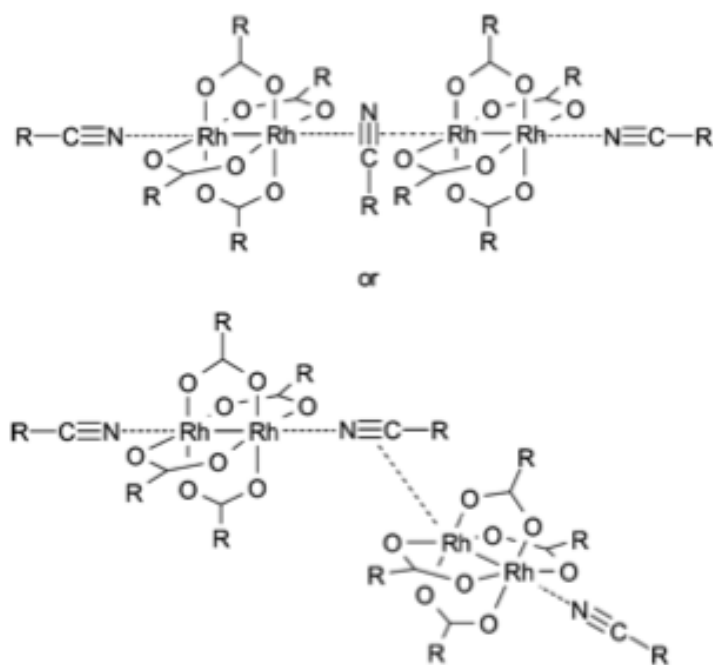


Figure 10. Tentative binding modes at bridging nitrile molecule.¹²

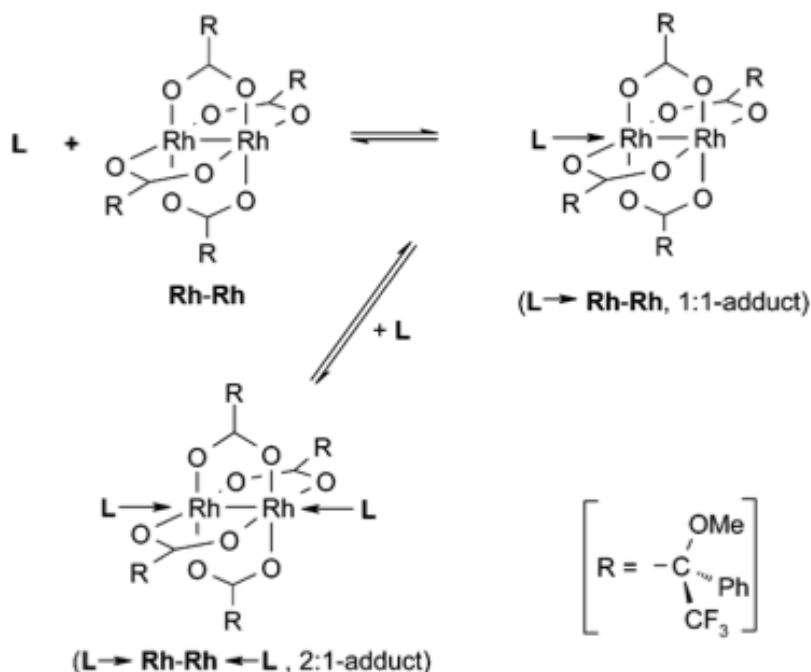


Figure 11. Adduct formation between ligand molecules (L) and dirhodium complex $\text{Rh}_2[(\text{R})\text{-MTPA}_4]$ (Rh-Rh; MTPA-H \equiv methoxytrifluoromethylphenylacetic acid = Mosher acid).¹²

Rozwadowski's research continues to imply that, although the $\text{Rh-Rh} \leftarrow \text{N} \equiv \text{C}$ should be linear, and the $\text{N} \equiv \text{C}$ complexes via its π -electron, $\text{Rh-Rh} \leftarrow \text{N} \equiv \text{C}$ is not linear. Because axial nitrile ligands have a tendency to form a dimer of dimers by bridging two Rh-Rh adducts, $\text{Rh-Rh} \leftarrow \text{N} \equiv \text{C}$ is nonlinear.¹² Hameed, who also studied $\text{Rh}_2[(\text{R})\text{-MTPA}_4]$, discovered that the R-N-C bond angle deviates from linearity (166° in $[\text{Rh}_2(\text{CH}_3\text{CN})_{10}]^{4+}$ cation), and bond angles of $[\text{Rh}(\text{CN})_6]^{4-}$ are nonlinear.¹³ If the axial $\text{C} \equiv \text{N}$ ligands deviate greatly from linearity, this suggests that σ -bonding is dominant over π -backbonding.

1.3 X-ray Crystallography Introduction

A crystal is composed of atoms arranged in a pattern that repeats periodically in three-dimensional space.¹⁴ A unit cell is the simplest repeating unit of atoms in a 3D crystal structure, which is always parallelepiped and defined by its

lattice points. Lattice points are where the atoms of a crystal vibrate. A unit cell containing n lattice points has a volume of n times the volume of a primitive cell in the same lattice. By describing the structure of the unit cell of a particular crystal, the arrangement of the atoms in a crystal can be predicted.

Max von Laue proposed that the periodic (repeating) structure of a crystal might be used to diffract X-rays in a similar way to how gratings generate diffraction patterns with visible light. His idea was based on the assumption that: crystals are periodic, and X-rays are waves. The X-ray wavelength is of the same order of magnitude as the repeat distance in crystals. William Lawrence Bragg discovered that the geometry of the crystal was analogous to the reflection of light by a plane mirror. This discovery generated the Bragg equation, which calculates the distance between planes of atoms in a crystal from the pattern of diffraction of X-rays of a known wavelength: $n\lambda = 2d \sin(\theta)$.¹⁴

During X-ray crystallography analysis, a crystal is mounted onto a goniometer loop on a magnetic holder, which is placed onto a goniometer and is immersed in X-rays of a specific wavelength (0.71075 Å). The crystal is rotated continuously about one of the unit cell axes, and the incident X-ray beam is normal to this axis.¹⁴ As the crystal is rotated, the atoms in a crystal structure absorb X-ray radiation and emit the radiation outward, creating both constructive and destructive interference, called diffraction. These rays of diffracted radiation are sent out in the different directions, and the constructive interference from diffracted beams creates a diffraction pattern on the photographic plate. The intensity of the diffraction patterns depends on the size of the crystal, the condition of the crystal, and the thermal vibrations in the crystal structure. From the angles of the X-ray beams and intensities determined by diffraction patterns, the 3D structure of the atoms of the crystal can be constructed. The angles of the diffraction beams also give insight on the specific details of the structure of the atoms, such as the distances of the bonds of the atoms.¹⁵

1.4 X-ray Characteristics

In order to determine the positions of the atoms within a unit cell, the atomic

structural parameters (temperature, thermal motion, partial occupancy of atomic sites, etc.) can be refined to produce more accurate measurements of the unit cell. Because an atom does not vibrate equally in all directions (anisotropically), it is difficult to pinpoint the exact location of an atom. Adjusting these parameters would result in a change of the values of the structure factors. The best set of parameters is that which will produce the most accurate values of interatomic distances and bond angles.¹⁴ The measure of correctness of a structure is given by the residual or R-value calculated by the following formula:

$$R = \frac{\sum |F_{\text{observed}} - F_{\text{calculated}}|}{\sum |F_{\text{observed}}|}$$

F is the structure factor, which is related to the intensity of the reflection. An R of 0.20 may indicate a correct structure, with the best possible values of the experimental atomic parameters; however, R should be considerably less than 0.20, and an R value of 0.10 or less implies that the results are probably very reliable. By refining the atomic parameters, a low R value of 0.10 should be obtained.¹⁴

“Residual” is the term used to describe a quantity remaining after another quantity has been subtracted. In crystallography, “residual” refers to the discrepancy index R. For example, when the calculated value of a variable is subtracted from the observed value, the difference is called a residual value. The goodness of fit indicator refers to the measure of the extent to which calculated model values of a set of quantities compare to the observed data values. The goodness of fit is indicated by the residual R-values, which should be low to indicate a reliable structure. Maximum peak in final difference map refers to the space where the probability of the electron density of the model is highest, and the minimum peak in the final difference map refers to the space of the lowest probability of finding the model’s electron density.¹⁶

To describe the unit cell, the symmetry of the unit cell can be classified by crystal systems and Bravais lattices. There are seven crystal systems and fourteen Bravais lattices; however, we will only focus on monoclinic and triclinic crystal

systems, as well as the C-centered and primitive Bravais lattices (see Figure 13). A system of reference points can be obtained by choosing a point in the unit cell, and all the points that are identical with this point constitute what is known as the lattice points. The lattice points have the same surroundings and are identical relatively in position to one another in the unit cell.¹⁴

A crystal is monoclinic if the given unit cell has $\alpha=90^\circ$ and $\gamma=90^\circ$, with no other conditions on the dimensions and shape of the cell. The C-centered monoclinic unit cell has a centering on the C face, which is the face of the unit cell bound by the a and b axes. A point in the center of a face is shared by two unit cells, therefore the C-centered unit cell has two lattice points. A unit cell with lattice points only at the corners is a primitive unit cell. In a triclinic system, no symmetry restrictions occur because the unit cell “cube” is not symmetrical, and therefore only a primitive cell be used.¹⁴

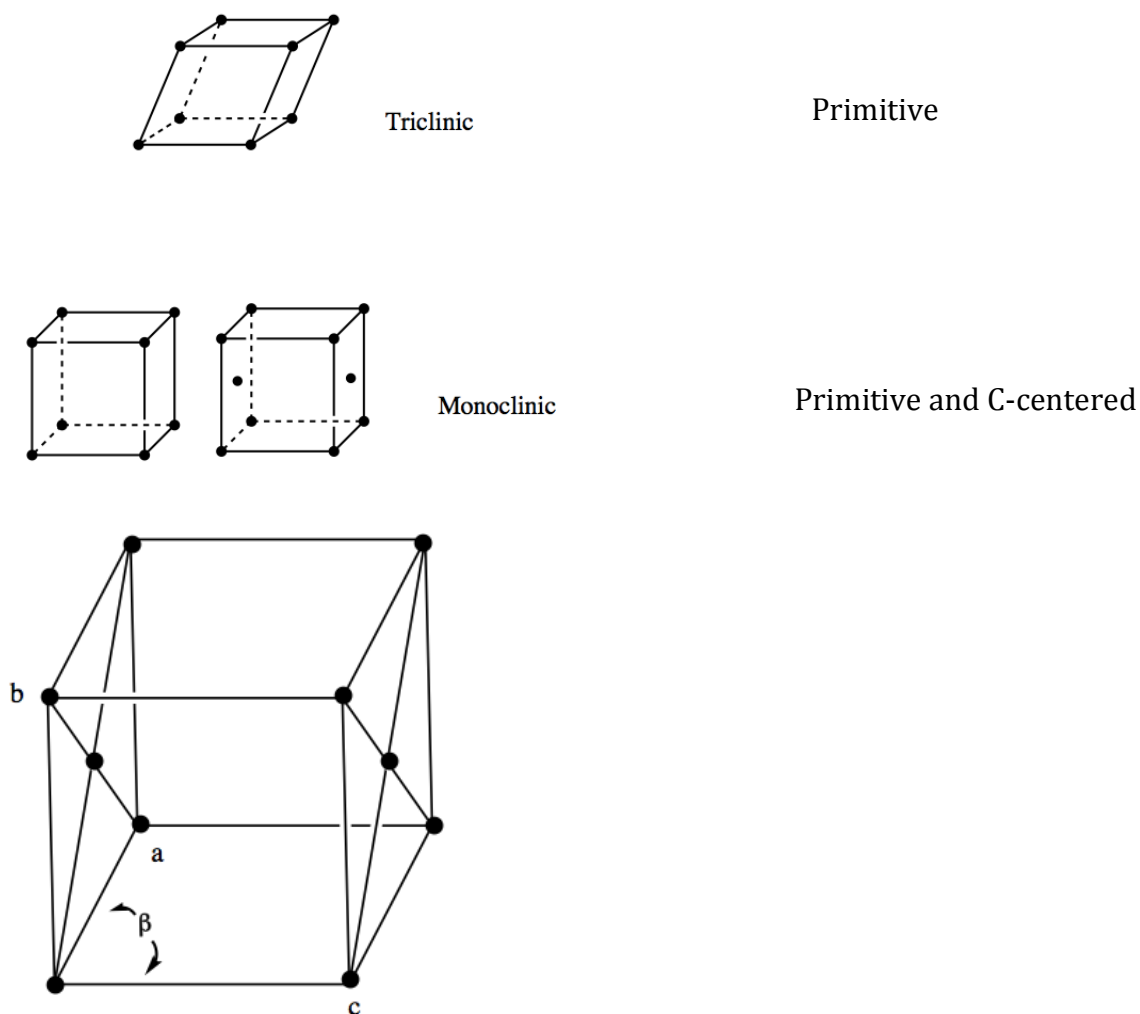


Figure 12. Bravais lattices of triclinic and monoclinic structures (above); C-centered monoclinic unit cell (below). Lattice points are at $0,0,0$ and at $\frac{1}{2},\frac{1}{2},0$; $\alpha=\gamma=90^\circ$.

The bond lengths, bond angles, and torsion angles are all properties of molecular geometry. The bond length of two atoms is the average distance between the two nuclei of the atoms, and the strength and bond dissociation energy are inversely correlated to the bond length. Bond length of the $C\equiv N$ functional group is significant because it gives insight into σ -bonding and π -backbonding. The bond lengths of interest are Rh-Rh and $C\equiv N$ functional group's bond lengths. The bond angle is measured by the angle formed by three atoms bonded together. The bond angle of C-N-Rh bears significance because of its ability to influence π -backbonding. The torsion angle refers to the degree to which four atoms bonded together twist,

and the torsion angle is varied by the distance and orientation between the first and fourth atoms. When the fourth atom is orientation to where it eclipses the first atom, the angle is 0° , but when it is in the opposite position, the angle is 180° . The torsion angles of N-Rh-Rh-O and N-Rh-Rh-N are of interest because they would give some insight as to whether σ -bonding or π -backbonding is dominant.

2. Methods

2.1 Synthesis of $[\text{Rh}_2(\text{NPhCOCH}_3)_4]$

The first isolation of the 2,2-*trans* $[\text{Rh}_2(\text{NPhCOCH}_3)_4]$ isomer was performed by Eagle and co-workers using a Soxhlet extractor to react $[\text{Rh}_2(\text{COOCH}_3)_4]$ with an excess of *N*-phenylacetamide, reflux condenser, and round bottom flask under nitrogen gas, which afterwards, was separated by flash column chromatography (medium pressure liquid chromatography). A mixture of $[\text{Rh}_2(\text{COOCH}_3)_4]$ and *N*-phenylacetamide in chlorobenzene was refluxed for over 7 days via Soxhlet extractor. The thimble in the soxhlet extractor contained an oven-dried mixture of sodium carbonate and sand, which was replaced every 24 hours. Three tetrakis(*N*-phenylacetamidate) dirhodium(II) isomers, the 2,2-*trans*, 2,2-*cis*, and 3,1 isomers, were then separated through flash column chromatography on silica gel.¹ This method was reproduced for this research in the isolation of the 2,2-*trans* tetrakis(*N*-phenylacetamide) dirhodium(II) isomer for this synthesis.

Synthesizing the tetrakis(*N*-phenylacetamide) dirhodium(II) starting compound required using a Soxhlet extractor and reflux condenser system. *N*-phenylacetamide and $[\text{Rh}_2(\text{COOCH}_3)_4]$ were added in over a 10:1 excess. In a 250 mL round bottom flask, 0.312 g (0.843 mmol) of $[\text{Rh}_2(\text{COOCH}_3)_4]$ and 3.72 g (372. mmol) *N*-phenylacetamide were dissolved in chlorobenzene, and the reaction solution turned bright green. The Soxhlet extractor was attached to the round bottom flask. The mixture inside the thimble was about 10 g of coarse sand and about 10 g of sodium carbonate, with a small layer of sand on top of the mixture until the thimble was about $\frac{3}{4}$ full. Eight of these thimbles were oven dried for three days at 125°C prior to use. The Soxhlet extractor was fitted with a condenser, and

the round bottom flask was heated via a curved heating mantle for 7 days. Nitrogen gas was blown through a three-way valve at the top of the condenser into a bubbler, creating a blanket of nitrogen gas for the reflux condenser system. The Soxhlet extractor and round bottom flask were wrapped with a layer of fiberglass and wool, with a layer of aluminum foil on top for insulation. Every 24 hours, the heating mantle was turned off and the reaction system was allowed to cool under N₂ gas; this was done so that the thimble could be replaced with a fresh thimble by using a pair of long tongs. After replacing the thimble, the heating mantle was turned on again, and the reaction flask was monitored to ensure the solution in the flask did not boil over before left to continue refluxing. After seven days, the reaction mixture was cooled under N₂ gas. Since sand from one of the thimbles was found in the main compartment of the Soxhlet extractor and reaction flask, Na₂CO₃ potentially contaminated the reaction flask.¹⁷ Gravity filtration was used to remove the sand and any precipitated *N*-phenylacetamide, and 2.286 g of the crude reaction mixture was recovered in another round bottom flask. The remaining solvent was removed using a rotary evaporation apparatus in combination with a water vacuum pump for several hours over the course of 6 days. Some of the chlorobenzene was bypassing the primary trap of the rotary evaporation, escaping the secondary trap of a 500 mL Erlenmeyer flask in an ice bath, and coming out of the water vacuum pump. The water vacuum pump was replaced with a water aspirator. The remaining green, crude reaction mixture containing *N*-phenylacetamide and [Rh₂(NPhCOCH₃)₄] solid was capped and stored.¹⁷

After about a month of storage, the crude [Rh₂(NPhCOCH₃)₄] compound was then separated into four fractions by flash column chromatography for six days. The first layer in the condenser on the bottom was a small layer of glass wool, then a 1" layer of sand on top of the first layer, 7" layer of silica gel, and then 1" layer of sand on top. The reaction mixture containing [Rh₂(NPhCOCH₃)₄] was dissolved in 6 mL of dichloromethane and was added into the column gradually with a pipette. Because the crude [Rh₂(NPhCOCH₃)₄] was colored, the separate fractions were also colored and could be visually seen moving through the column; therefore each colored band was defined as a separate fraction. The first fraction was eluted with a 20:80

mixture of ethyl acetate and hexane as a green band. The next fraction was eluted with a 30:70 mixture of ethyl acetate and hexane, and was purple in color. The third and fourth fractions were eluted with a 50:50 mixture of ethyl acetate and hexane, and both were brownish black in color. The amount of ethyl acetate in the eluent was increased until 100% to ensure there were not any remaining bands. The fractions were collected into Erlenmeyer flasks and were labeled with their corresponding fraction numbers. Each different band was considered as a "fraction," and was checked by spotting with thin layer chromatography (TLC). A drop of each fraction was added with a capillary tube onto a TLC plate coated with adsorbent silica gel, and the TLC plate was placed into a chamber made by covering a 250 mL beaker containing a 4 mL 50:50 solvent mixture of hexane and ethyl acetate with aluminum foil. Once the solvent mixture was drawn up the plate onto the solvent front, the TLC plate was removed, and fractions whose TLC spots were similar were combined together in the same flask. Each separated band or fraction of $[\text{Rh}_2(\text{NPhCOCH}_3)_4]$ had about five 250 mL Erlenmeyer flasks worth of solution, and were combined during rotary evaporation. Each isolated fraction was rotary evaporated in combination with a vacuum pump for more than a total of 7 hours each to remove any solvent. Next, each fraction was then heated in a vacuum oven at 125°C to further remove any remaining solvent. Each fraction, without solvent, was stored as solids separately in 1-dram vials. To determine which isomer was contained in each vial, ^1H NMR was used. The NMR Fraction I was green, Fraction II was purple, and Fractions III and IV were black. However, after adding CDCl_3 , an NMR solvent, Fraction II formed a green solution, which was the same color as Fraction I in solution, prior to being subjected to a vacuum. Fraction I was the 2,2-*trans* $[\text{Rh}_2(\text{NPhCOCH}_3)_4]$ isomer and was utilized for this research, and both Fraction I and Fraction II were identified by ^1H NMR spectroscopy. However, the subsequent Fractions III and IV did not contain identifiable Rh_2 species. After being dried with the vacuum pump, Fractions III and IV were black and had a melted appearance; instead of having a powdery texture, they had the appearance of a solid that had melted, then cooled and hardened into a black clump. After ^1H NMR analysis of Fractions III and IV, the peaks were determined to not correspond to the

expected peaks, and thus Fractions III and IV were claimed to have been decomposed. Several possible reasons why the decomposition could have occurred include: 1) the crude $[\text{Rh}_2(\text{NPhCOCH}_3)_4]$ was left sitting for about a month; 2) the crude $[\text{Rh}_2(\text{NPhCOCH}_3)_4]$ was separated into fractions through flash column chromatography over six days; 3) the most likely cause: Na_2CO_3 contaminated the solution and reacted with the $[\text{Rh}_2(\text{COOCH}_3)_4]$, or some of the $[\text{Rh}_2(\text{NPhCOCH}_3)_4]$. Because the some of the sand was found outside the thimble and in the condenser, the Na_2CO_3 probably reacted with the crude $[\text{Rh}_2(\text{COOCH}_3)_4]$ to displace the *N*-phenylacetamide.

The weight of the non-decomposed the fractions was 46 mg for Fraction I and 132 mg for Fraction II. The actual yield for the synthesis of $[\text{Rh}_2(\text{NPhCOCH}_3)_4]$ was 0.178 g; the theoretical yield was calculated as 0.524 g; therefore, the percent yield was 34.0%. This low yield was probably a result of the decomposition of Fractions III and IV, as their weights were not included in the actual yield.

The NMR solvent chosen was deuterated chloroform (CDCl_3). Although the proton from CHCl_3 in the CDCl_3 solvent overlaps proton peaks in the phenyl region, most compounds dissolve in CDCl_3 , and CDCl_3 had less of a chance of reacting with or changing the sample being analyzed (CDCl_3 will not exchange its deuterium with the protons in the sample molecule). For example, the carbonyl group in DMSO, another NMR solvent, could potentially displace nitrile ligands from the axial site of the dirhodium complex. Some deuterated solvents are prepared by catalytic exchange of protonated solvent with deuterium oxide, and then purified by distillation; residual water is a result of H_2O in equilibrium exchange with D_2O .¹⁸ The peaks around 1.60 ppm represent a solvent impurity (H_2O) from the CDCl_3 .

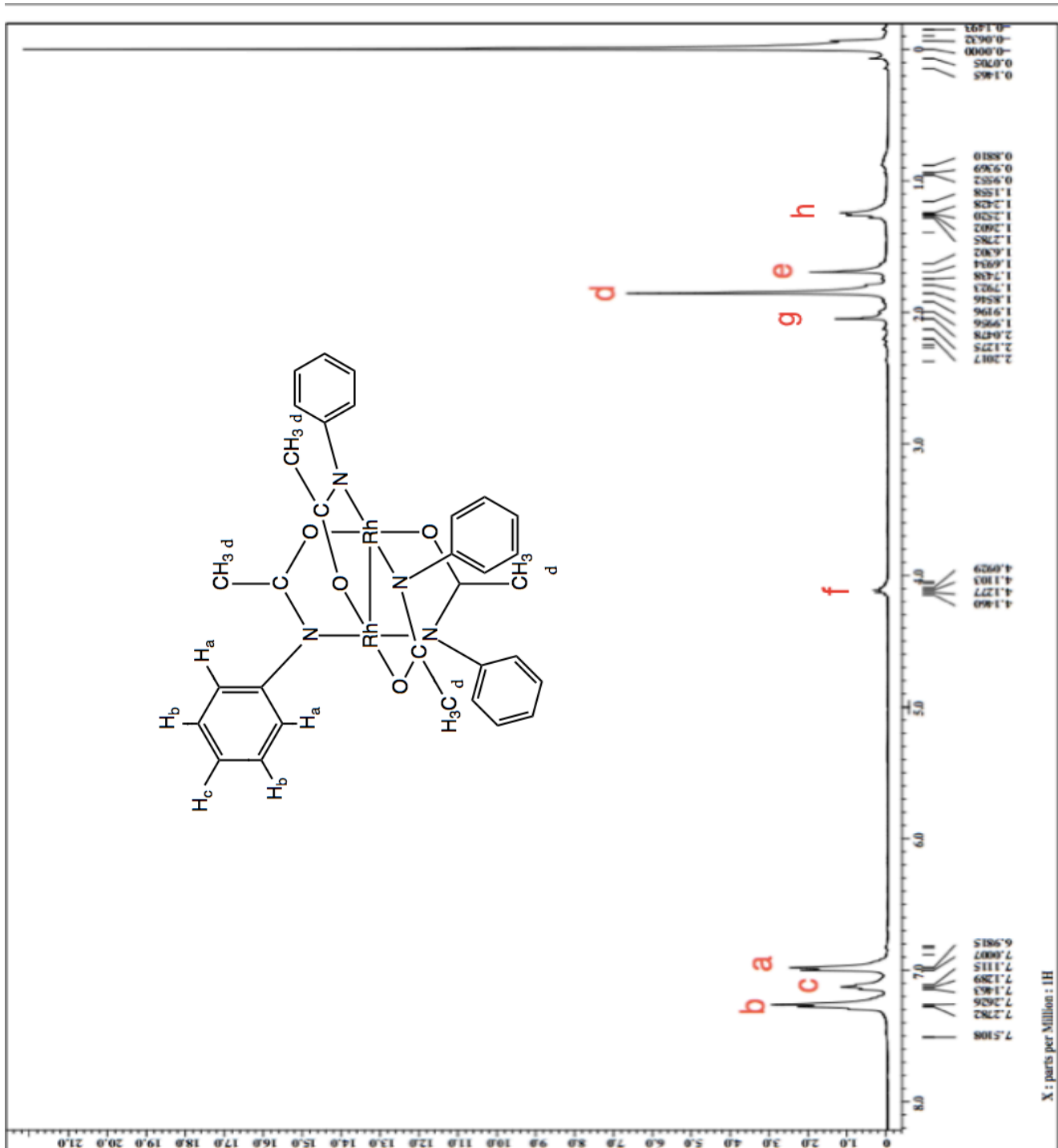


Figure 13. ¹H NMR of Fraction I.

Fraction I	
Peak	(ppm)
a	6.982
b	7.263
c	7.129
d	1.855
e	1.693
f	4.110
g	2.048
h	1.260

Table 2. ^1H NMR of Fraction I.

Because the solutions were dilute, the TMS peak in the ^1H NMR spectra of Fractions I-IV is much higher compared to the other peaks. For Fraction I, the triplet peaks at about 7.12 ppm represents the H attached to the benzene rings of the *N*-phenylacetamide, as shown in Figure 14.

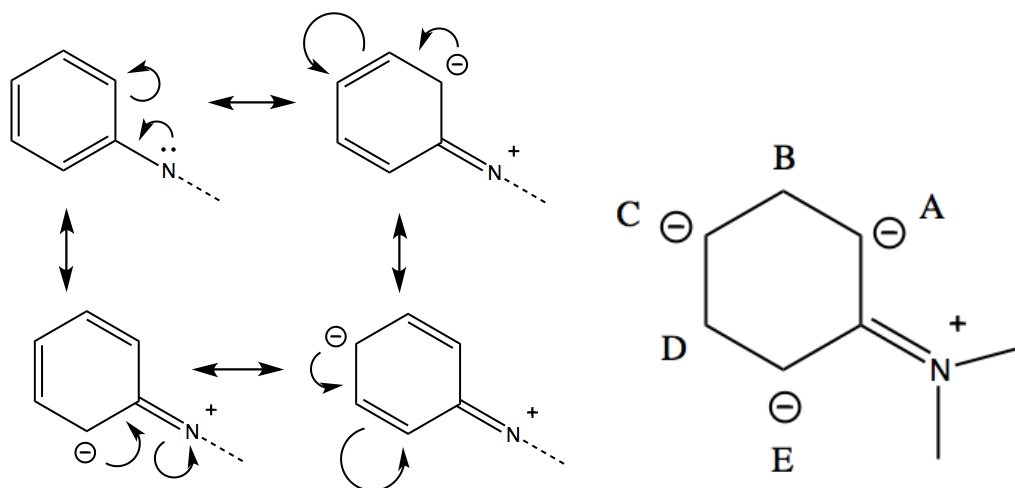


Figure 14. Resonance of benzene ring attached *N*-phenylacetamide (left), proton locations on benzene ring attached *N*-phenylacetamide (right)

Due to the resonance of the benzene ring and the lone pair of electrons (e^-) from the nitrogen, the protons in positions labeled A, C, and E in Figure 14 shown above in the ortho and para positions are more shielded, and therefore appear more

upfield in the ^1H NMR graph (6.982 ppm, 7.129 ppm, and 1.693 ppm.) Since there are twice as many protons H_a from Fraction I than H_c , the taller, upfield peak in the triplet represents the H_a proton labeled in the structure from Figure 13 on the NMR spectrum at 6.982 ppm. Since H_b is not as shielded as H_a or H_c , its peak will appear most downfield from H_a and H_c at 7.263 ppm. Even though the nitrogen is an electron withdrawing species, the Rh is a metal and is an electron donor. The Rh donates electrons to the nitrogen, and the H_a protons are shielded, and thus the peaks appear more upfield.

The H_a proton is split by H_b ; therefore the H_a is shown as a doublet. The H_b proton is split by both H_a and H_c ; and therefore H_b is shown as a triplet. The 7.26 ppm peak is an overlap of the proton from CHCl_3 in the CDCl_3 solvent, and this peak masks the H_b triplet, making it appear as a doublet instead. The H_c proton is split by H_b ; therefore H_c should be a doublet, but appears as a triplet. This may have occurred due to an overlapping peak from impurity, or through long distance coupling from non-adjacent protons, such as the H_a protons. The peak at d is in the methyl region of the NMR spectrum. All four of the CH_3 groups produced one singlet at peak d. The solvent impurities at f, g, e, and h are solvents from synthesis or column chromatography that weren't completely removed. The f and g peaks are from ethyl acetate; the e peak is from H_2O in the CDCl_3 ; the h peak is from hexane.

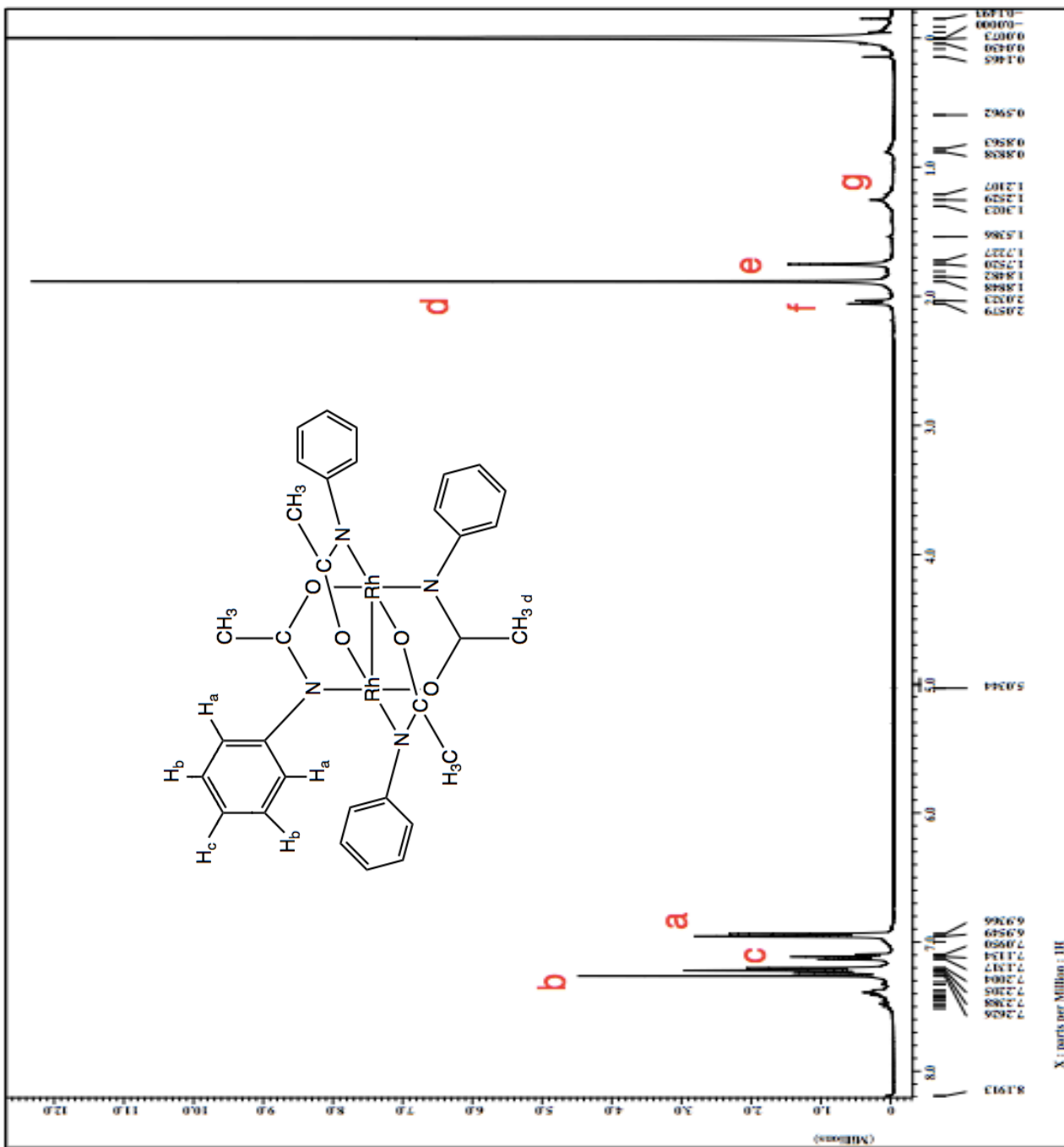


Figure 15. ^1H NMR of Fraction II.

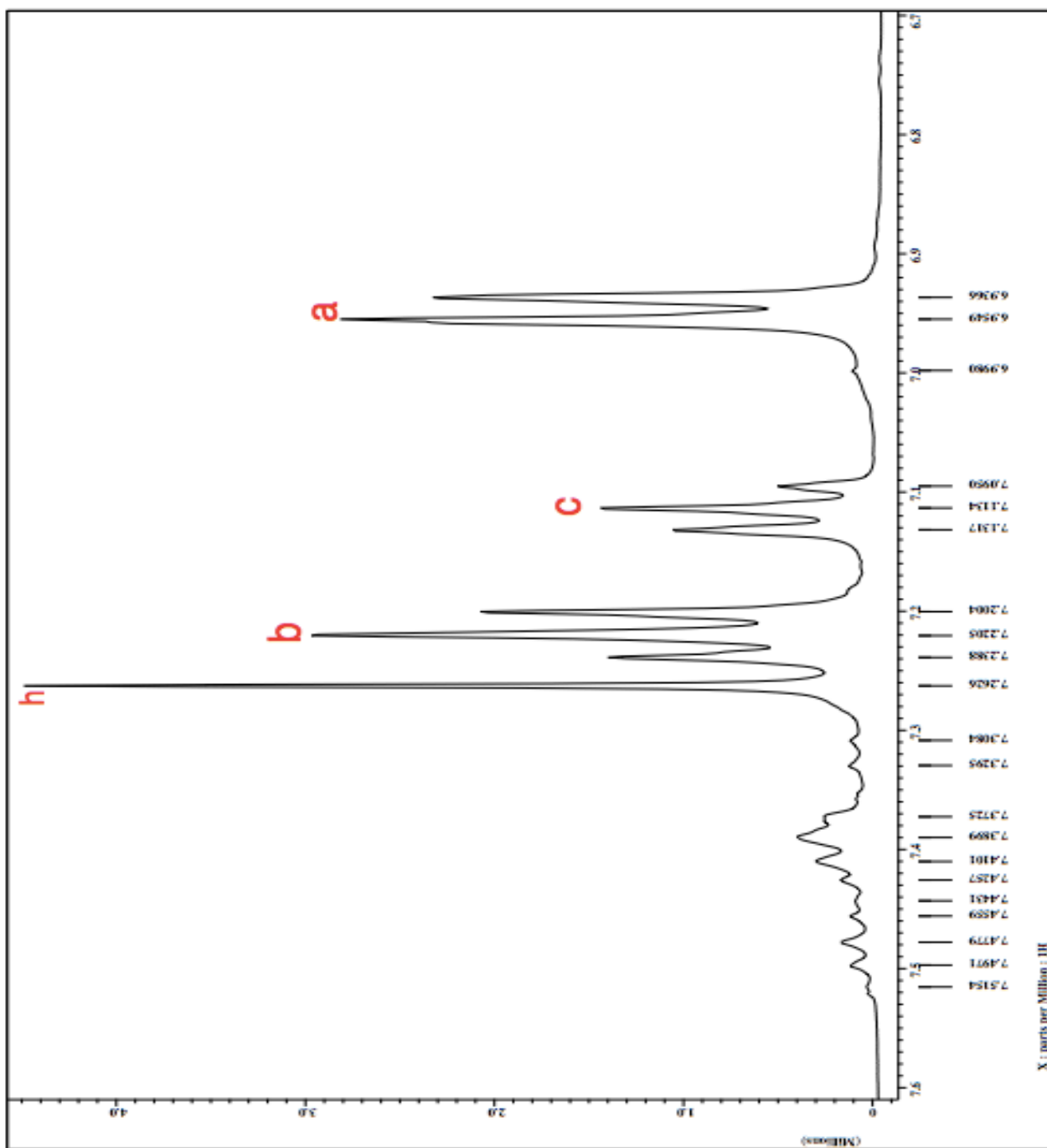


Figure 16. ^1H NMR of Fraction II from 6.7 to 7.6 ppm, expanded to show the region.

Fraction II	
Peak	(ppm)
a	6.955
b	7.221
c	7.113
d	1.885
e	1.693
f	2.058
g	1.253
h	7.263

Table 3. ^1H NMR of Fraction II.

The ^1H NMR spectrum for Fraction II was similar to the ^1H NMR spectrum of Fraction I. For the peaks in the phenyl region around (7.0 ppm to 7.6 ppm) those peaks represent the protons attached to the benzene rings of the *N*-phenylacetamide, as shown above. The 7.26 ppm peak, labeled h, is an overlap of the proton from CHCl_3 in the CDCl_3 solvent. Both Fraction I and Fraction II were compared with literature data to confirm that Fraction I was the *2,2-trans* tetrakis(*N*-phenylacetamidate) dirhodium(II) and Fraction II was the *2,2-cis* tetrakis(*N*-phenylacetamidate) dirhodium(II).¹⁹

The H_a proton is split by H_b ; therefore the H_a is shown as a doublet. The H_b proton is split by both H_a and H_c ; and therefore H_b is shown as a triplet. The 7.26 ppm peak is an overlap of the proton from CHCl_3 in the CDCl_3 solvent, and this peak masks the H_b triplet, making it appear as a doublet instead. The H_c proton is split by H_b ; therefore H_c should be a doublet, but appears as a triplet. This may have occurred due to an overlapping peak from an impurity, or through long distance coupling from non-adjacent protons, such as the H_a protons. The solvent impurities at f, g, and e are solvents from synthesis and column chromatography that weren't completely removed via vacuum procedures. The f peak is from ethyl acetate; the e peak is from H_2O in the CDCl_3 ; the g peak is from hexane.

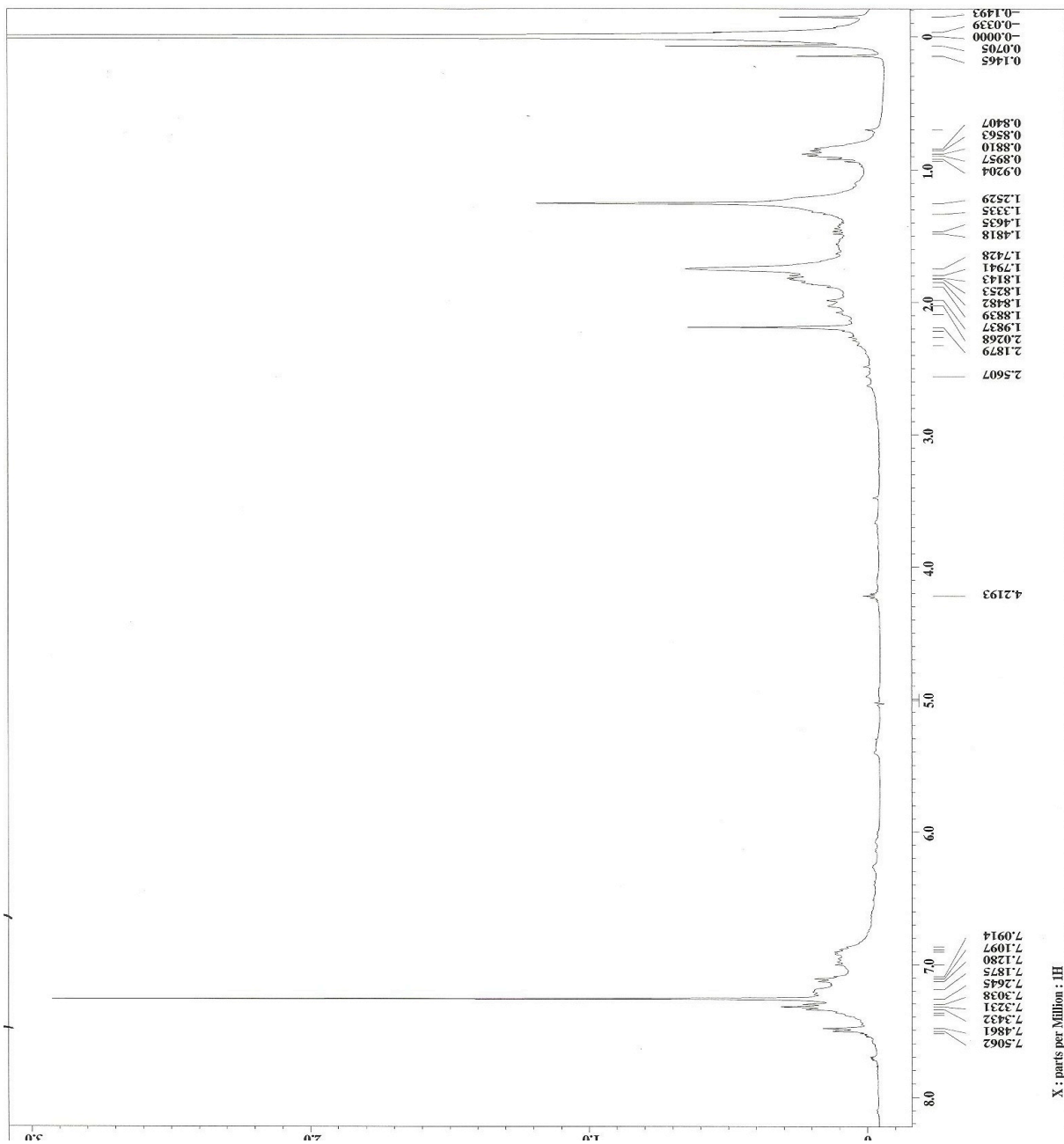


Figure 17. ¹H NMR of Fraction III

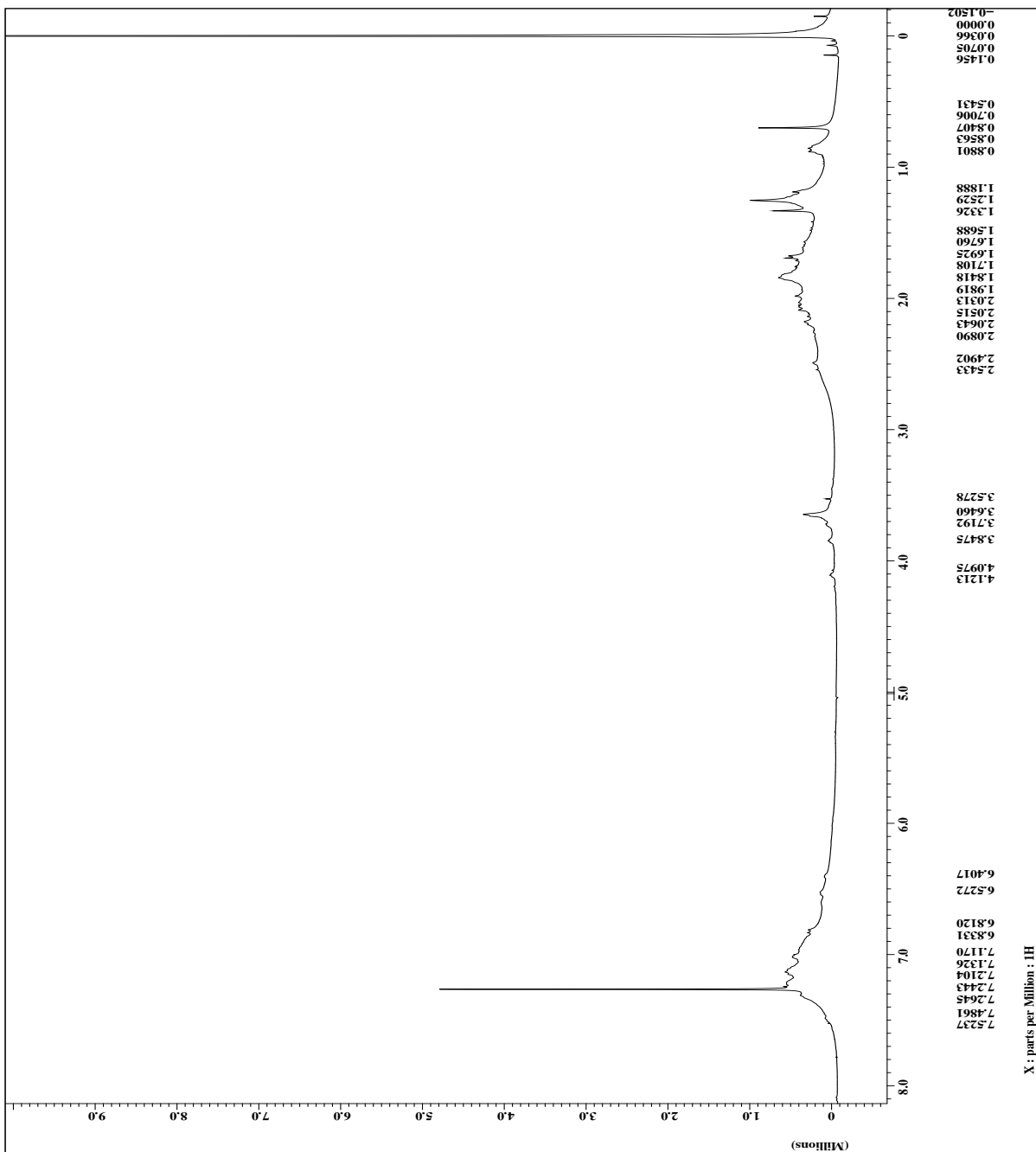


Figure 18. ¹H NMR of Fraction IV

The ¹H NMR peaks from Fractions III and IV do not clearly represent any protons from *N*-phenylacetamide. There are not many protons of distinctness, but

the peaks of solvents can be identified. The distinct peak at 7.26 ppm is from the proton from CHCl_3 in the CDCl_3 solvent. In Figure 17, the 2.03 ppm peak is from ethyl acetate. The peak at 0.88 ppm is from hexane. The peak at 1.25 ppm is a overlap from both hexane and ethyl acetate. The peak at 1.81 ppm is from the methyl group (CH_3) from $[\text{Rh}_2(\text{NPhCOCH}_3)_4]$. In Figure 18, the 1.25 ppm peak is from ethyl acetate and hexane. The peak at 0.84 ppm is from hexane.

2.2 Synthesis of 2,2-*trans* $[\text{Rh}_2(\text{NPhCOCH}_3)_4]$ • nitriles

For this study, we chose three axial ligands: benzonitrile, o-tolunitrile, and m-tolunitrile. First, 0.02 g of 2,2-*trans* $[\text{Rh}_2(\text{NPhCOCH}_3)_4]$ was dissolved in 5 mL of dichloromethane for each synthesis of 2,2-*trans* $[\text{Rh}_2(\text{NPhCOCH}_3)_4]$ and nitrile ligand, and the amount of nitrile that gave a 2:1 molar ratio of nitrile to 2,2-*trans* $[\text{Rh}_2(\text{NPhCOCH}_3)_4]$ was added by using a gas tight syringe to a reaction vial. (Glassware was rinsed with acetone and dried in an oven 120°C for a day prior to use.) Different sets of solvents were used in vapor diffusion for crystallization, including: ethyl acetate, ethanol, acetone, toluene, methanol, water, acetonitrile, hexane, and toluene.

1. Benzonitrile adduct of 2,2-*trans* $[\text{Rh}_2(\text{NPhCOCH}_3)_4]$

0.02 g (0.028 mmol) of 2,2-*trans* $[\text{Rh}_2(\text{NPhCOCH}_3)_4]$ were dissolved in 5 mL of dichloromethane in a 50 mL round bottom flask and clamped to a stand. Then, 6.31 μL (0.061 mmol) of benzonitrile were added by using gas tight syringe. The solution turned from green to blue.

2. o-tolunitrile adduct of 2,2-*trans* $[\text{Rh}_2(\text{NPhCOCH}_3)_4]$

0.02 g (0.028 mmol) of 2,2-*trans* $[\text{Rh}_2(\text{NPhCOCH}_3)_4]$ were dissolved in 5 mL of dichloromethane in a 50 mL round bottom flask and clamped to a stand. Then, 6.38 μL (0.054 mmol) of o-tolunitrile were added by using gas tight syringe. The solution turned from green to blue.

3. m-tolunitrile adduct of 2,2-*trans* $[\text{Rh}_2(\text{NPhCOCH}_3)_4]$

0.02 g (0.028 mmol) of 2,2-*trans* $[\text{Rh}_2(\text{NPhCOCH}_3)_4]$ were dissolved in 5 mL of dichloromethane in a 50 mL round bottom flask and clamped to a

stand. Then, 6.50 μL (0.054 mmol) of m-tolunitrile were added by using gas tight syringe. The solution turned from green to blue.

2.3 Crystallization process of 2,2-*trans* $[\text{Rh}_2(\text{NPhCOCH}_3)_4] \cdot \text{nitriles}$

1. Benzonitrile adduct of 2,2-*trans* $[\text{Rh}_2(\text{NPhCOCH}_3)_4]$

The reaction solution was divided into 10 vials (seven of them were 1/2-dram, three were 2-dram). Seven 1/2-dram vials were used for vapor diffusion, and the other three 2-dram vials were used for liquid diffusion. To perform the vapor diffusion, the 1/2-dram vials were placed into 6-dram vials each containing a different solvent. The seven solvents used in the 6-dram vials were ethyl acetate, ethanol, acetone, toluene, methanol, water, and acetonitrile. The 6-dram vials containing the 1/2-dram vials and solvents were capped and left to crystallize for a week. If disturbed, the product reaction vial (the 1/2-dram vial) was centered inside the larger vial with tweezers. This was done to prevent the solvent in the 6-dram vial from entering the 1/2-dram vial via capillary action. To perform liquid diffusion, 2-dram vials were used with three solvents: acetone, toluene, and ethanol. To the first vial, acetone was carefully added dropwise; to the second vial, toluene was added; and lastly, ethanol was added to the third vial. However, even after a month of waiting for crystals to form, the contents in the vial remained in solution.

2. o-tolunitrile adduct of 2,2-*trans* $[\text{Rh}_2(\text{NPhCOCH}_3)_4]$

The process for vapor diffusion of the o-tolunitrile ligand was similar to the benzonitrile. Liquid diffusion was not performed because of the previous unsuccessfulness of crystal growth via liquid diffusion during the 2,2-*trans* $[\text{Rh}_2(\text{NPhCOCH}_3)_4] \cdot \text{benzonitrile}$ trial (see 2.4.1). The reaction solution was divided into 7 vials (1/2-dram). To perform the vapor diffusion, the 1/2-dram vials were placed into 6-dram vials each containing a different solvent. The seven solvents used in the 6-dram vials were ethyl acetate,

ethanol, acetone, toluene, methanol, water, and acetonitrile. The solutions in the vials were left to crystallize for a week.

3. m-tolunitrile adduct of 2,2-*trans* [Rh₂(NPhCOCH₃)₄]

The process for vapor diffusion of the m-tolunitrile ligand was the same as the o-tolunitrile. The solvents used were the same as the ones used for the o-tolunitrile series.

After crystals were grown, several crystals were taken for X-ray crystallography analysis. However, after three trials of unsuccessfully solving the crystal structure, it was concluded that the crystal samples were too thin for analysis. The 2,2-*trans* [Rh₂(NPhCOCH₃)₄]•m-tolunitrile crystals were regrown to produce thicker crystals. In this second and third m-tolunitrile trials, 0.02 g of 2,2-*trans*-[Rh₂(NPhCOCH₃)₄] were dissolved in 4 mL of dichloromethane in a 50 mL round bottom flask and clamped to a stand. Then, 6.50 μL of m-tolunitrile were added by using gas tight syringe. Six solvents were used in the 6-dram outer vial: ethyl acetate, ethanol, methanol, water, and hexane. The same vapor diffusion procedure was performed as the first 2,2-*trans* [Rh₂(NPhCOCH₃)₄]•m-tolunitrile trial. But once again, the crystals were still long and thin, and X-ray diffraction was difficult due to the crystal dimensions.

A different approach to crystal growth was taken. To the solid crystals, five drops of acetone were added. Five drops of acetone is equal to approximately 250.0 μL, which is much greater than the 6.50 μL of m-tolunitrile, which was added previously. The ½ dram vials were re-submerged in the 6-dram vials, which contained liquids for vapor diffusion. After one week, this method produced some crystals that were X-ray quality.

2.4 X-ray Crystallography

To prepare a crystal sample for analysis, a sewing needle was used to apply a small amount of STP onto a microscope slide. Viable crystals were separated from the reaction vials using the same needle and viewed under a microscope. After

analyzing potential crystals, a single crystal was isolated and mounted onto a mitogen loop via sewing needle to be placed inside the X-ray diffractometer. Using the Rigaku Mercury375R/M CCD (XtaLAB mini) diffractometer, the spatial arrangement of atoms in the molecules of the crystal was analyzed.

3. Results and Discussion

3.1 ^1H NMR:

- 3.11: benzonitrile
- 3.12: 2,2-*trans* $[\text{Rh}_2(\text{NPhCOCH}_3)_4] \cdot 2\text{NC}(\text{C}_6\text{H}_4)$
- 3.13: o-tolunitrile
- 3.14: 2,2-*trans* $[\text{Rh}_2(\text{NPhCOCH}_3)_4] \cdot 2 \text{o-NC}(\{2\text{-CH}_3\}\text{C}_6\text{H}_4)$
- 3.15: m-tolunitrile
- 3.16: 2,2-*trans* $[\text{Rh}_2(\text{NPhCOCH}_3)_4] \cdot \text{m-NC}(\{3\text{-CH}_3\}\text{C}_6\text{H}_4)$

For the following ^1H NMR (Nuclear Magnetic Resonance) discussions, the term “deshielded” refers to a peak shift downfield, to the left of the NMR spectrum. “Shielded” protons are protons that have shifted upfield, to the right of the NMR spectrum. The NMR instrument used was the 400 MHz JEOL NMR.

3.11 Benzonitrile

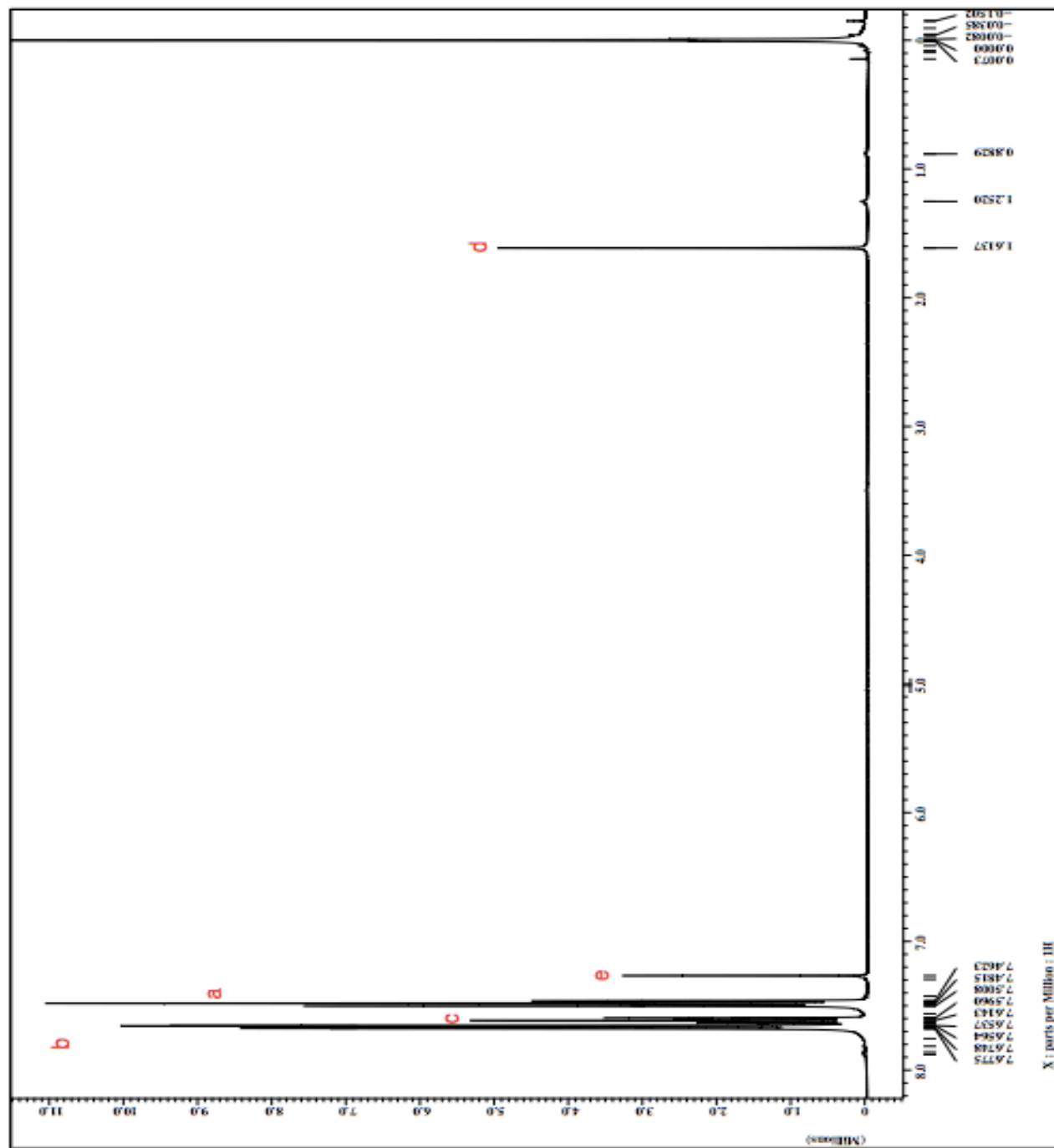


Figure 19. ^1H NMR of benzonitrile from 0-8 ppm.

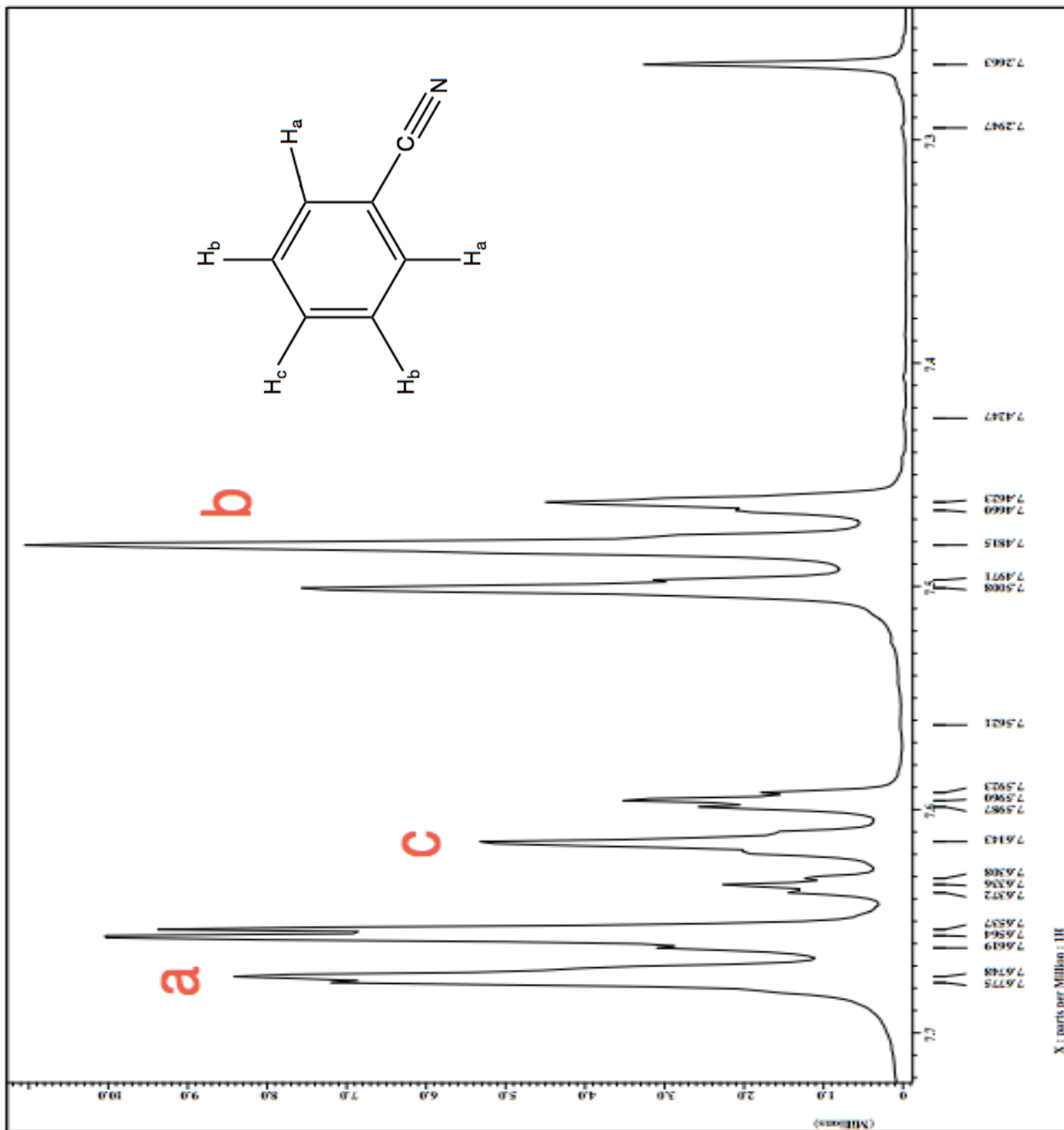


Figure 20. ^1H NMR of benzonitrile from 7.2-7.7 ppm, expanded to show the region.

Phenyl peaks (ppm)
7.678
7.675
7.656
7.654
7.614
7.596
7.501
7.482
7.462
7.266

Table 4. Benzonitrile phenyl protons. See Figure 20.

The protons in the ortho and para positions (H_a and H_c) to the $C\equiv N$ functional group in benzonitrile are the most deshielded due to inductive and resonance effects. The C in the $C\equiv N$ functional group is electron deficient and deshields the hydrogens closest to it (H_a). The H_a protons (7.656 ppm) in the ortho position are the most deshielded by the e^- donated by the nitrogen, and thus appear more upfield. The H_a protons are split by H_b and appear as doublet. The H_c protons (7.614 ppm) are split by both H_b and H_a , and thus appear as a triplet. The H_b protons (7.482 ppm) are split by both H_c and H_a , and thus also appear as a triplet. Since there are twice as many H_a and H_b , the a and b peaks are longer than the c peaks. The d peak at 1.61 ppm is a solvent impurity, (H_2O from the $CDCl_3$.) The 7.26 ppm peak (peak e) is the proton from $CHCl_3$ in the $CDCl_3$ solvent (see Figure 19).

3.12: 2,2-*trans* [Rh₂(NPhCOCH₃)₄]• 2NC(C₆H₄)

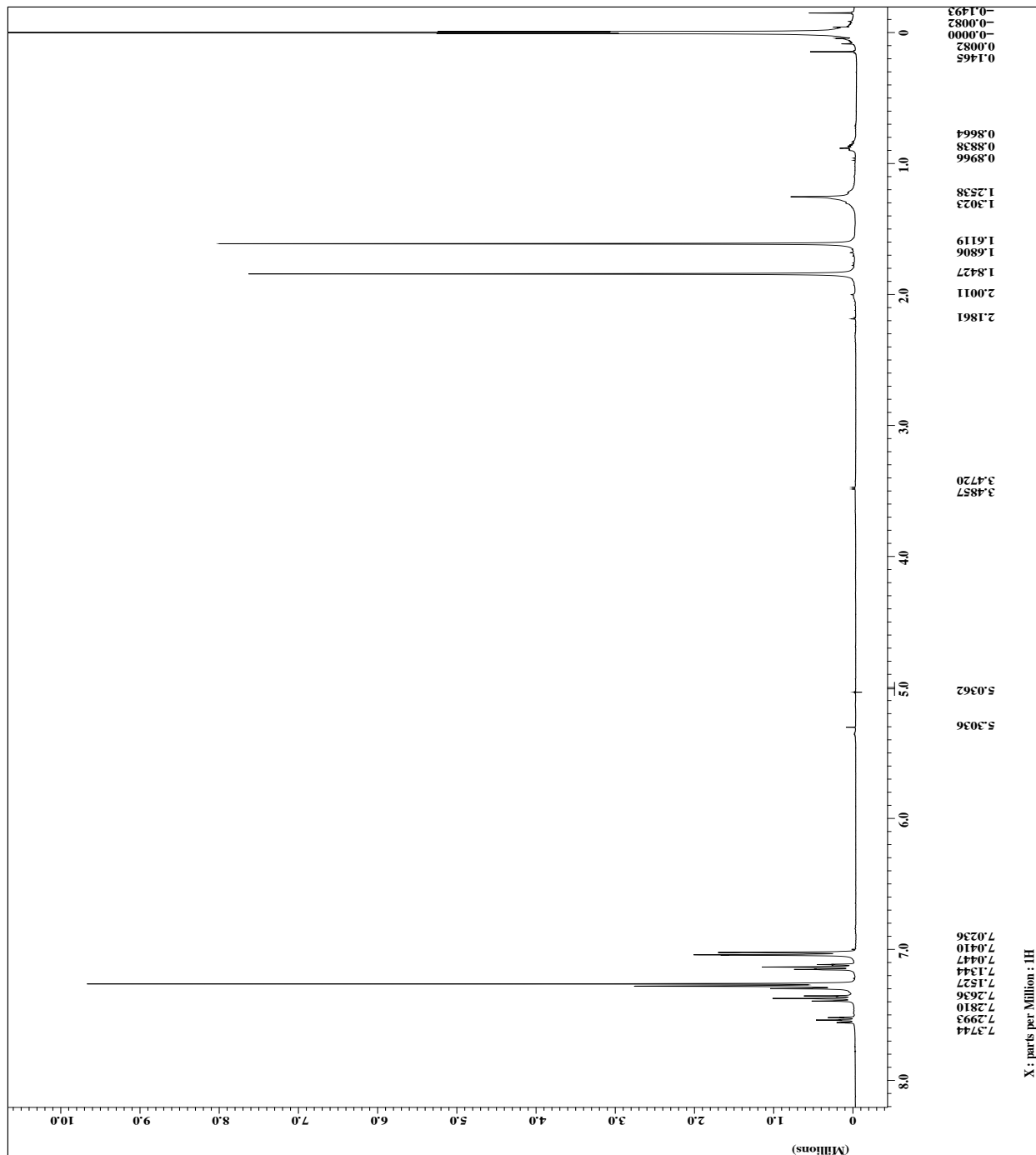


Figure 21. ¹H NMR of 2,2-*trans* [Rh₂(NPhCOCH₃)₄]• 2NC(C₆H₄) from 0.0-8.0 ppm.

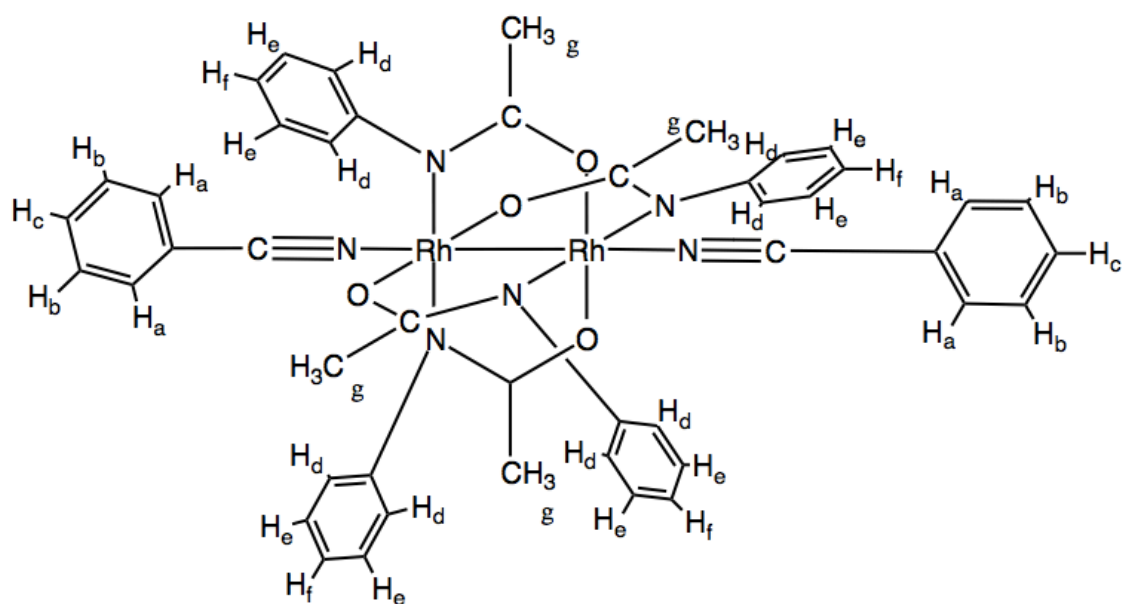


Figure 22. Proton labels for $2,2\text{-trans} [\text{Rh}_2(\text{NPhCOCH}_3)_4] \cdot 2\text{NC}(\text{C}_6\text{H}_4)$.

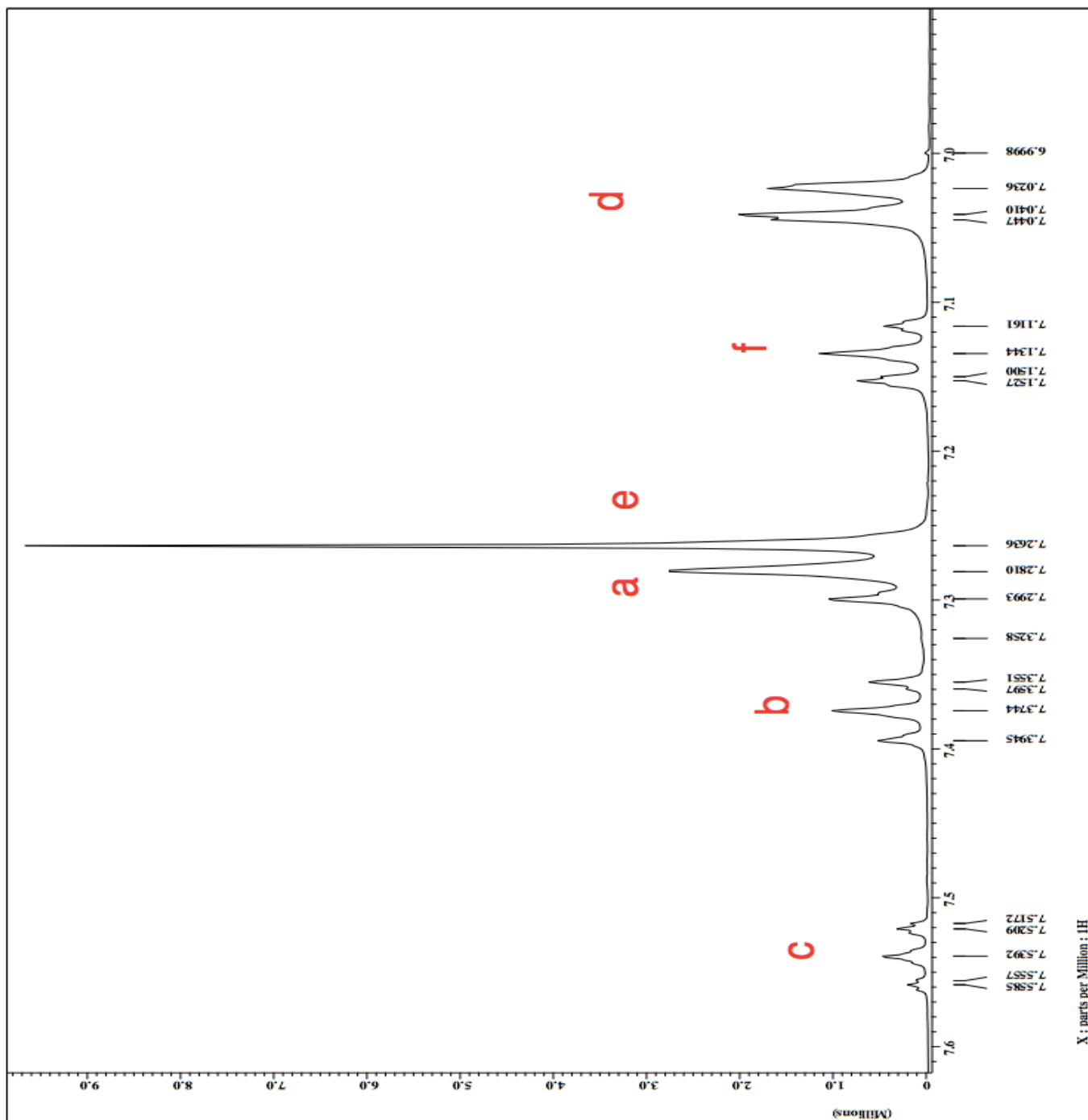


Figure 23. ^1H NMR of 2,2-*trans* $[\text{Rh}_2(\text{NPhCOCH}_3)_4] \cdot 2\text{NC}(\text{C}_6\text{H}_4)$ from 6.0-7.6 ppm.

The rhodium atom, because it is a metal bound to the $\text{C}\equiv\text{N}$ functional group, manipulates the $\text{C}\equiv\text{N}$ functional group's properties from functioning as an electron withdrawing group to functioning similar to an electron donating group. The

protons on the phenyl ring of the benzonitrile are deshielded by the $C\equiv N$ functional group, but the protons in the ortho position are less deshielded than the para position. The H_a protons (7.281 ppm) are more shielded through the inductive effect than the H_b or H_c protons because they are the closest to the $C\equiv N$. The H_a protons should appear as a doublet, but the peaks are masked by the $CHCl_3$ solvent peak at 7.26 ppm. Similarly, through the same effect, the H_b protons (7.374 ppm) are also shielded by the $C\equiv N$ functional group; however, since the H_b protons are not as close to the $C\equiv N$ functional group as the H_a protons, the H_b appear slightly more downfield to the H_a protons. The H_b protons appear as a triplet because they are split by the H_a and H_c protons. The H_c protons (7.539 ppm) para to the $C\equiv N$ functional group are the most deshielded by the $C\equiv N$ functional group. The H_c protons appear as a triplet because they are split by the H_b and H_a protons.

The phenyl protons (H_d , H_e , and H_f) are attached to the electron withdrawing N (from the *N*-phenylacetamide). The protons ortho and para to the electron withdrawing group would be shielded because the electrons are delocalized by the N-C-O group on the 2,2-*trans* $[Rh_2(NPhCOCH_3)_4] \cdot 2NC(C_6H_4)$ adduct. Because the H_d protons (7.041 ppm) are the closest to the N, the H_d protons ortho to the N are the most shielded, and appear as a doublet because of the splitting by the H_e protons (7.264 ppm). The H_e peaks meta to the N are the most deshielded, and therefore appear downfield. The H_e peaks should appear as a triplet, but the peaks are masked by the $CHCl_3$ solvent peak at 7.26 ppm. The H_f protons (7.134 ppm) appear in between the H_e and H_d peaks as a triplet, split by two neighboring H_e protons.

Phenyl peaks (ppm)
7.559
7.556
7.539
7.521
7.517
7.395
7.374
7.360
7.355
7.326
7.299
7.281
7.264
7.153
7.150
7.134
7.116
7.045
7.041
7.024
7.000

Table 5. *2,2-trans* [Rh₂(NPhCOCH₃)₄]• 2NC(C₆H₄) phenyl protons. See Figure 23.

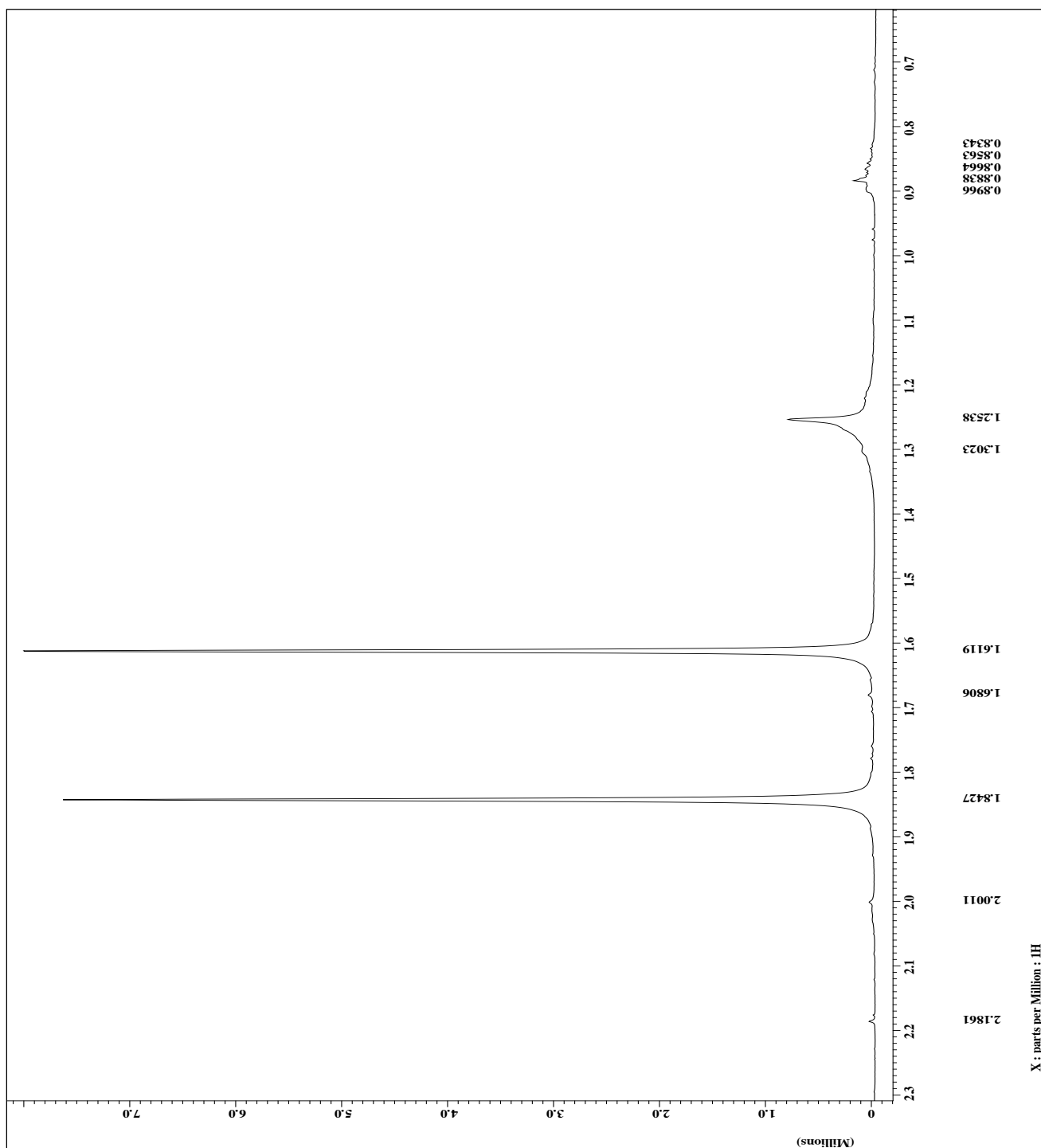


Figure 24. ¹H NMR of 2,2-*trans* [Rh₂(NPhCOCH₃)₄] • 2NC(C₆H₄) from 0.7-2.3 ppm.

The peak at 1.843 ppm (H_g) represents the proton of the methyl group of the *N*-phenylacetamide equatorial ligand. The peak at 1.61 ppm is a solvent peak, H_2O .

3.13: *o*-tolunitrile

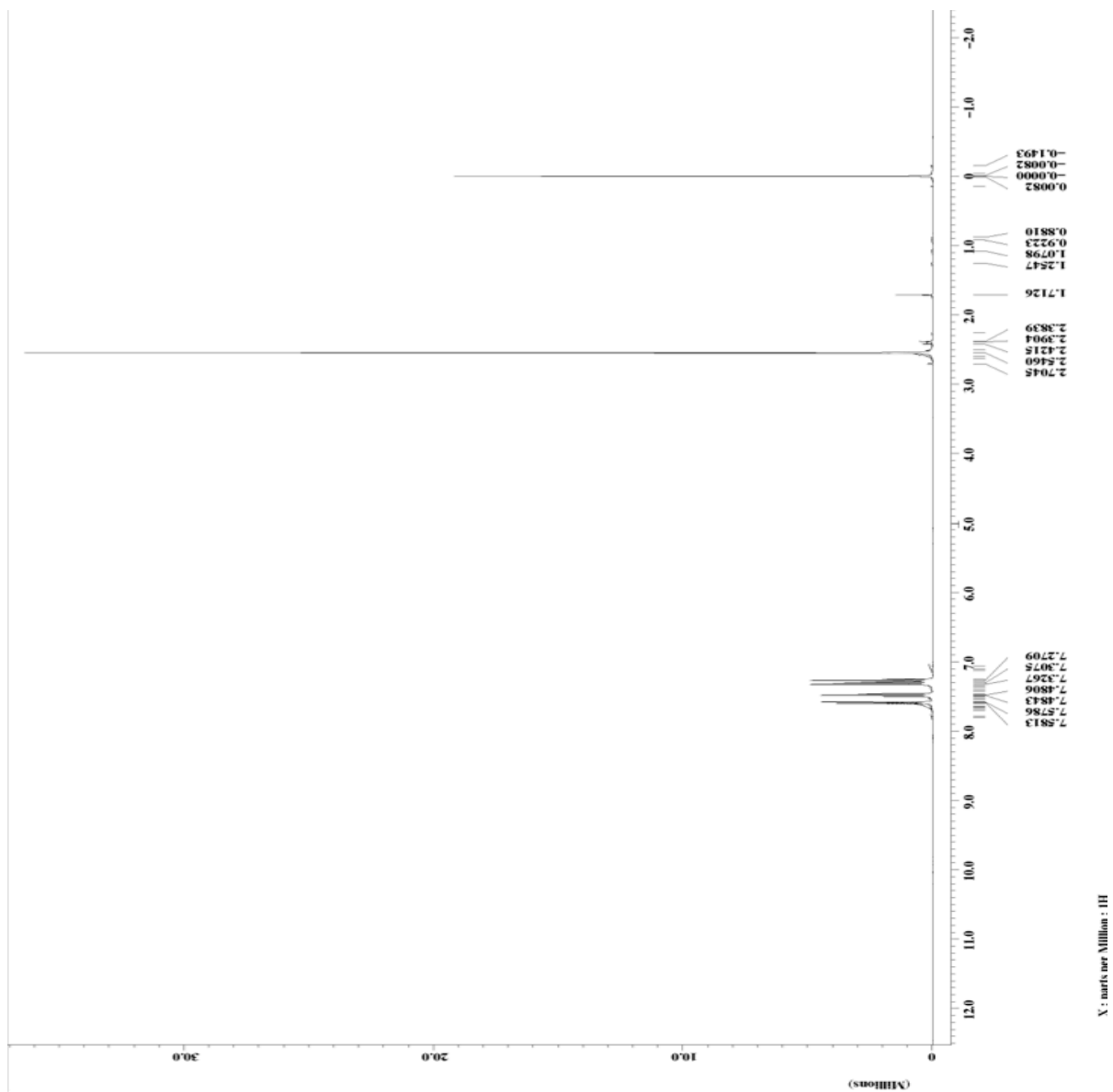


Figure 25. 1H NMR of *o*-tolunitrile.

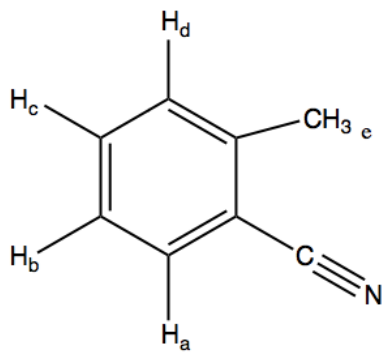


Figure 26. 1H labels for o-tolunitrile.

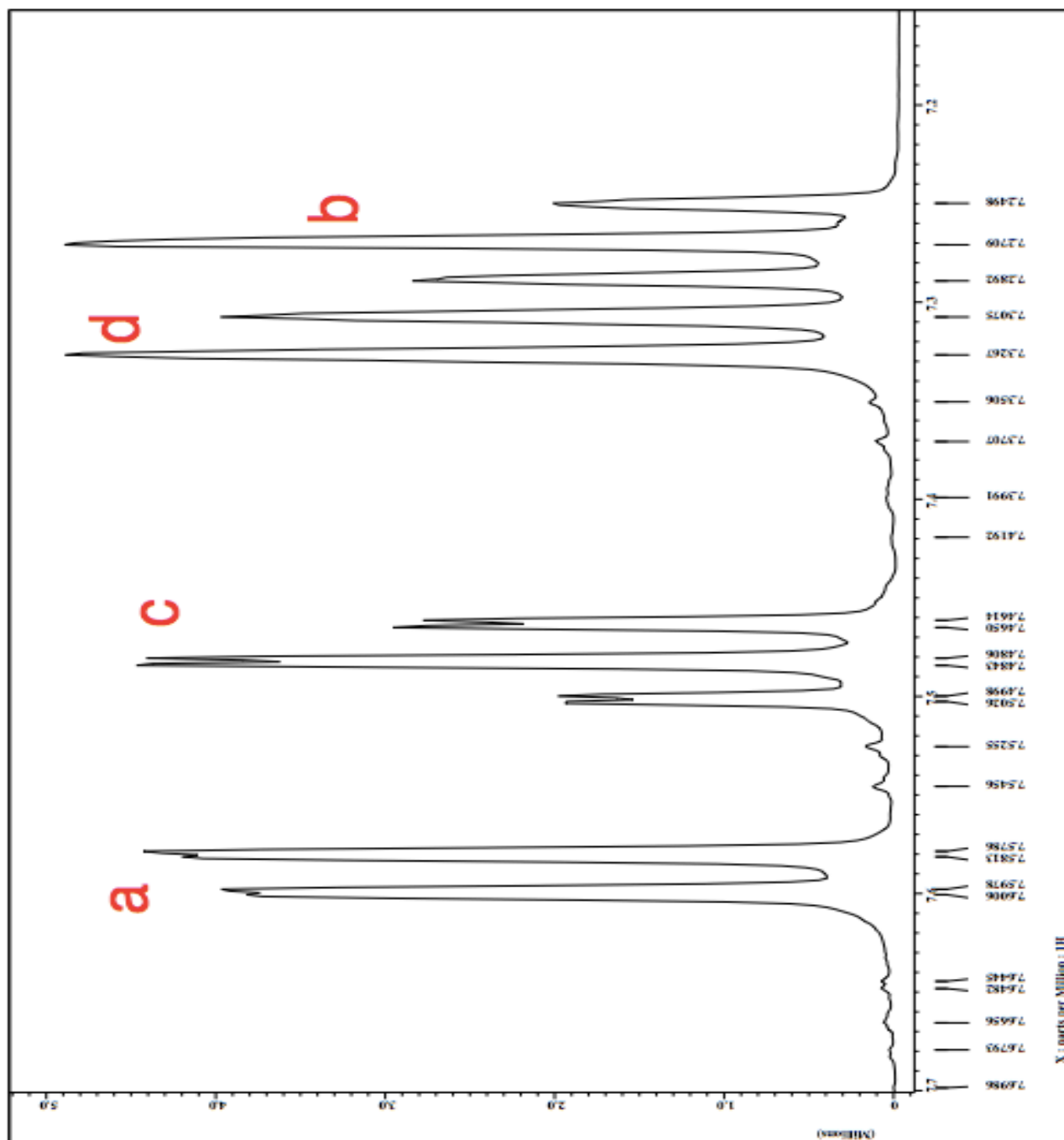


Figure 27. ^1H NMR of o-tolunitrile from 7.2 ppm to 7.7 ppm.

The protons ortho to the $\text{C}\equiv\text{N}$ functional group (H_a) appear the most downfield because it is deshielded by the $\text{C}\equiv\text{N}$ functional group. The H_a peaks (7.576 ppm) are split by H_b , and thus appear as a doublet. The H_c protons (7.465

ppm) para to the C≡N functional group appears the downfield because it is also deshielded by C≡N functional group. The H_c peaks are split by H_b and H_d, and thus appear as a triplet. The H_d peaks (7.327 ppm) are split by H_c, and thus appear as a doublet. The H_b protons (7.271 ppm) meta to the C≡N functional group appears upfield because it is shielded by C≡N functional group; these H_b peaks are split by H_a and H_c, and thus appear as a triplet. The 7.26 ppm peak is an overlap of the proton from CHCl₃ in the CDCl₃ solvent.

Phenyl peaks (ppm)
7.601
7.598
7.581
7.579
7.503
7.500
7.484
7.481
7.465
7.461
7.327
7.308
7.289
7.271
7.250

Table 6. o-tolunitrile phenyl protons. See Figure 27.

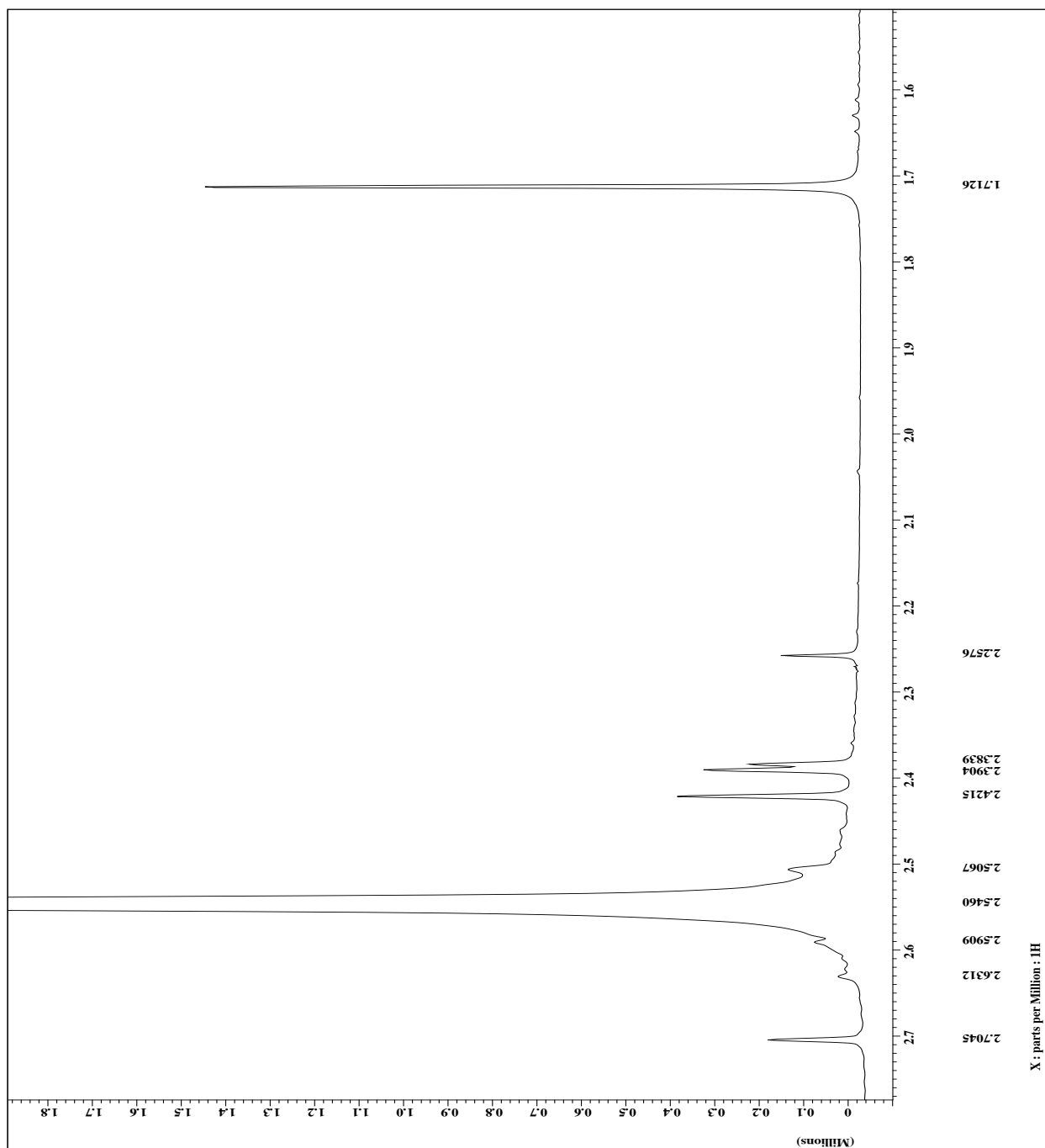


Figure 28. ^1H NMR of o-tolunitrile from 1.6 ppm to 2.7 ppm.

The H_e that appears at 2.54 ppm is from the CH_3 of the o-tolunitrile. The 1.71 ppm peak is H_2O from the NMR solvent. The peaks at 2.70 ppm, 2.42 ppm, 2.39 ppm,

2.38 ppm and 2.26 ppm represent peaks are the result of ^{13}C coupling to the H_e proton (of the methyl group.) ^{13}C has only about 1.1% natural abundance rate of carbon atoms. Due to the low abundance, ^1H - ^{13}C coupling is negligible and usually not observed in the spectrum. Because the sample was concentrated and the spectrum was enlarged, the peaks of the ^1H - ^{13}C coupling were visible.²⁰

3.14: 2,2-*trans* [Rh₂(NPhCOCH₃)₄] • 2 o-NC({2-CH₃)C₆H₄)

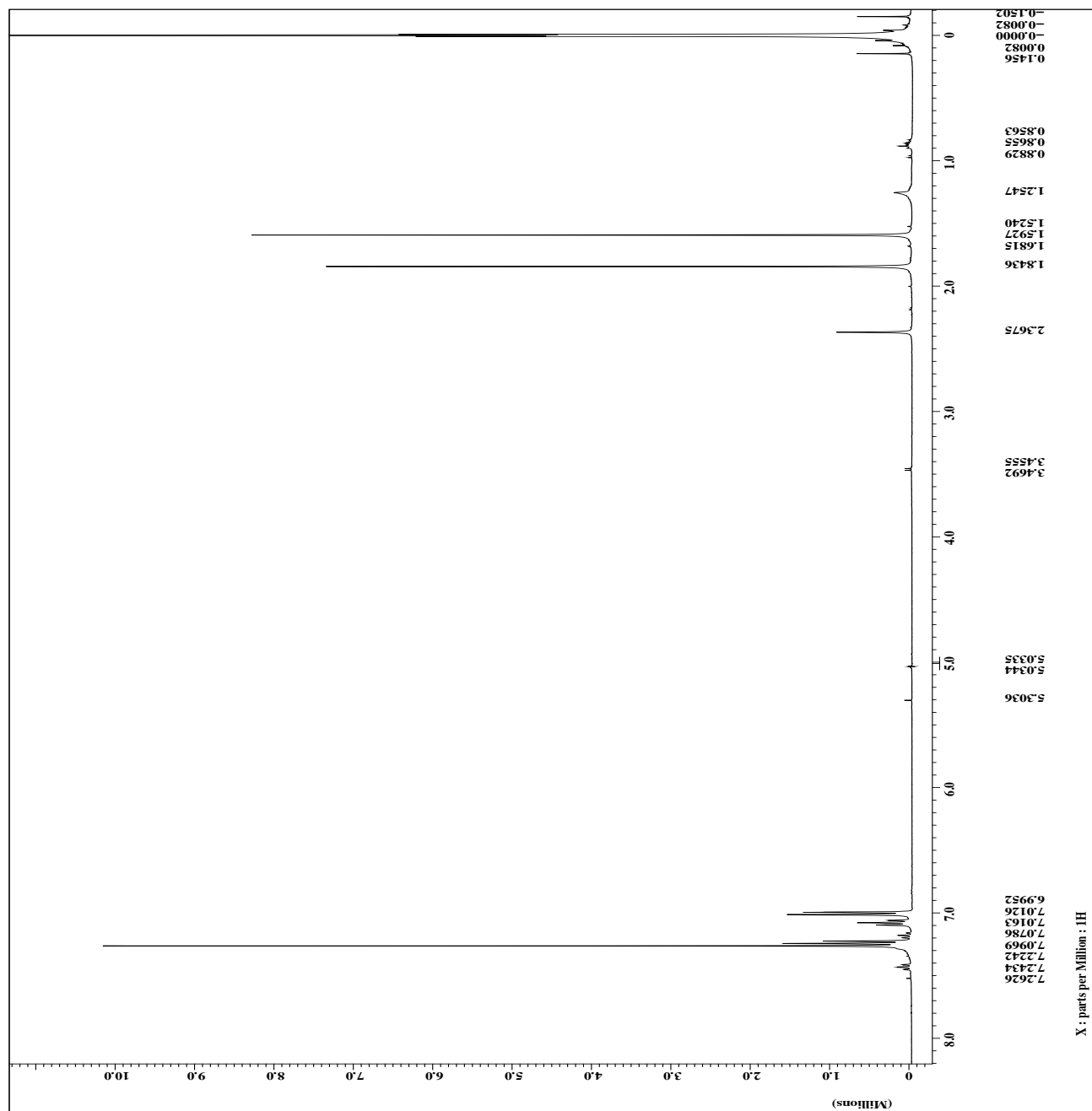


Figure 29. ¹H NMR of 2,2-*trans* [Rh₂(NPhCOCH₃)₄] • 2 o-NC({2-CH₃)C₆H₄).

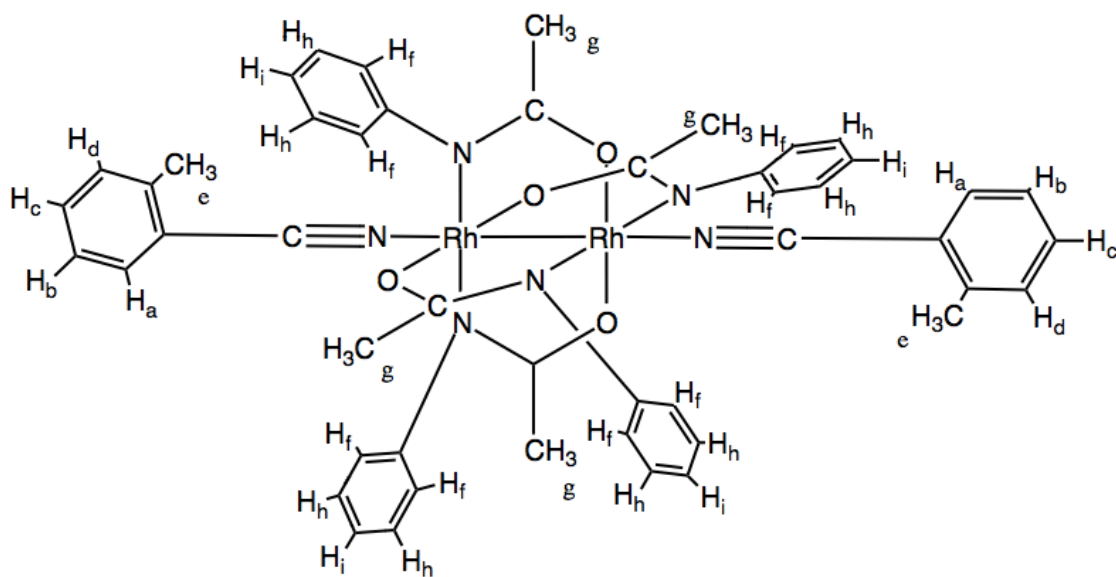


Figure 30. Proton labels for 2,2-*trans* [Rh₂(NPhCOCH₃)₄]• 2 o-NC({2-CH₃}C₆H₄).

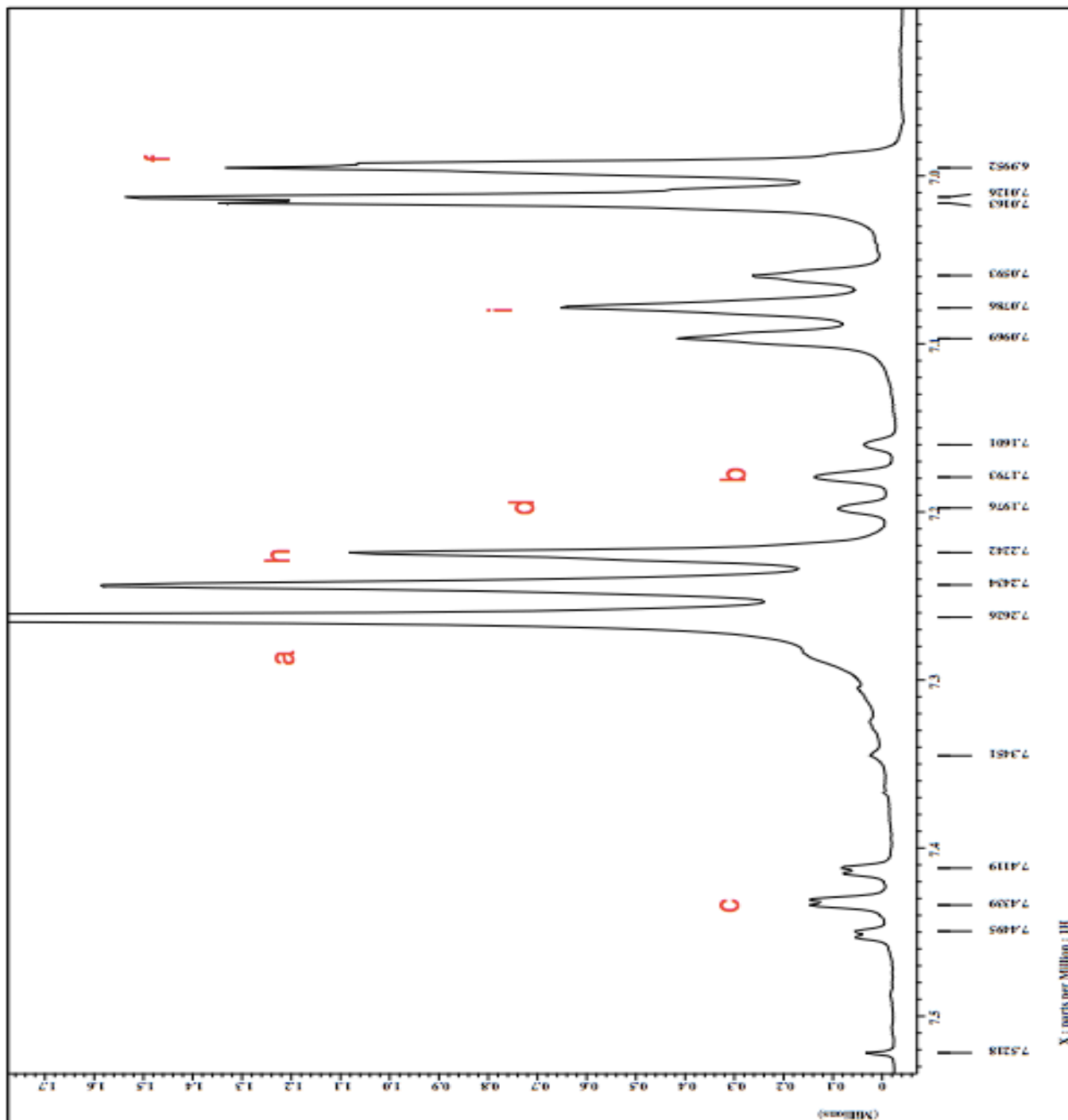


Figure 31. ¹H NMR of 2,2-*trans* [Rh₂(NPhCOCH₃)₄] • 2 o-NC({2-CH₃)C₆H₄) from 6.0-7.8 ppm, expanded to show the region.

Similarly to the 2,2-*trans* [Rh₂(NPhCOCH₃)₄]• 2NC(C₆H₄) ¹H NMR data, the rhodium atom is a metal bound to the C≡N functional group. Because it is a metal, this property manipulates the C≡N's properties from functioning as an electron withdrawing group to functioning similar to an electron donating group. The protons on the phenyl ring of the *o*-tolunitrile are shielded by the C≡N functional group, but the protons in the para position are more shielded. The H_b proton (7.1793 ppm) is shielded by the C≡N functional group; however, since the H_b proton appears more upfield because the H_b proton is para to the CH₃, an electron donating group. The H_b protons appear as a triplet because they are split by the H_a and H_c protons. The H_a protons (7.263 ppm) are shielded through resonance and inductive effect because they are the closer to the C≡N functional group. The H_a protons should appear as a doublet, but the peaks are masked by the CHCl₃ solvent peak at 7.26 ppm. The H_c proton (7.434 ppm) para to the C≡N functional group is the most deshielded by the C≡N functional group. The H_c protons appear as a triplet because they are split by the H_b and H_a protons. The H_d proton should appear as a doublet, but the peaks are masked by the CHCl₃ solvent peak at 7.26 ppm. The methyl group in the ortho position on the phenyl ring (e) is an electron donating group; however, an alkyl group does not shift the signal as much as C≡N functional group.

The phenyl protons (H_f, H_h, and H_i) are attached to N (of the *N*-phenylacetamide equatorial ligand), an electron withdrawing group. The protons ortho and para to the electron withdrawing group would be shielded because the electrons are delocalized by the N-C-O group on the 2,2-*trans* [Rh₂(NPhCOCH₃)₄] • 2 *o*-NC({2-CH₃)C₆H₄) adduct. Because the H_f protons (7.013 ppm) are the closest to the N, the H_f protons ortho to the N are the most shielded, and appear as a doublet because of the splitting by the H_e protons. Through inductive and resonance effects, the H_i protons on the phenyl group are more deshielded than the H_f protons; the H_i proton is not as close to the electron withdrawing N (from the *N*-phenylacetamide equatorial ligand). The H_i peaks (7.079 ppm) appear as a triplet because H_i protons are split by two H_h protons. The H_h peaks (7.224 ppm) meta to the N are the most deshielded through resonance effect, and therefore the H_h peaks should appear as a triplet, but the peaks are masked by the CHCl₃ solvent peak at 7.26 ppm.

Phenyl peaks (ppm)
7.450
7.434
7.412
7.263
7.243
7.224
7.198
7.179
7.160
7.097
7.079
7.059
7.016
7.013
6.995

Table 7. *2,2-trans* [Rh₂(NPhCOCH₃)₄] • 2 o-NC({2-CH₃}C₆H₄) phenyl protons. See Figure 31.

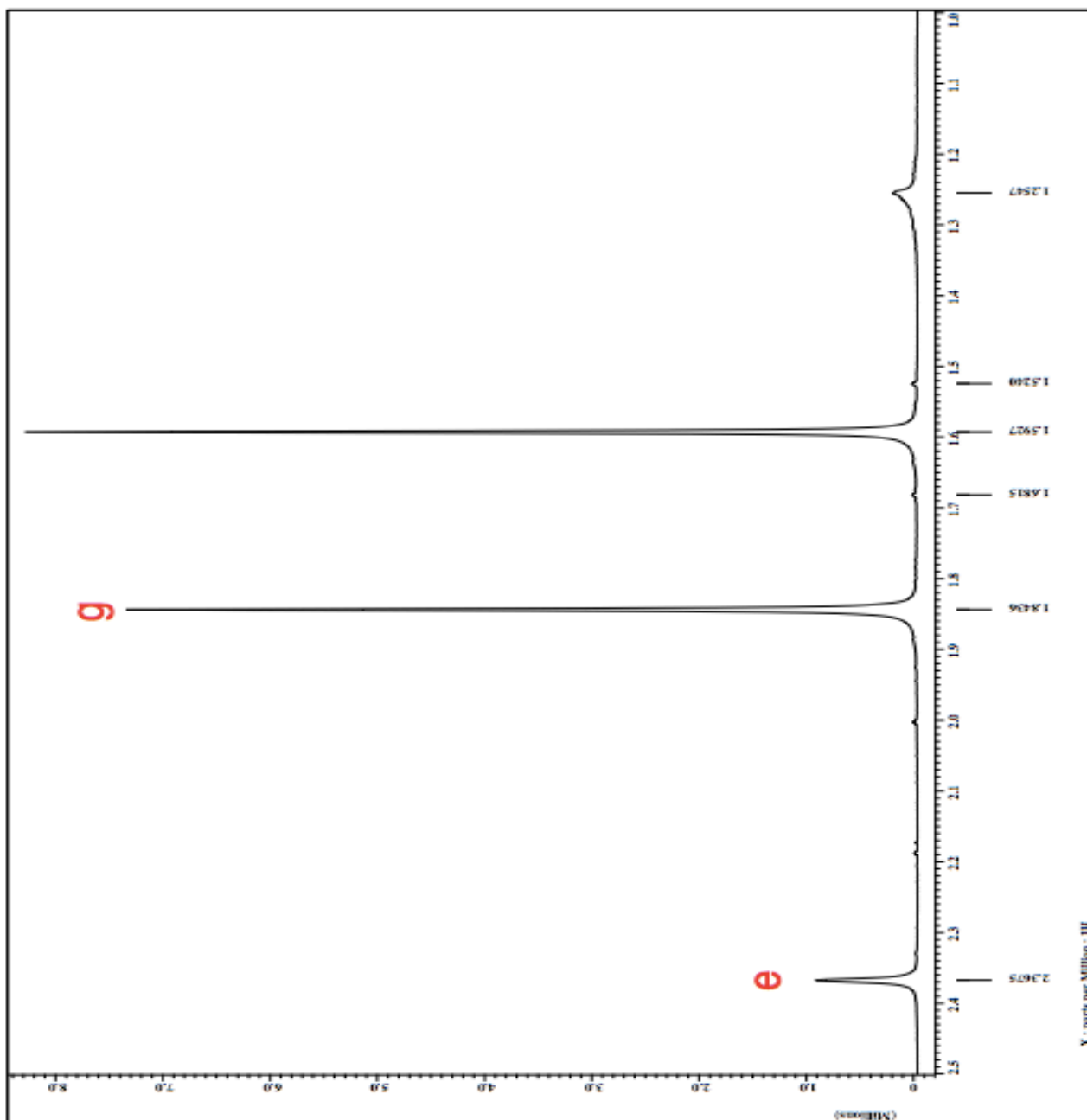


Figure 32. ^1H NMR of $2,2\text{-trans} [\text{Rh}_2(\text{NPhCOCH}_3)_4] \cdot 2 \text{ o-NC}(\{2\text{-CH}_3\}\text{C}_6\text{H}_4)$ from 2.5-1 ppm, expanded to show the region.

The protons H_e and H_g are methyl protons; H_g protons are located on the rhodium adduct, while the H_e protons exist on the *o*-tolunitrile ligand. The g peak

(1.8 ppm) appears more intense than the e peak (2.34 ppm) because the H_g protons exist in a 12:6 ratio of H_g:H_e.

3.15: m-tolunitrile

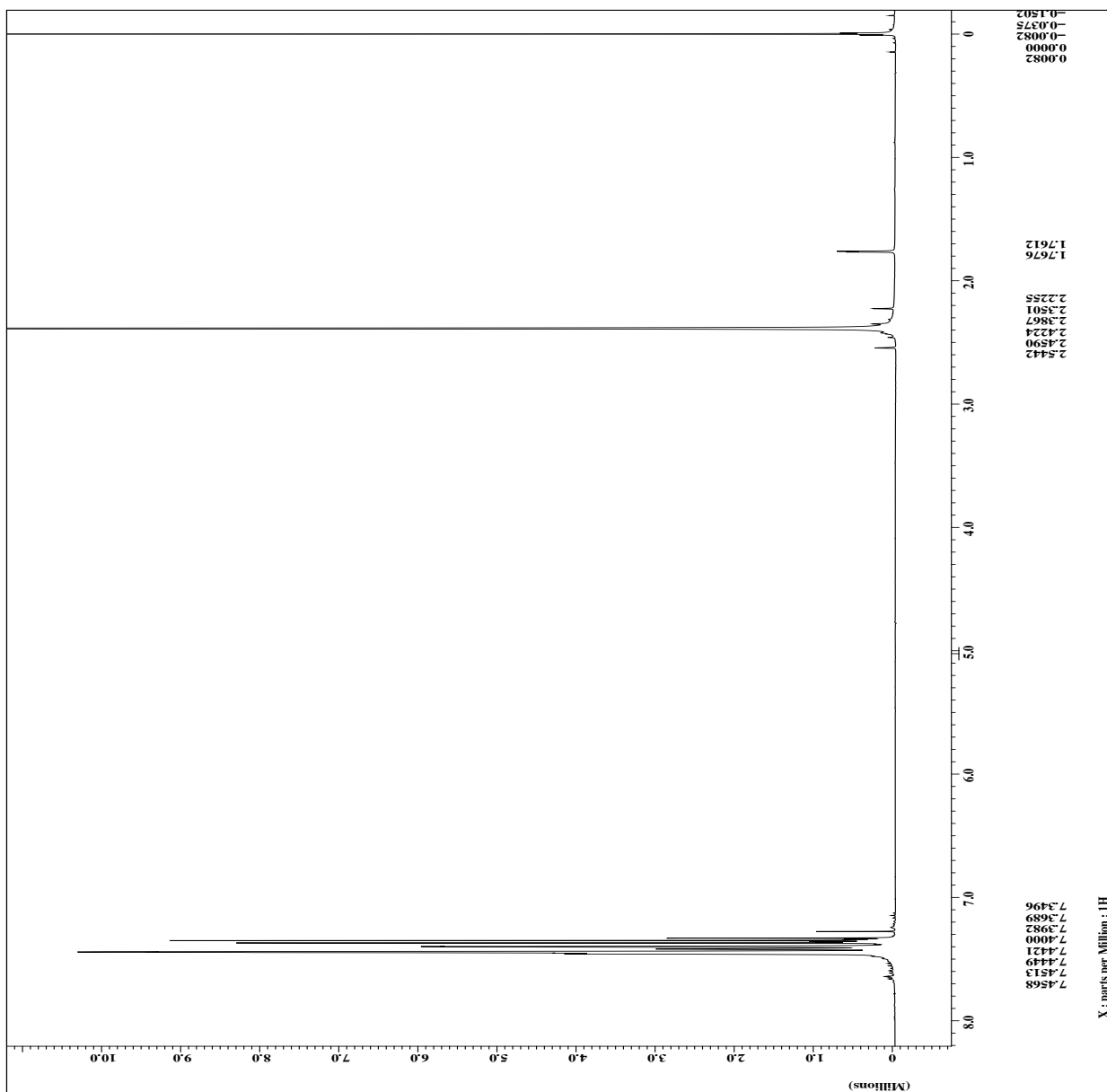


Figure 33. ¹H NMR of m-tolunitrile.

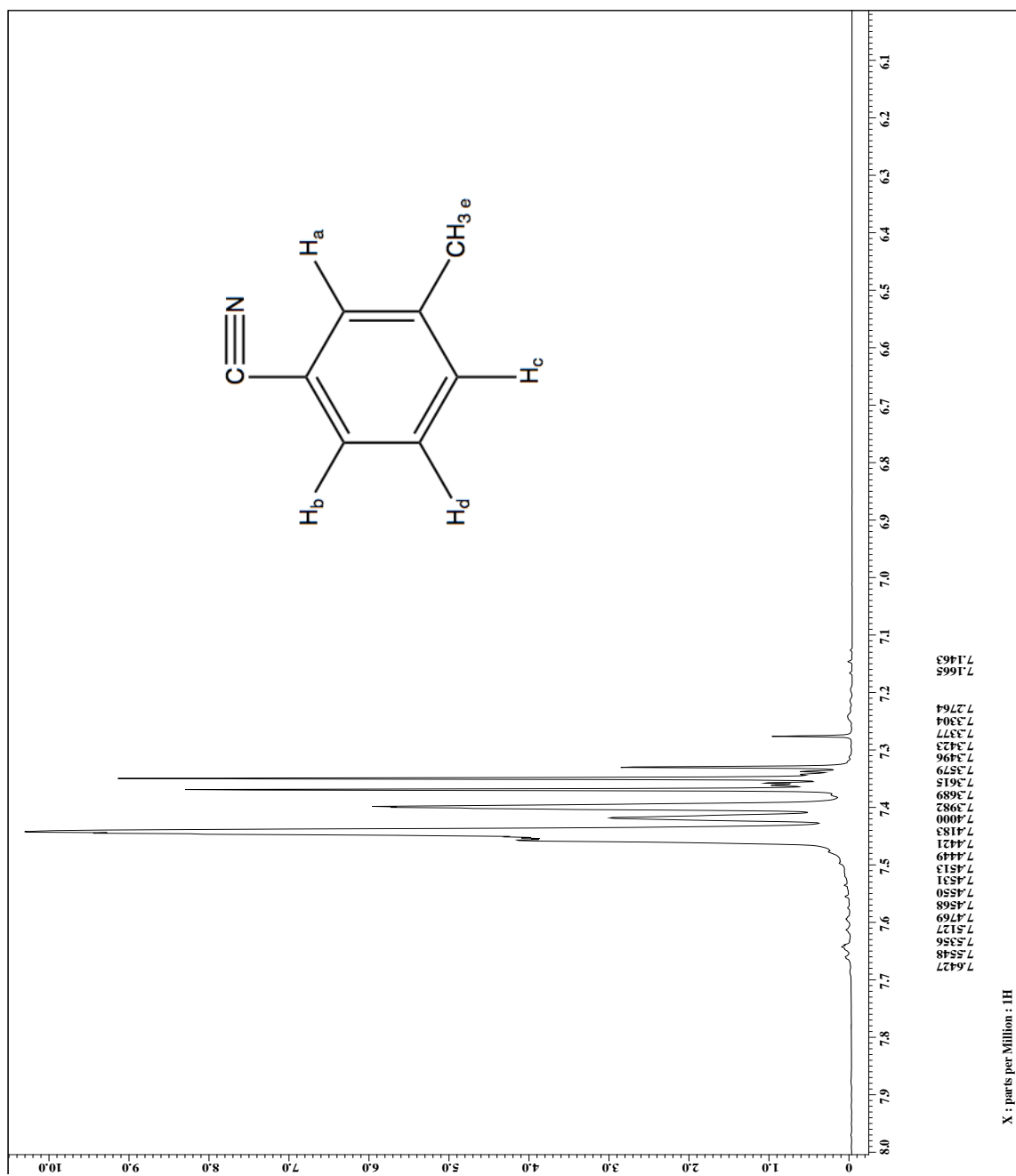


Figure 34. ¹H NMR of m-tolunitrile from 6.0 ppm to 8.0 ppm.

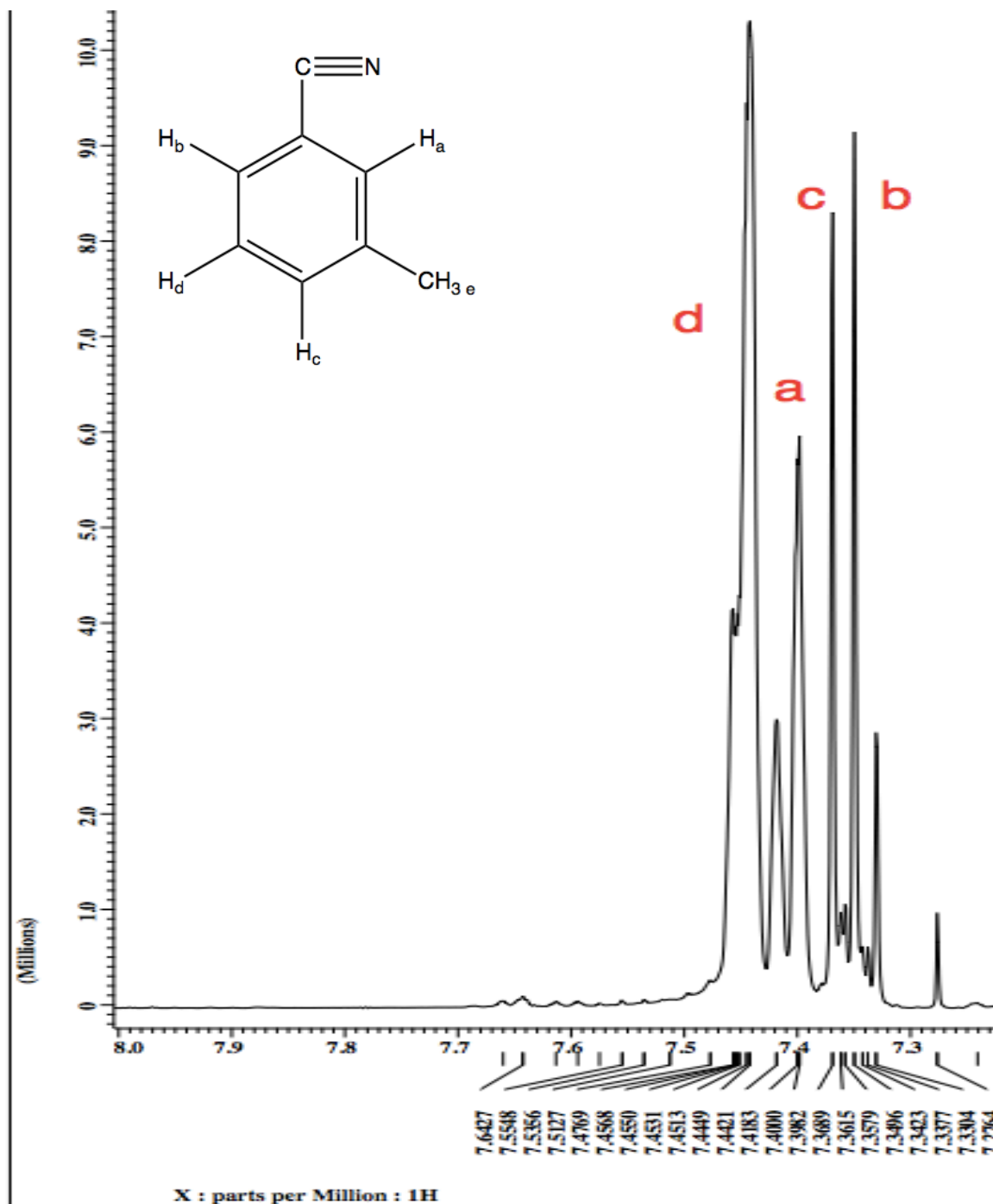


Figure 35. ^1H NMR of m-tolunitrile from 7.3–8.0 ppm, expanded to show the region.

The $\text{C}\equiv\text{N}$ functional group in the m-tolunitrile is an electron withdrawing group. The H_a proton appears the most downfield because H_a proton (7.451 ppm) is deshielded by both the $\text{C}\equiv\text{N}$ functional group and CH_3 group through inductive

effect. The H_a proton (7.442 ppm) ortho to the C≡N functional group appears downfield because it is deshielded by the C≡N functional group. The H_b proton (7.342 ppm) and the H_c proton (7.369 ppm) peaks overlapped. The peaks appear to be a triplet, but have smaller doublet peaks amongst the triplet peaks. The H_b peaks should appear as a doublet, split by H_d. The H_c peaks should appear as a triplet, also split by H_d. The H_a peak is not split, and thus the H_a peak appears as a singlet. The 7.28 ppm peak is an overlap of the proton from CHCl₃ in the CDCl₃ solvent.

Phenyl peaks (ppm)
7.455
7.445
7.442
7.418
7.398
7.369
7.362
7.358
7.350
7.338
7.330
7.276

Table 8. m-tolunitrile phenyl protons. See Figure 35.

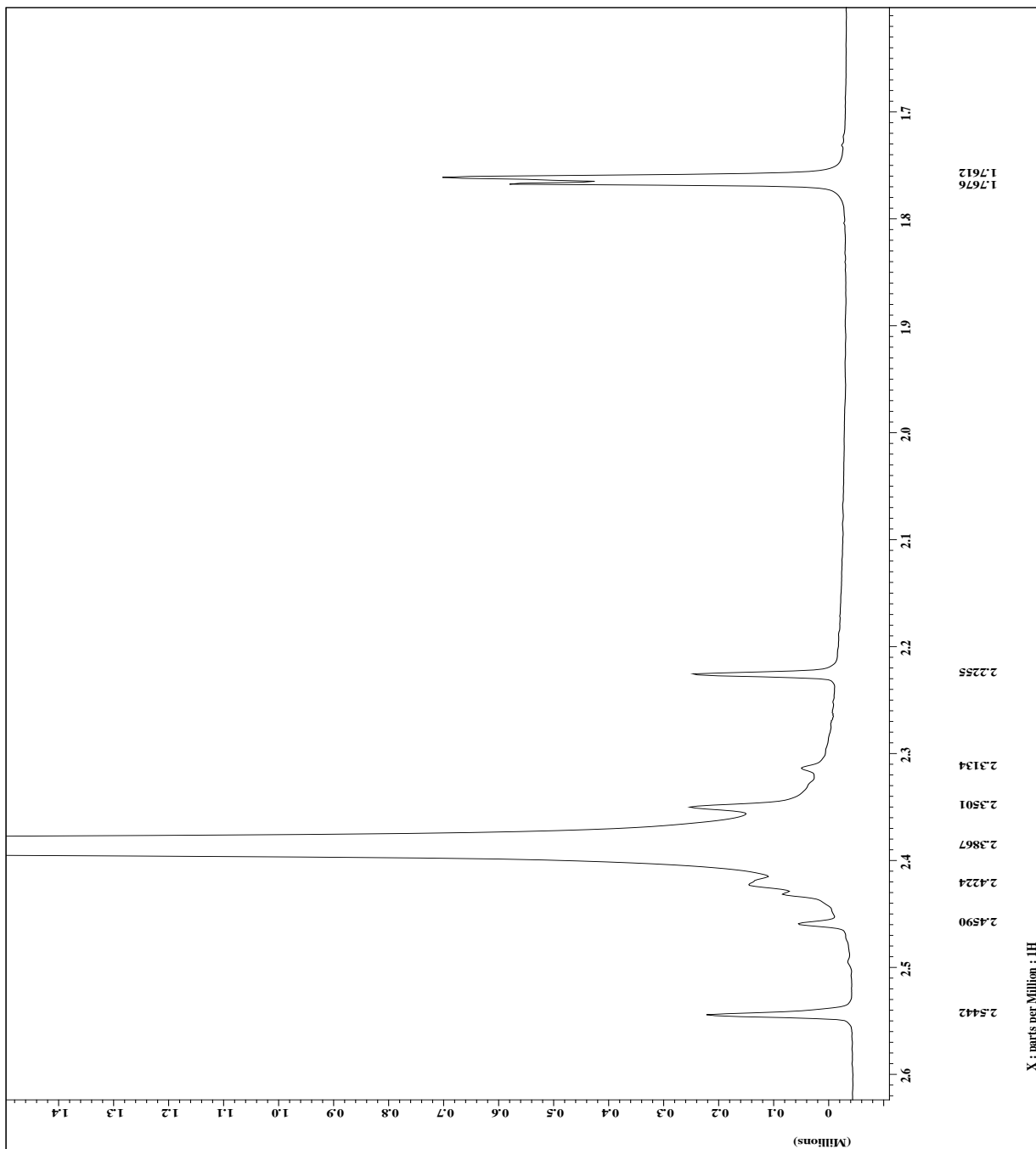


Figure 36. ^1H NMR of m-tolunitrile from 2.6 ppm to 1.7 ppm.

The peak at 2.39 ppm represents the H_e protons from the methyl group. The 1.76 ppm peak represents H_2O from the NMR solvent. The peaks at 2.54 ppm and 2.23

ppm are the result of ^1H - ^{13}C coupling to the H_e proton (of the methyl group.) ^{13}C has only about 1.1% natural abundance rate of carbon atoms. Due to the low abundance, ^1H - ^{13}C coupling is negligible and usually not observed in the spectrum. Because the sample was concentrated and the spectrum of the 2.39 ppm peak was enlarged, the peaks of the ^{13}C coupling were visible.²⁰

3.16: *2,2-trans* $[\text{Rh}_2(\text{NPhCOCH}_3)_4] \cdot m\text{-NC}(\{3\text{-CH}_3\}\text{C}_6\text{H}_4)$

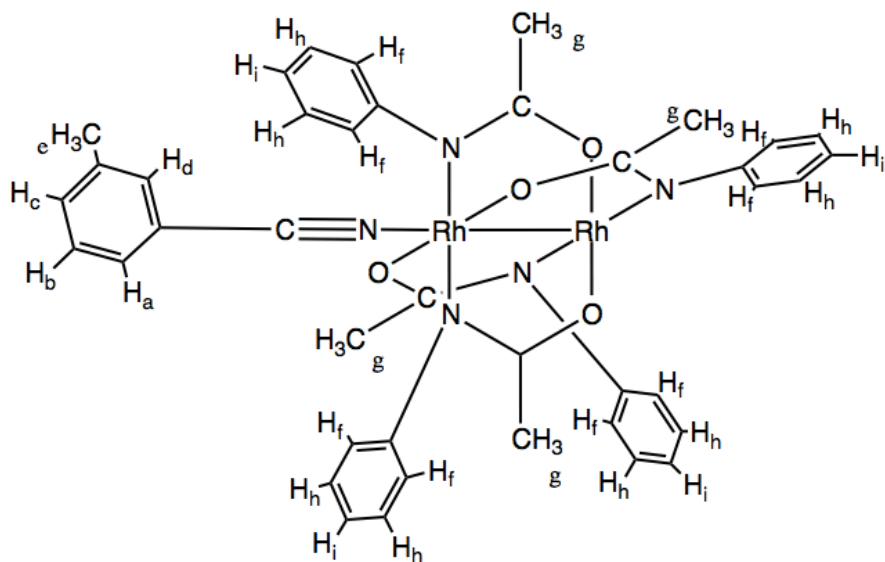


Figure 37. Proton labels for *2,2-trans* $[\text{Rh}_2(\text{NPhCOCH}_3)_4] \cdot m\text{-NC}(\{3\text{-CH}_3\}\text{C}_6\text{H}_4)$.

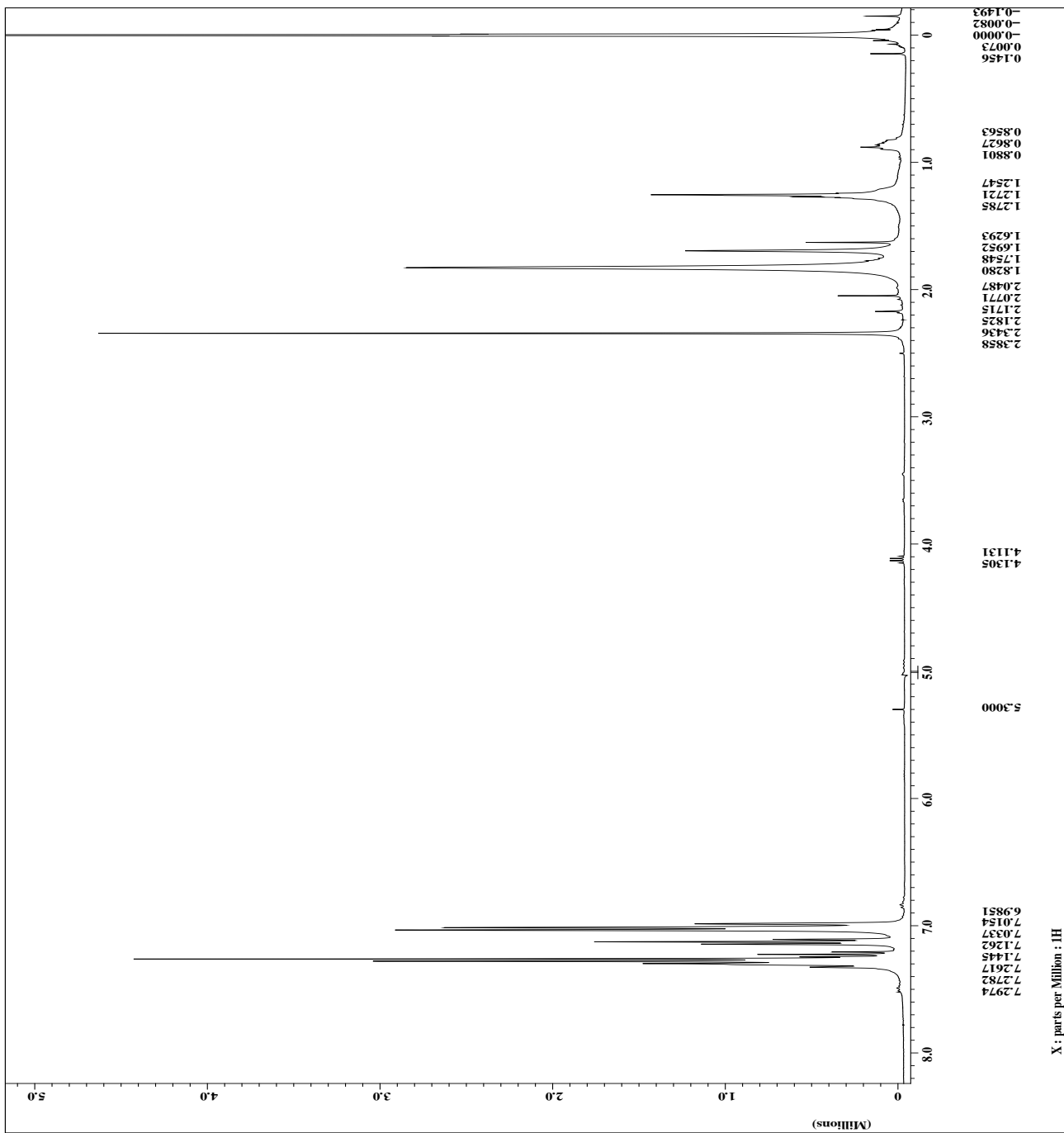


Figure 38. ^1H NMR of 2,2-*trans* $[\text{Rh}_2(\text{NPhCOCH}_3)_4] \cdot m\text{-NC}(\{3\text{-CH}_3\}\text{C}_6\text{H}_4)$.

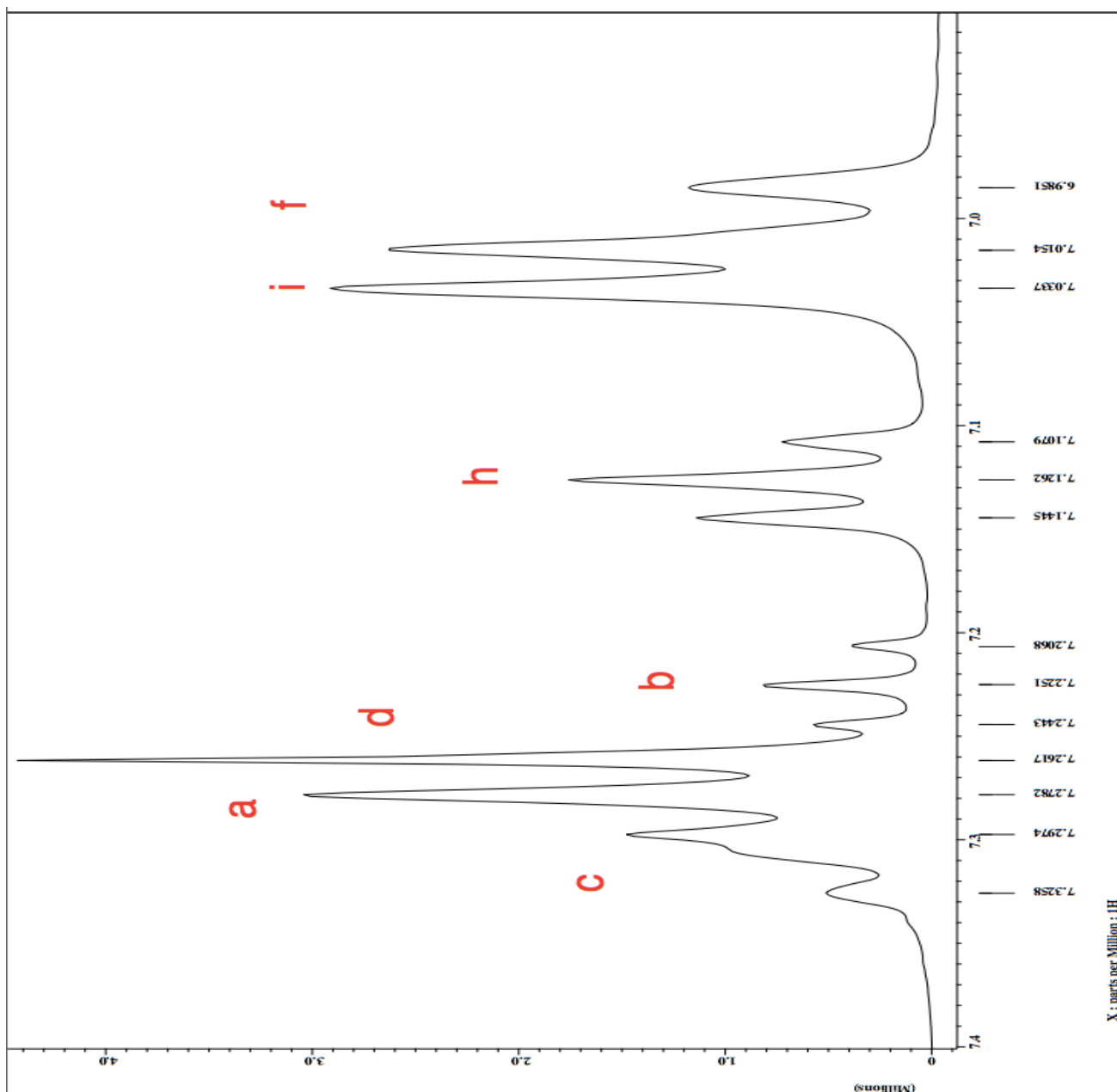


Figure 39. ^1H NMR of 2,2-*trans* $[\text{Rh}_2(\text{NPhCOCH}_3)_4] \cdot \text{m-NC}(\{3\text{-CH}_3\}\text{C}_6\text{H}_4)$ from 6.0 to 7.4 ppm.

Similarly to the 2,2-*trans* $[\text{Rh}_2(\text{NPhCOCH}_3)_4] \cdot 2\text{NC}(\text{C}_6\text{H}_4)$, the rhodium atom manipulates the $\text{C}\equiv\text{N}$'s properties from functioning as an electron withdrawing group to functioning similar to an electron donating group. The protons on the phenyl ring of the *m*-tolunitrile are shielded by the $\text{C}\equiv\text{N}$. The H_b proton (7.225 ppm)

is most shielded by being para to the $C\equiv N$ functional group and meta to the CH_3 . The H_b peak is split by the H_c and H_a protons, resulting in a triplet peak for H_b . The H_d protons (7.262 ppm) are the next most shielded through the inductive effect because the H_d protons are the closest to the $C\equiv N$ functional group and CH_3 . The H_a , H_c , and H_d proton peaks are masked by the $CHCl_3$ solvent peak at 7.26 ppm. The H_a protons (7.278 ppm) should appear as a doublet, but the peaks are masked by the $CHCl_3$ proton peak. The H_b proton peaks should appear as a triplet, split by H_a and H_c . The H_c proton (7.297 ppm) peaks should appear as a doublet, split by the H_b proton. The H_d proton peak appears as a singlet, as it is not being split by neighboring protons.

The phenyl protons of the 2,2-*trans* $[Rh_2(NPhCOCH_3)_4] \cdot m-NC(\{3-CH_3\}C_6H_4)$ adduct (H_f , H_h , and H_i) are attached to the electron withdrawing N (from the *N*-phenylacetamide). The protons ortho and para to the electron withdrawing group would be shielded because the electrons are delocalized by the N-C-O group on the 2,2-*trans* $[Rh_2(NPhCOCH_3)_4] \cdot m-NC(\{3-CH_3\}C_6H_4)$ adduct. Because the H_f protons (7.015 ppm) are the closest to the N, the H_f protons ortho to the N are the most shielded, and appear as a doublet because of the splitting by the H_e protons. Through inductive and resonance effects, the H_i protons on the phenyl group appear are more deshielded than the H_f protons; the H_i proton is not as close to the electron withdrawing group N. The H_i proton (7.034 ppm) peaks appear as a triplet because H_i protons are split by two H_h protons. The H_h proton (7.126 ppm) peaks meta to the N are the most deshielded through resonance effect, and therefore the H_h peaks should appear as a triplet, but the peaks are masked by the $CHCl_3$ solvent peak at 7.26 ppm. The 7.26 ppm peak is an overlap of the proton from $CHCl_3$ in the $CDCl_3$ solvent.

Phenyl peaks (ppm)
7.326
7.297
7.278
7.262
7.244
7.225
7.207
7.145
7.126
7.108
7.034
7.015
6.985

Table 9. *2,2-trans* [Rh₂(NPhCOCH₃)₄] • *m*-NC({3-CH₃)C₆H₄) phenyl peaks.

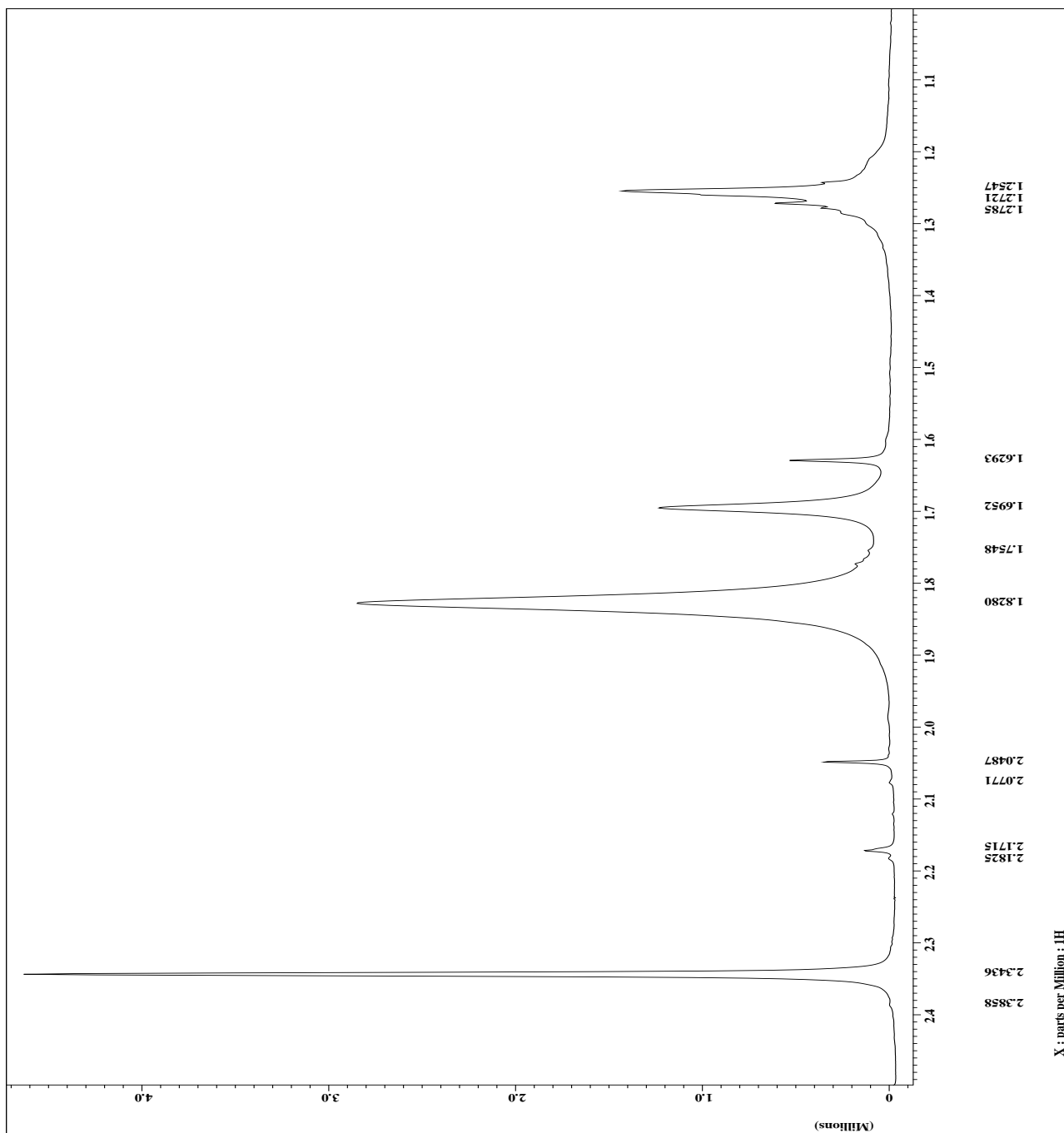


Figure 40. ¹H NMR of 2,2-*trans* [Rh₂(NPhCOCH₃)₄]• m-NC({3-CH₃}C₆H₄) from 1.1 to 2.4 ppm.

3.2 FTIR data

Fourier transform infrared spectroscopy (FTIR) is an instrument that measures the absorption of a sample to produce an infrared spectrum. The FTIR instrument used was the Shimadzu IR Prestige-21. When π -backbonding occurs with a $C\equiv N$ functional group bond, the bond becomes weaker, and thus has lower energy. The stretching frequency usually decreases during π backbonding because the energy a molecule has is proportionate to its wave number (cm^{-1}). However, the $C\equiv N$ functional group's FTIR peaks for both the 2,2-*trans* $[\text{Rh}_2(\text{NPhCOCH}_3)_4] \cdot 2$ o-NC($\{2\text{-CH}_3\}\text{C}_6\text{H}_4$) and the 2,2-*trans* $[\text{Rh}_2(\text{NPhCOCH}_3)_4] \cdot m\text{-NC}(\{3\text{-CH}_3\}\text{C}_6\text{H}_4)$ complexes increased instead of decreased compared to the respective nitrile ligand by itself. The 2,2-*trans* $[\text{Rh}_2(\text{NPhCOCH}_3)_4] \cdot 2$ o-NC($\{2\text{-CH}_3\}\text{C}_6\text{H}_4$) was 2320.37 cm^{-1} ; the o-tolunitrile $C\equiv N$ functional group's stretching frequency was 2223.92 cm^{-1} . The 2,2-*trans* $[\text{Rh}_2(\text{NPhCOCH}_3)_4] \cdot m\text{-NC}(\{3\text{-CH}_3\}\text{C}_6\text{H}_4)$ was 2310.72 cm^{-1} ; the m-tolunitrile $C\equiv N$ functional group's stretching frequency was 2227.78 cm^{-1} .

The increases in shifts of stretching frequency in the FTIR spectra upon nitrile bonding to $[\text{Rh}_2(\text{NPhCOCH}_3)_4]$ for 2,2-*trans* $[\text{Rh}_2(\text{NPhCOCH}_3)_4] \cdot 2$ o-NC($\{2\text{-CH}_3\}\text{C}_6\text{H}_4$) and 2,2-*trans* $[\text{Rh}_2(\text{NPhCOCH}_3)_4] \cdot m\text{-NC}(\{3\text{-CH}_3\}\text{C}_6\text{H}_4)$ imply that σ -bonding is dominant over π -backbonding. During IR analysis, the $C\equiv N$ functional group's stretching was difficult to see or masked, so the number of scans was increased to 3200.

The ^1H NMR spectra were taken with the samples in solution state. The FTIR and X-ray crystallography data were collected with the samples in a solid state. If the peaks for the NMR spectra had been integrated, the 2,2-*trans* $[\text{Rh}_2(\text{NPhCOCH}_3)_4] \cdot 2\text{NC}(\text{C}_6\text{H}_4)$ and 2,2-*trans* $[\text{Rh}_2(\text{NPhCOCH}_3)_4] \cdot 2$ o-NC($\{2\text{-CH}_3\}\text{C}_6\text{H}_4$) complexes would have had a 1:2 ratio of nitrile axial ligand phenyl protons and 2,2-*trans* $[\text{Rh}_2(\text{NPhCOCH}_3)_4]$ phenyl protons (6H:12H). For 2,2-*trans* $[\text{Rh}_2(\text{NPhCOCH}_3)_4] \cdot m\text{-NC}(\{3\text{-CH}_3\}\text{C}_6\text{H}_4)$, the ratio of nitrile axial ligand phenyl protons and 2,2-*trans* $[\text{Rh}_2(\text{NPhCOCH}_3)_4]$ phenyl protons would have been 1:4 (3H:12H).

Although nitriles have both σ -bonding and π -backbonding capabilities, the Rh-N (of nitrile) bonds of the three compounds, 2,2-*trans* [Rh₂(NPhCOCH₃)₄] • 2NC(C₆H₄), 2,2-*trans* [Rh₂(NPhCOCH₃)₄] • 2 *o*-NC({2-CH₃}C₆H₄), and 2,2-*trans* [Rh₂(NPhCOCH₃)₄] • *m*-NC({3-CH₃}C₆H₄) are predominantly σ -bonding because of the increase in shifts of the C \equiv N functional group's stretching frequencies in the IR spectra. This dominance of σ -bonding can affect the function of carbenoid species during cyclopropanation reactions.

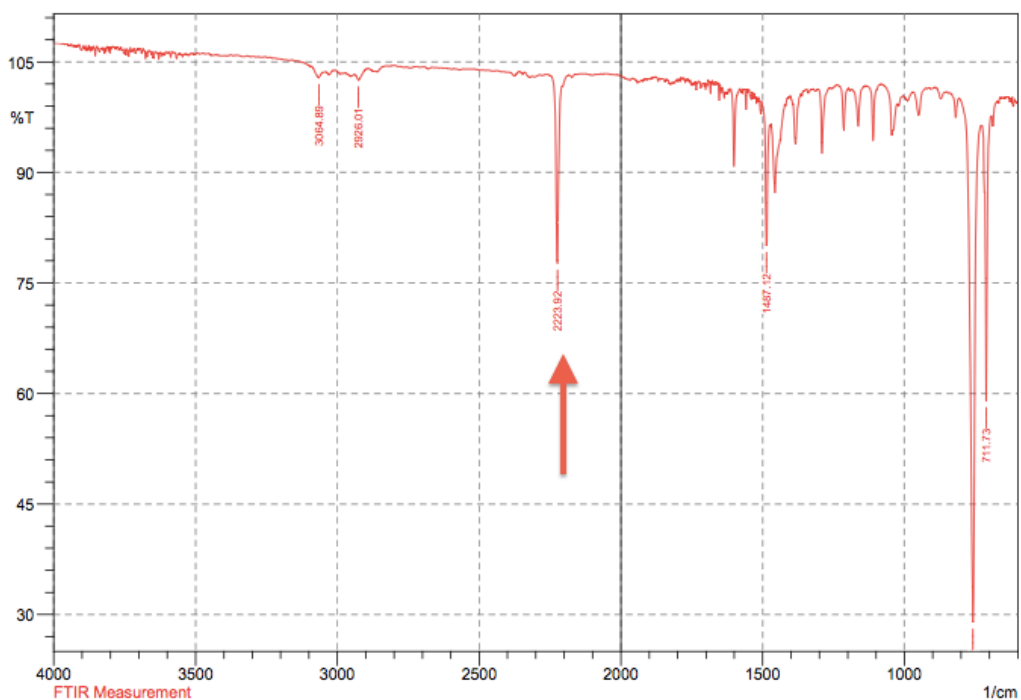


Figure 41. IR spectrum of *o*-tolunitrile. C \equiv N functional group's stretching frequency at 2223.92 cm⁻¹.

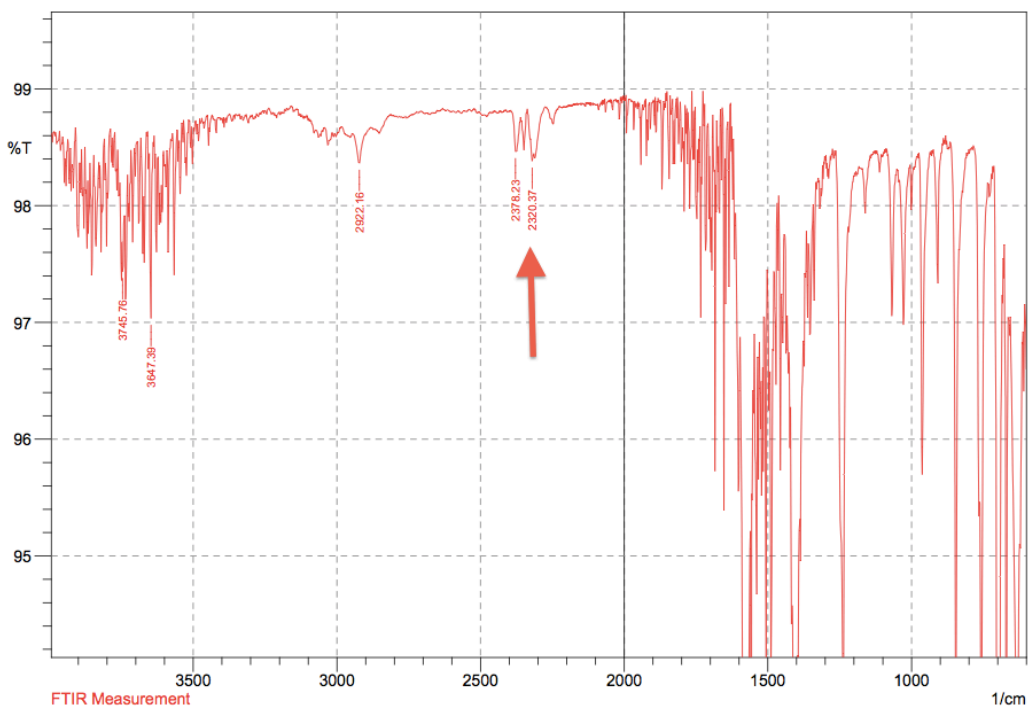


Figure 42. IR spectrum of 2,2-*trans* [Rh₂(NPhCOCH₃)₄] • 2 *o*-NC({2-CH₃)C₆H₄). C≡N functional group's stretching frequency at 2320.37 cm⁻¹.

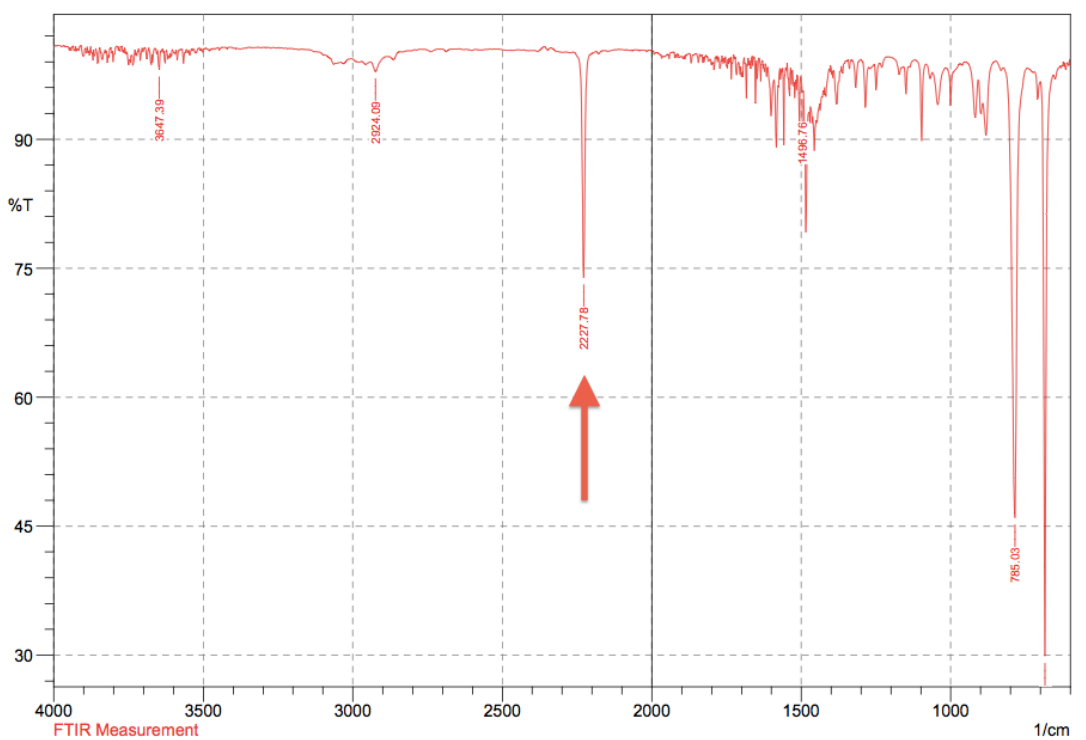


Figure 43. IR spectrum of *m*-tolunitrile. C≡N functional group's stretching frequency at 2227.78 cm⁻¹.

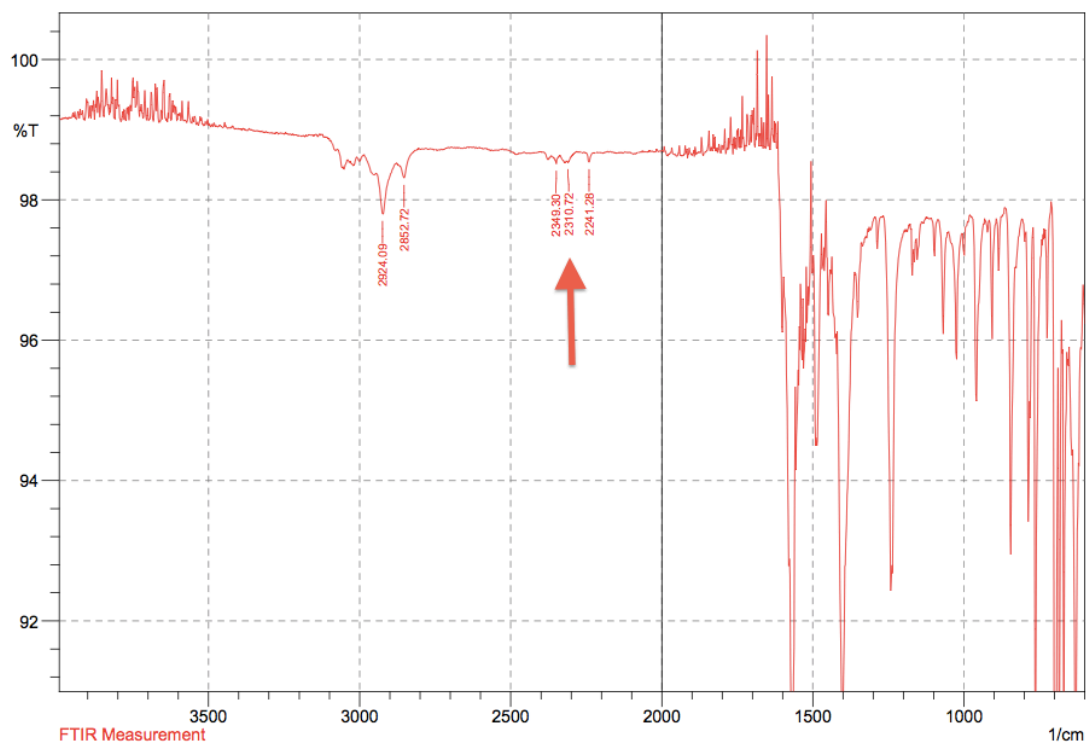


Figure 44. IR spectrum of 2,2-*trans* [Rh₂(NPhCOCH₃)₄]• *m*-NC({3-CH₃)C₆H₄) C≡N functional group's stretching frequency at 2310.72 cm⁻¹.

3.3 X-ray Diffraction data

X-ray quality crystals produced				
	Axial ligand			
	benzonitrile	<i>o</i> -tolunitrile	<i>m</i> -tolunitrile	<i>m</i> -tolunitrile (2 nd trial)
ethyl acetate	no	no	no, red	yes, blue
ethanol	yes, purple	yes, purple	yes, purple	yes, blue
acetone	no	no	no	--
toluene	yes, red	yes, purple	no	--
methanol	yes, red	yes, purple	no, blue	yes, red
H ₂ O	yes, red	yes, purple	no, red	yes, red
acetonitrile	yes, red	yes, red	no, red	yes, red
hexane	--	--	--	no

Table 10. X-ray quality crystals and solvent in the formation of: 2,2-*trans* [Rh₂(NPhCOCH₃)₄]• 2NC(C₆H₄); 2,2-*trans* [Rh₂(NPhCOCH₃)₄]• 2 *o*-NC({2-CH₃)C₆H₄); and 2,2-*trans* [Rh₂(NPhCOCH₃)₄]• *m*-NC({3-CH₃)C₆H₄).

Crystal yield produced was a variety of red, blue, and purple crystals; all were brittle, thin, spikey, and long in shape. The 2,2-*trans* [Rh₂(NPhCOCH₃)₄]• m-NC({3-CH₃}C₆H₄) crystals were especially long and thin, and thus did not diffract X-rays well enough to produce reliable data. Therefore, there was a need for a second trial of crystal growing. We have shown that the nitrile ligands form in a variety of solvents; however, acetone was the only solvent used in the outer 6-dram vial that consistently did not produce crystals. All measurements were made on a Rigaku Mercury375R/M CCD (XtaLAB mini) diffractometer using graphite monochromated Mo-Ka radiation.

2,2-trans [Rh₂(NPhCOCH₃)₄]• 2NC(C₆H₄):

Crystal Dimensions	0.14 X 0.11 X 0.08 mm
Crystal System	monoclinic
Lattice Type	C-centered
Lattice Parameters	a = 30.238(7) Å b = 10.605(2) Å c = 26.091(6) Å β = 90.539(7) ° V = 8366.2(33) Å ³
Temperature	25.0°C
Exposure Rate	30.0 sec./°
Residuals: R1 (I>2.00s(I))	0.0686
Residuals: R (All reflections)	0.1341
Residuals: wR2 (All reflections)	0.1355
Goodness of Fit Indicator	1.038
Max Shift/Error in Final Cycle	0.001
Maximum peak in Final Diff. Map	0.70 e ⁻ /Å ³
<u>Minimum peak in Final Diff. Map</u>	<u>-0.57 e⁻/Å³</u>

Table 11. 2,2-trans [Rh₂(NPhCOCH₃)₄]• 2NC(C₆H₄) X-ray crystallography data.

The 2,2-trans [Rh₂(NPhCOCH₃)₄]• 2NC(C₆H₄) was a red block-shaped crystal having the approximate dimensions of 0.33 x 0.12 x 0.12 mm mounted on a glass fiber. The crystal to detector distance was 50.00 mm. The lattice parameters measured for the crystal's unit cell determined that the 2,2-trans [Rh₂(NPhCOCH₃)₄]• 2 o-NC({2-CH₃}C₆H₄) crystal system was a monoclinic C-centered cell. The number of molecules per unit cell is represented by the letter Z. For Z=2 and formula weight=976.74 g/mol, the calculated density was 1.463 g/cm³. The data was collected at a temperature of 25± 1°C. A total of 540 oscillation images were collected. The exposure rate was 30.0 [sec./°].

2,2-trans [Rh₂(NPhCOCH₃)₄] • 2 o-NC({2-CH₃}C₆H₄):

Number and type of atoms	C ₄₈ H ₄₆ N ₆ O ₄ Rh ₂
Crystal Dimensions	0.33 X 0.12 X 0.12 mm
Crystal System	triclinic
Lattice Type	Primitive
Lattice Parameters	a = 9.7912(7) Å b = 14.7873(10) Å c = 16.3592(11) Å α = 103.837(7) ° β = 99.173(7) ° γ = 99.772(7) ° V = 2216.4(3) Å ³
Temperature	25.0°C
Exposure Rate	16.0 sec./°
Residuals: R1 (I>2.00s(I))	0.0368
Residuals: R (All reflections)	0.0541
Residuals: wR2 (All reflections)	0.0798
Goodness of Fit Indicator	1.037
Max Shift/Error in Final Cycle	0.002
Maximum peak in Final Diff. Map	0.62 e ⁻ /Å ³
<u>Minimum peak in Final Diff. Map</u>	<u>-0.51 e⁻/Å³</u>

Table 12. 2,2-trans [Rh₂(NPhCOCH₃)₄] • 2 o-NC({2-CH₃}C₆H₄) X-ray crystallography data.

The 2,2-trans-[Rh₂(NPhCOCH₃)₄] • 2 o-NC({2-CH₃}C₆H₄) was a long, red block-shaped crystal having the approximate dimensions of 0.33 x 0.12 x 0.12 mm mounted on a glass fiber. The crystal to detector distance was 50.00 mm. The lattice parameters measured for the crystal's unit cell determined that the 2,2-trans-

[Rh₂(NPhCOCH₃)₄]• 2 o-NC({2-CH₃}C₆H₄) crystal system was a primitive triclinic cell. For Z=2 and formula weight=976.74 g/mol, the calculated density was 1.463 g/cm³. The data was collected at a temperature of 25± 1°C. A total of 540 oscillation images were collected. The exposure rate was 16.0 [sec./°].

2,2-trans [Rh₂(NPhCOCH₃)₄]• m-NC({3-CH₃)C₆H₄):

Number and type of atoms	C ₄₈ H ₄₆ N ₆ O ₄ Rh ₂
Crystal Dimensions	0.16 X 0.08 X 0.07 mm
Crystal System	triclinic
Lattice Type	Primitive
Lattice Parameters	a = 11.7109(13) Å b = 13.0181(14) Å c = 13.3980(14) Å α = 72.337(5) ° β = 66.780(5) ° γ = 82.742(6) ° V = 1788.6(3) Å ³
Temperature	25.0°C
Exposure Rate	30.0 sec./°
Residuals: R1 (I>2.00s(I))	0.0491
Residuals: R (All reflections)	0.0859
Residuals: wR2 (All reflections)	0.1014
Goodness of Fit Indicator	1.036
Max Shift/Error in Final Cycle	0.001
Maximum peak in Final Diff. Map	0.73 e ⁻ /Å ³
<u>Minimum peak in Final Diff. Map</u>	<u>-0.84 e⁻/Å³</u>

Table 13. 2,2-trans [Rh₂(NPhCOCH₃)₄]• m-NC({3-CH₃)C₆H₄) X-ray crystallography data.

The 2,2-trans-[Rh₂(NPhCOCH₃)₄]• m-NC({3-CH₃)C₆H₄) was a long, blue block-shaped crystal having the approximate dimensions of 0.16 x 0.08 x 0.07 mm mounted on a glass fiber. The crystal to detector distance was 50.00 mm. The lattice parameters measured for the crystal's unit cell determined that the 2,2-trans-

[Rh₂(NPhCOCH₃)₄]• m-NC({3-CH₃)C₆H₄) crystal system was a primitive triclinic cell. For Z=2 and formula weight=873.60.74 g/mol, the calculated density was 1.622 g/cm³. The data was collected at a temperature of 25± 1°C. A total of 540 oscillation images were collected. The exposure rate was 30.0 [sec./°].

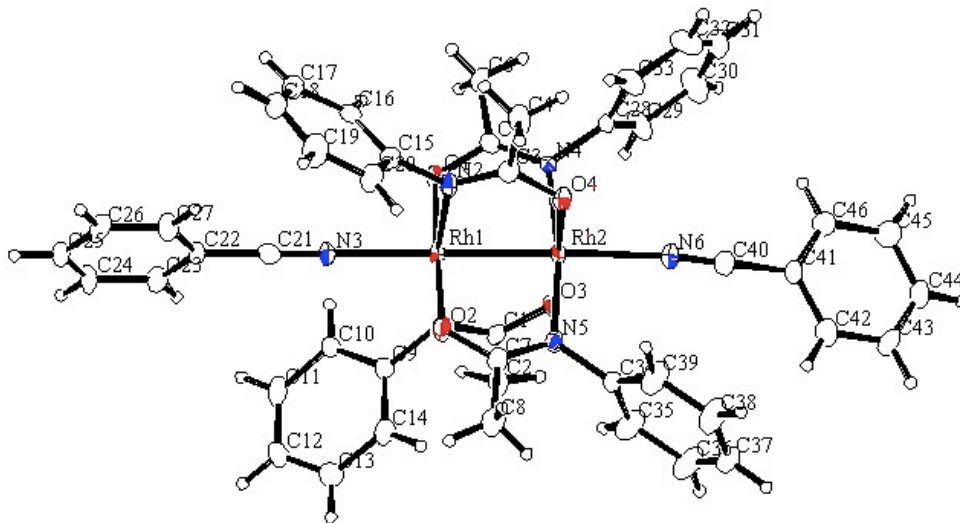


Figure 45. ORTEP of 2,2-*trans*-[Rh₂(NPhCOCH₃)₄]• 2NC({2-CH₃)C₆H₄)

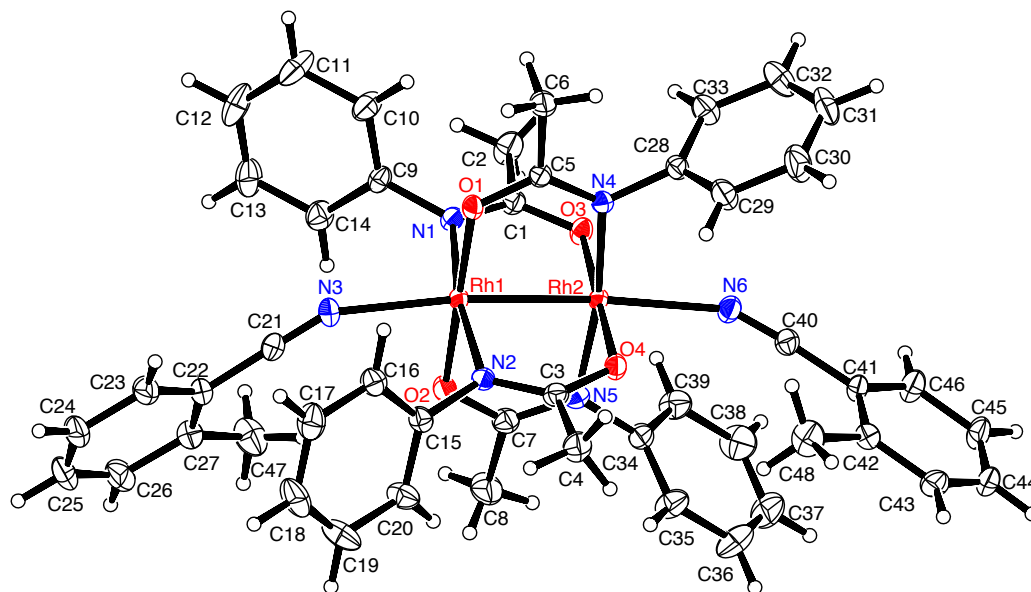


Figure 46. ORTEP of 2,2-*trans*-[Rh₂(NPhCOCH₃)₄]• 2 o-NC({2-CH₃)C₆H₄)

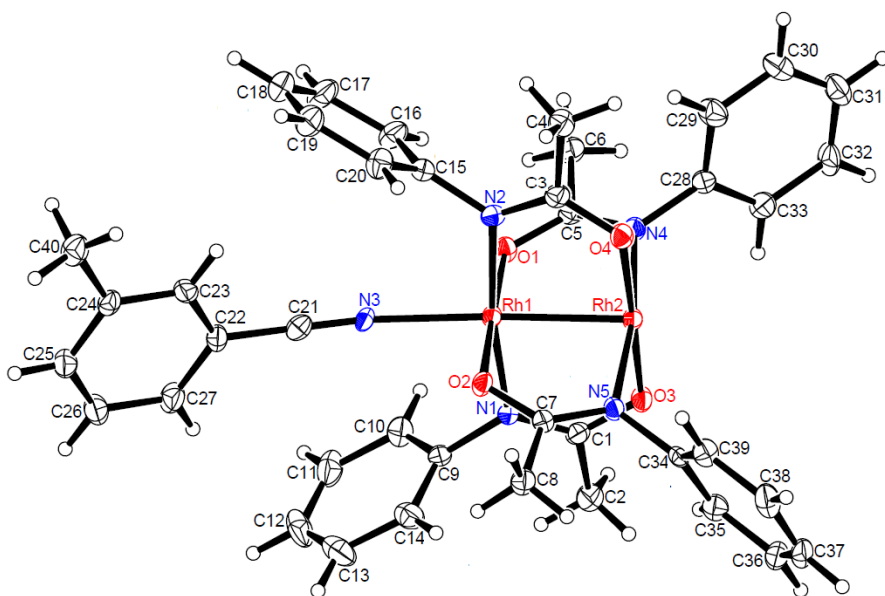


Figure 47. ORTEP of 2,2-*trans* [Rh₂(NPhCOCH₃)₄]• *m*-NC({3-CH₃)C₆H₄)

	From 2,2- <i>trans</i> [Rh ₂ (NPhCOCH ₃) ₄]• x L			
	bond	bond length (Å)	bond angle (°)	torsion angle (°)
L=benzonitrile	Rh1-Rh2	2.4207(8)		
x=2	C21-N3	1.156(8)		
	C40-N6	1.130(8)		
	Rh1-N3-C21		177.8(5)	
	Rh2-N6-C40		169.2(5)	
	N2-Rh1-Rh2-O4			9.50(1)
	N3-Rh1-Rh2-N6			45.03(6)
	N4-Rh1-Rh2-O1			10.84(1)
	O2-Rh1-Rh2-N5			11.26(1)
	N1-Rh1-Rh2-O3			12.71(2)
L=o-tolunitrile	Rh1-Rh2	2.4241(4)		
x=2	C21-N3	1.132(4)		
	C40-N6	1.137(4)		
	Rh1-N3-C21		151.6(3)	
	Rh2-N6-C40		152.5(3)	
	N5-Rh2-Rh1-O2			4.79(5)
	N6-Rh2-Rh1-N3			71.6(9)
	O1-Rh1-Rh2-N4			4.07(5)
	N2-Rh1-Rh2-O4			6.82(7)
	N1-Rh1-Rh2-O3			6.87(7)
L=m-tolunitrile	Rh1-Rh2	2.4039(7)		
x=1	C21-N3	1.140(8)		
	Rh1-N3-C21		166.3(3)	
	N2-Rh1-Rh2-O4			12.69(1)
	N1-Rh1-Rh2-O3			12.55(1)
	N4-Rh2-Rh1-O1			14.04(8)
	N5-Rh2-Rh1-O2			13.28(8)

Table 14. X-ray Crystallography bond lengths, bond angles, and torsion angles (x=1 or x=2).

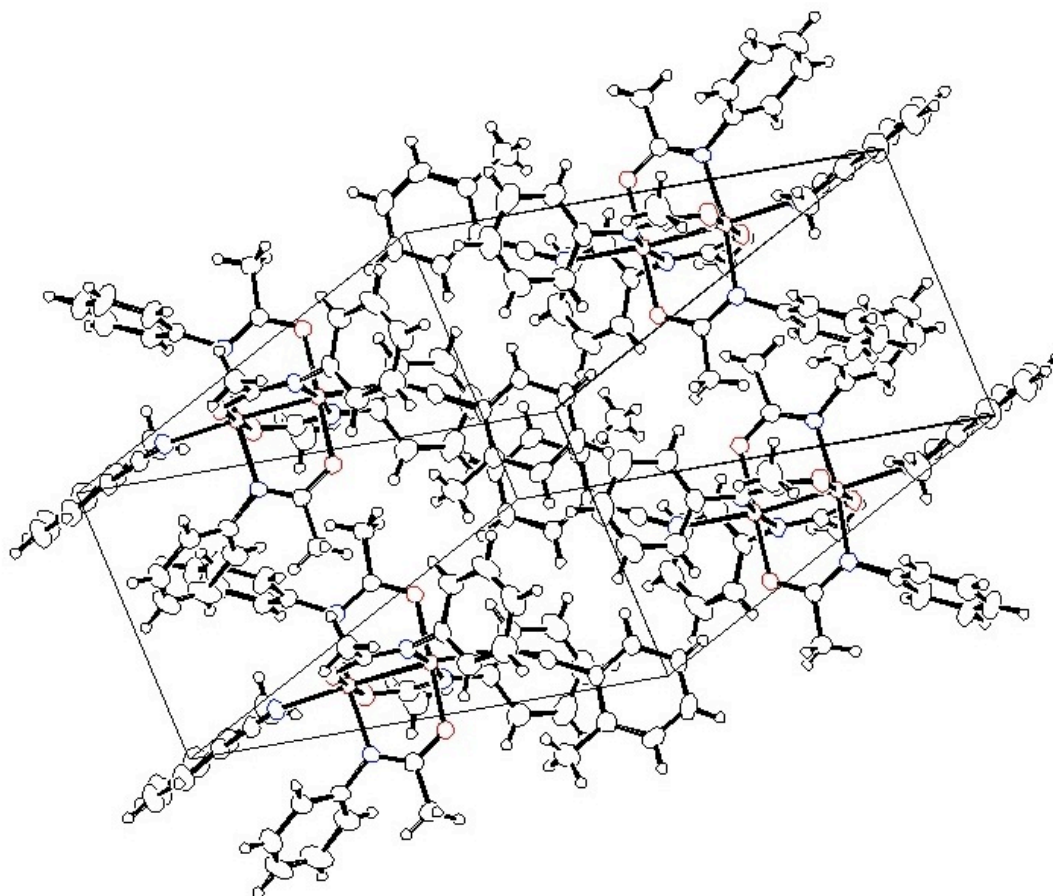


Figure 48. Packing diagram of 2,2-*trans* [Rh₂(NPhCOCH₃)₄]• 2 o -NC({2-CH₃}C₆H₄)

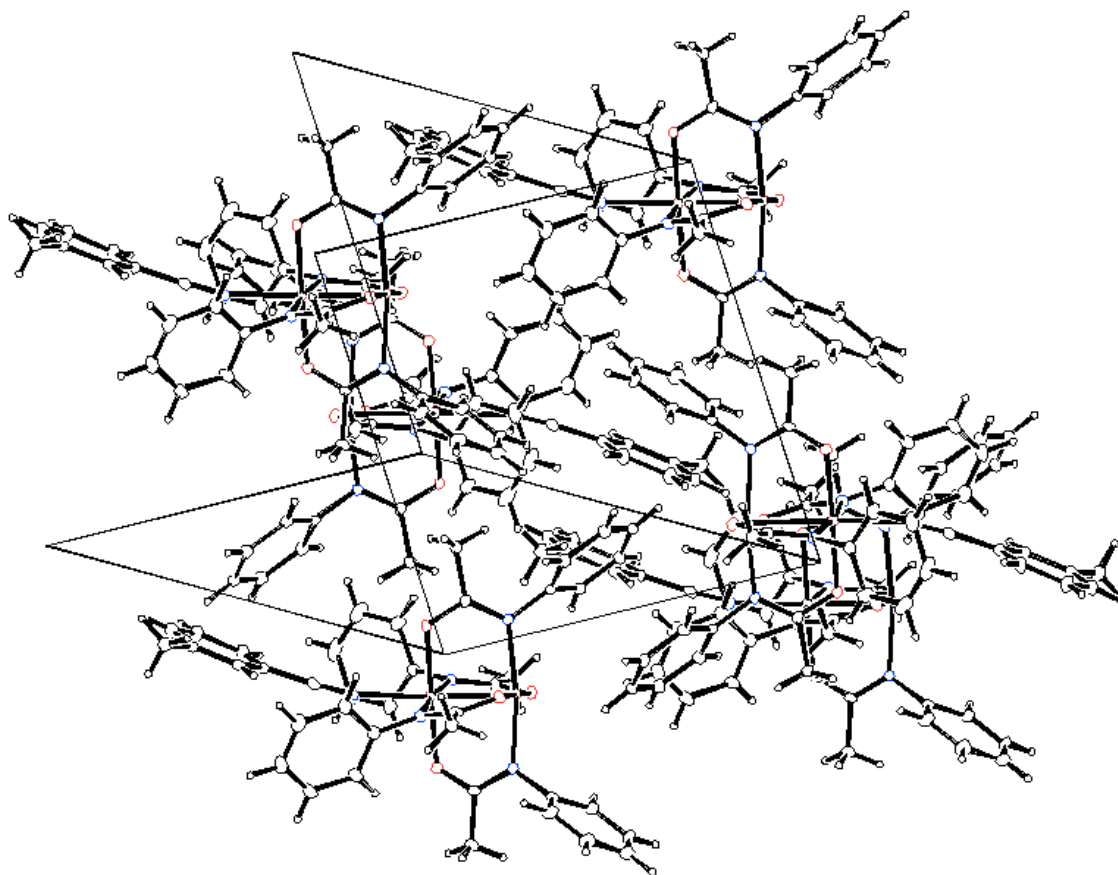


Figure 49. X-ray crystallography packing diagram of 2,2-*trans* [Rh₂(NPhCOCH₃)₄] • *m*-NC({3-CH₃}C₆H₄)

(The following abbreviations will be used for simplification: “Nax” for an axial nitrile ligand, either benzonitrile, *o*-tolunitrile, or *m*-tolunitrile; and “Neq” for an equatorial *N*-phenylacetamide ligand.)

3.31 Bond lengths

For 2,2-*trans* [Rh₂(NPhCOCH₃)₄] • 2NC(C₆H₄), the bond lengths were 2.4207(8) Å (Rh1-Rh2), 1.156(8) Å (C21-N3_{ax}), and 1.130(8) Å (C40-N6_{ax}).

For 2,2-*trans* [Rh₂(NPhCOCH₃)₄] • 2 *o*-NC({2-CH₃}C₆H₄), the bond lengths were 2.4241(4) Å (Rh1-Rh2), 1.132(4) Å (C21-N3_{ax}), and 1.137(4) Å (C40-N6).

For 2,2-*trans* [Rh₂(NPhCOCH₃)₄] • m-NC({3-CH₃)C₆H₄), the bond lengths were 2.4039(7) Å (Rh1-Rh2) and 1.140(8) Å (C21-N3_{ax}).

For the three compounds, 2,2-*trans* [Rh₂(NPhCOCH₃)₄] • 2NC(C₆H₄), 2,2-*trans* [Rh₂(NPhCOCH₃)₄] • 2 o-NC({2-CH₃)C₆H₄), and 2,2-*trans* [Rh₂(NPhCOCH₃)₄] • m-NC({3-CH₃)C₆H₄), the bond lengths of the corresponding Rh-Rh and C≡N functional group are all similar: the Rh-Rh bond is around 2.4 Å; the C≡N functional group's bond lengths are about 1.13-1.15 Å. So bond strength and bond dissociation energy did not change much because of the change of axial nitrile ligands (benzonitrile, o-tolunitrile, or m-tolunitrile.)

3.33 Bond angles

For 2,2-*trans* [Rh₂(NPhCOCH₃)₄] • 2NC(C₆H₄), the bond angles were: 177.8(5)° (Rh1-N3-C21_{ax}) and 169.2(5)° (Rh2-N6-C40_{ax}).

For 2,2-*trans* [Rh₂(NPhCOCH₃)₄] • 2 o-NC({2-CH₃)C₆H₄), the bond angles were: 151.6(3)° (Rh1-N3-C21_{ax}) and 152.5(3)° (Rh2-N6-C40_{ax}).

For 2,2-*trans* [Rh₂(NPhCOCH₃)₄] • m-NC({3-CH₃)C₆H₄), the bond angle was 166.3(3)° (Rh1-N3-C21_{ax}).

2,2-*trans* [Rh₂(NPhCOCH₃)₄] • 2 o-NC({2-CH₃)C₆H₄) had the smallest Rh-N-C bond angle, which is the angle that is least linear out of the three complexes. Due to the σ-bond and π-bonds from the triple bond of the C≡N functional group, the Rh-N-C bond angle should be linear, ideally. However, it was expected that the bond that would experience the most bending would be the 2,2-*trans* [Rh₂(NPhCOCH₃)₄] • 2 o-NC({2-CH₃)C₆H₄) complex because of the position of the CH₃ from the o-tolunitrile axial ligand. In the ortho position, the CH₃ substituent of the o-tolunitrile positioned closest to 2,2-*trans* [Rh₂(NPhCOCH₃)₄] • 2 o-NC({2-CH₃)C₆H₄) adduct, which forces Rh-N-C to become nonlinear due to steric forces from the CH₃ substituent of the o-tolunitrile. The Rh-N-C of 2,2-*trans* [Rh₂(NPhCOCH₃)₄] • m-NC({3-CH₃)C₆H₄) did not bend as much as the Rh-N-C of 2,2-*trans* [Rh₂(NPhCOCH₃)₄] • 2 o-NC({2-CH₃)C₆H₄), but it the angle was still smaller than the Rh-N-C of 2,2-*trans* [Rh₂(NPhCOCH₃)₄] • 2NC(C₆H₄). Similarly to 2,2-*trans* [Rh₂(NPhCOCH₃)₄] • 2 o-NC({2-CH₃)C₆H₄), the CH₃ substituent of the m-tolunitrile influences the linearity of the Rh-

N-C angle. In the meta position, the CH₃ substituent of the m-tolunitrile positioned close to 2,2-*trans* [Rh₂(NPhCOCH₃)₄] • m-NC({3-CH₃}C₆H₄) adduct, which forces Rh-N-C to bend slightly due to steric forces from the CH₃ substituent of the m-tolunitrile. None of the Rh-C≡N bond angles of any of the three complexes were completely linear (180°), but had bond angles less than 180°, possibly suggesting that neither σ-bonding nor π-backbonding is responsible for the nonlinear bond angles.

In comparison with Rozwadowski's research, tetrakis(carboxylate) dirhodium(II) was used instead of 2,2-*trans* tetrakis(carboxylamide) dirhodium(II). However, Rozwadowski also found Rh-Rh ← N≡C to be nonlinear because these Rh-Rh adducts tend to form a dimer of dimers with axial nitrile ligands, using these nitrile ligands as bridging molecules, which in turn influence the geometry of the molecules. (A dimer is formed when two rhodium atoms are bound together; a dimer of dimers forms when two dirhodium complexes are bound together by a nitrile.) Although it is unclear what is responsible for the deviation from linearity, the weak bonds of the bridging ligands to the Rh may have influenced Rh-Rh ← N≡C to be nonlinear.¹² For the 2,2-*trans* [Rh₂(NPhCOCH₃)₄] • 2NC(C₆H₄), 2,2-*trans* [Rh₂(NPhCOCH₃)₄] • 2 o-NC({2-CH₃}C₆H₄), and 2,2-*trans* [Rh₂(NPhCOCH₃)₄] • m-NC({3-CH₃}C₆H₄) complexes, because the Rh-Rh adduct was tetrakis(carboxylamide) dirhodium(II) instead of tetrakis(carboxylate) dirhodium(II), the phenyl substituents attached to the nitrogens of the tetrakis(carboxylamide) dirhodium(II) may have had steric influences that could have blocked or prevented the axial nitrile ligands from bridging the Rh-Rh adducts.

3.34 Torsion angles

For 2,2-*trans* [Rh₂(NPhCOCH₃)₄] • 2NC(C₆H₄), the torsion angles were: 9.50(1)° (N2-Rh1-Rh2-O4), 45.03(6)° (N3-Rh1-Rh2-N6), 10.84(1)° (N4-Rh2-Rh1-O1), 11.26(1)° (O2-Rh1-Rh2-N5), and 12.71(2)° (N1-Rh1-Rh2-O3).

For 2,2-*trans* [Rh₂(NPhCOCH₃)₄] • 2 *o*-NC({2-CH₃)C₆H₄), the torsion angles were: 4.79(5)° (N5-Rh2-Rh1-O2), 71.6(9)° (N6-Rh2-Rh1-N3), 4.07(5)° (O1-Rh1-Rh2-N4), 6.82(7)° (N2-Rh1-Rh2-O4), and 6.87(7)° (N1-Rh1-Rh2-O3).

For 2,2-*trans* [Rh₂(NPhCOCH₃)₄] • *m*-NC({3-CH₃)C₆H₄), the torsion angles were 12.69(1)° (N2-Rh1-Rh2-O4), 12.55(1)° (N1-Rh1-Rh2-O3), 14.04(8)° (N4-Rh2-Rh1-O1), and 13.28(8)° (N5-Rh2-Rh1-O2).

The torsion angles could be a consequence of either steric or electronic influences. Specifically, the torsion angles could result from steric influences from the methyl groups on the nitrile axial ligands. The methyl groups could “push” away from other surrounding molecules, thus resulting in greater torsion angles. The (N-Rh-Rh-O) torsion angles of the 2,2-*trans* [Rh₂(NPhCOCH₃)₄] • 2 *o*-NC({2-CH₃)C₆H₄) were smaller than the 2,2-*trans* [Rh₂(NPhCOCH₃)₄] • 2NC(C₆H₄). However, the (N_{ax}-Rh-Rh-N_{ax}) torsion angle of 2,2-*trans* [Rh₂(NPhCOCH₃)₄] • 2 *o*-NC({2-CH₃)C₆H₄) was greater than that of 2,2-*trans* [Rh₂(NPhCOCH₃)₄] • 2NC(C₆H₄) because of the methyl groups(_{ax}). The 2,2-*trans* [Rh₂(NPhCOCH₃)₄] • *m*-NC({3-CH₃)C₆H₄) did not have a (N_{ax}-Rh-Rh-N_{ax}) torsion angle because it only had one axial nitrile ligand. The (N-Rh-Rh-O) torsion angles of 2,2-*trans* [Rh₂(NPhCOCH₃)₄] • *m*-NC({3-CH₃)C₆H₄) were greater than the (N-Rh-Rh-O) torsion angles 2,2-*trans* [Rh₂(NPhCOCH₃)₄] • 2 *o*-NC({2-CH₃)C₆H₄) and 2,2-*trans* [Rh₂(NPhCOCH₃)₄] • 2NC(C₆H₄). This resulted because the 2,2-*trans* [Rh₂(NPhCOCH₃)₄] • *m*-NC({3-CH₃)C₆H₄) had only one axial nitrile ligand, allowing it to have more freedom to “twist.” The methyl group(_{ax}) in the meta position also could have caused these greater torsion angles.

3.35 Packing diagrams

The packing diagrams for 2,2-*trans* [Rh₂(NPhCOCH₃)₄] • 2 *o*-NC({2-CH₃)C₆H₄) and 2,2-*trans* [Rh₂(NPhCOCH₃)₄] • *m*-NC({3-CH₃)C₆H₄) can be found in Figures 48 and 49.

Packing diagrams were then generated to analyze the influence of packing forces. The small torsion angles of 2,2-*trans* [Rh₂(NPhCOCH₃)₄] • 2 *o*-NC({2-CH₃)C₆H₄) implies that the N and O (N-Rh-Rh-O) and the N and N' (N-Rh-Rh-N') almost eclipse each other. From the packing diagrams, the phenyl groups (from the

N-phenylacetamide) fit tightly in the spaces in between the 2,2-*trans* [Rh₂(NPhCOCH₃)₄]• 2 *o*-NC({2-CH₃)C₆H₄) adducts, suggesting that the steric bulk from the phenyl groups(_{eq}) is forcing (N-Rh-Rh-O) to twist slightly to have torsion angles slightly greater than zero. The large (N-Rh-Rh-N') torsion angle of 71.6(9)° may have resulted due to a combination of the packing forces of the phenyl groups(_{ax}) and the methyls on the phenyl groups(_{ax}).

After analysis of the X-ray crystallography data, it was determined that the benzonitrile and *o*-tolunitrile ligands bound on both axial sites of the 2,2-*trans* [Rh₂(NPhCOCH₃)₄]. However, the *m*-tolunitrile only bound to one side. The *o*-tolunitrile formed a 2:1 adduct, (L=*o*-tolunitrile axial ligand) L → Rh–Rh ← L, whereas the *m*-tolunitrile formed a 1:1-adduct, (L=*m*-tolunitrile ligand) L → Rh–Rh. It is not certain whether or not this occurred because of electronic influence or because not enough equivalents of the *m*-tolunitrile were added.

Packing forces could have influenced 2,2-*trans* [Rh₂(NPhCOCH₃)₄]• *m*-NC({3-CH₃)C₆H₄) to form a 1:1 adduct, L→Rh–Rh, whereas 2,2-*trans* [Rh₂(NPhCOCH₃)₄]• 2 *o*-NC({2-CH₃)C₆H₄) formed a 2:1 adduct, L→Rh–Rh←L. If the orientation of each 2,2-*trans* [Rh₂(NPhCOCH₃)₄]• *m*-NC({3-CH₃)C₆H₄) molecule in a unit cell prevented another *m*-tolunitrile ligand from binding to the axial site, the 1:1 adduct would be favored. A phenyl ring of another 2,2-*trans* [Rh₂(NPhCOCH₃)₄]• *m*-NC({3-CH₃)C₆H₄) could have been oriented toward that space (of the empty axial site) and occupied it, which would have blocked a second *m*-tolunitrile ligand from binding. However, after conducting a visual analysis of the space of the empty rhodium axial site, it was concluded that packing forces are not likely to have forced the *m*-tolunitrile to bind to only one axial site.

While it remains unknown as to why the *m*-tolunitrile bound only to one axial site of 2,2-*trans* [Rh₂(NPhCOCH₃)₄], there are several possible reasons that were postulated, including: steric hindrance, packing forces, electronic factors, or lack of enough equivalents of *m*-tolunitrile during synthesis of the 2,2-*trans* [Rh₂(NPhCOCH₃)₄] • *m*-NC({3-CH₃)C₆H₄).

According to Rozwadowski, the formation of the 2:1 adduct of L→Rh–Rh←L was energetically favored. However, the [Rh₂(NPhCOCH₃)₄] • *m*-NC({3-CH₃)C₆H₄)

contradicted this assumption. It was also unlikely that steric hindrance (of the CH₃ substituent on the m-tolunitrile) prevented the m-tolunitrile from binding to both axial sites of the 2,2-*trans* [Rh₂(NPhCOCH₃)₄] because if that were true, the methyl group on the o-tolunitrile would have also prevented the o-tolunitrile from binding to both axial sites of the 2,2-*trans* [Rh₂(NPhCOCH₃)₄].

4. Conclusion

The new method used to grow the 2,2-*trans* [Rh₂(NPhCOCH₃)₄] • m-NC({3-CH₃}C₆H₄) can be applied to grow X-ray quality crystals. After attempting to grow the crystals with dichloromethane, the crystals of 2,2-*trans* [Rh₂(NPhCOCH₃)₄] • m-NC({3-CH₃}C₆H₄) (that were not X-ray quality) were re-dissolved in acetone. The amount of acetone added was much greater than the amount of m-tolunitrile. Acetone should have competed with the m-tolunitrile ligand for the axial site, forcing the m-tolunitrile axial ligands out. However, since perhaps the m-tolunitrile ligands were already bound to the 2,2-*trans* [Rh₂(NPhCOCH₃)₄] compound, acetone did not bind to the axial site. The acetone may also have influenced m-tolunitrile bound to bind to only one axial site. Since growing the 2,2-*trans* [Rh₂(NPhCOCH₃)₄] • m-NC({3-CH₃}C₆H₄) crystals was difficult to do through the regular process, this method of using acetone was not attempted for the 2,2-*trans* [Rh₂(NPhCOCH₃)₄] • 2NC(C₆H₄) or 2,2-*trans* [Rh₂(NPhCOCH₃)₄] • 2 o-NC({3-CH₃}C₆H₄) complexes.

When synthesizing 2,2-*trans* [Rh₂(NPhCOCH₃)₄] • m-NC({3-CH₃}C₆H₄), only two molar equivalents of m-tolunitrile were added. Future research may attempt adding an excess of m-tolunitrile during synthesis to provide a greater probability of the m-tolunitrile to bind to both axial sites of the Rh-Rh adduct. Also, other possible future research may include molecular modeling to further investigate the influences behind the orientations of the atoms in 2,2-*trans* [Rh₂(NPhCOCH₃)₄] • m-NC({3-CH₃}C₆H₄). Other types of nitrile ligands can be synthesized with 2,2-*trans* [Rh₂(NPhCOCH₃)₄], such as p-tolunitrile, which, depending on whether or not p-tolunitrile forms a 2:1 adduct or 1:1 adduct with Rh-Rh, will give insight upon the forces influencing the bonding nature of axial nitrile ligands to 2,2-*trans*

$[\text{Rh}_2(\text{NPhCOCH}_3)_4]$. Also, 2,2-*cis* $[\text{Rh}_2(\text{NPhCOCH}_3)_4]$ or 3,1- $[\text{Rh}_2(\text{NPhCOCH}_3)_4]$ may be used as the Rh-Rh complex instead of 2,2-*trans* $[\text{Rh}_2(\text{NPhCOCH}_3)_4]$.

Because the *m*-tolunitrile ligand bound to one axial side of the dirhodium compound, the other site may be probed as a catalytic site. The *m*-tolunitrile ligand would serve as to block one axial site. We were able to successfully manipulate the electron density of 2,2-*trans* $[\text{Rh}_2(\text{NPhCOCH}_3)_4]$ through axial ligands, which can later be used as models for catalysis for future cyclopropanation research.

References

- ¹ Eagle, Cassandra T.; Farrar, David G.; Holder, Grant N.; Pennington, William T.; Bailey, Rosa D. "Structural and Electronic Properties of (2,2-*trans*)-Dirhodium(II) Tetrakis(N-phenylacetamidate)." *Journal of Organometallic Chemistry*, **2000**, 596, 90-94.
- ² Evans, Andrew P.; Tsuji, Jiro. *Rhodium(II) in 1,3-Dipole Formation: Modern Rhodium-Catalyzed Organic Reactions*; Wiley-VCH: Strauss GmbH, **2005**, p. 435.
- ³ Pirrung, Michael C.; Morehead Jr., Andrew T. "Electronic Effects in Dirhodium(II) Carboxylates. Linear Free Energy Relationships in Catalyzed Decompositions of Diazo Compounds and CO and Isonitrile Complexation." *Journal of the American Chemical Society*, **1994**, 116 (20), 8991-9000.
- ⁴ Eagle, Cassandra T.; Farrar, David G.; Holder, Grant N.; Hatley, Michelle L.; Humphrey, Shirley L.; Olson, Elizabeth V.; Quintos, Maria; Sadighi, Joseph; Wideman, Tom. "Cis-Enhanced Cyclopropanation Catalysts: Reaction Chemistry of Three isomers of Rh₂[N(C₆H₅)COCH₃]₄." *Tetrahedron Letters*, **2003**, 44 (12), 2593 - 2595.
- ⁵ McMurry, John E. *Organic Compounds: cycloalkanes and their stereochemistry. Organic Chemistry*, 7th ed.; Brooks Cole: Belmont, CA, Chapter 4.
- ⁶ Cotton, F. Albert; Thompson, J. Lon. "Preparation and Structural Characterization of Three Tetracarboxylato Dirhodium (Rh-Rh) Compounds with Bulky Ligands." *Inorganica Chimica Acta*, **1984**, 81, 193-203.
- ⁷ O'Brien, R.D. "Naturally Occurring Insecticides." *Insecticides, Action and Metabolism*, Academic Press, New York and London, **1967**, 164-171.
- ⁸ Parshall, George W.; Nugent, William A. "Homogeneous catalysis for agrochemicals, flavors, and fragrances. Part 3." *Chemtech*, **1988**, 18, (6), 376-83.
- ⁹ Wolf, Joffrey; Poli, Rinaldo; Xie, Jian-Hua; Nichols, Jason; Xi, Bin; Zavalij; Doyle, Michael P. "Removal of Metal-Metal Bonding in a Dimetallic Paddlewheel Complex: Molecular and Electronic Structure of Bis(phenyl) Dirhodium(III) Carboxamidate Compounds." *Organometallics*, **2008**, 27, 5836-5845.

-
- ¹⁰ Doyle, M.P.; Taunton, Jack; Pho, Hoan Q. "Conformational and electronic preferences in rhodium carboxylate and rhodium(II) carboxamide catalyzed carbon-hydrogen insertion reactions of *N,N*-disubstituted diazoacetoacetamides." *Tetrahedron Letters*, **1989**, 30 (40), 5397-5400.
- ¹¹ Doyle, M.P., et al; "Exceptionally High Trans (Anti) Stereoselectivity in Catalytic Cyclopropanation Reactions." *Journal of the American Chemical Society*, **1990**, 5 (112), 906-912.
- ¹² Rozwadowski, Zbigniew; Malik, Shahid; Tóth, Gábor; Tamás Gáti; Helmut Duddeck, Helmut. "Dirhodium tetraacylate complexes and monovalent ligands. Adduct formation in solution as monitored by NMR spectroscopy." *The Royal Society of Chemistry*, **2003**, 375-379.
- ¹³ Hameed, Shahid; Ahmad, Roshan; Duddeck, Helmut. "Chiral recognition of nitriles by ¹H NMR spectroscopy in the presence of a chiral dirhodium complex." *Magnetic Resonance in Chemistry*, **1998**, 36, 47-53.
- ¹⁴ Sands, Donald E. *Introduction to Crystallography*; Dover Publications, Inc: Mineola, NY, **1994**, 2, 11, 55-61, 88-92, 127.
- ¹⁵ Jesperen, Neil D.; Brady, James E.; Hyslop, Alison. X-ray Diffraction of Solids. *Chemistry: The Molecular Nature of Matter*, 6th ed.; John Wiley & Sons: Hoboken, NJ, **2012**, Chapter 12.
- ¹⁶ Glossary of statistical terms. IUCr Journals (accessed on June 11, 2012).
- ¹⁷ Refer to page 12 for the potential ramifications of contamination.
- ¹⁸ NMR Solvent Data Chart. Cambridge Isotope Laboratories, Inc. (accessed May 10, 2012).
- ¹⁹ This is further confirmed by X-ray crystallography results on pages 64-65.
- ²⁰ An Introduction: C-13 NMR. Institute of Pharmaceutical Sciences and Drug Research (accessed June 23, 2012).